

EVALUATION OF URBAN DEVELOPMENT IN KUNMING (CHINA) USING THE LOCAL CLIMATE ZONE SCHEME

Stéphanie Vandamme

01200266

Promoter: Prof. dr. Ir. Frieke Van Coillie

Copromoter: Prof. dr. Ir. Robert De Wulf

Tutor: Ir. Marie-Leen Verdonck

Thesis submitted in the fulfilment of the requirements of the degree of Master in Bioscience Engineering: Forest and Nature Management.

Academic year 2017-2018

Acknowledgements

Choosing a suitable topic for my master thesis was easier than expected. I was instantly drawn to the subject due to it being a combination of several of my interests such as remote sensing and investigating the impact of people on the environment. Of course, the pleasant people at the department of FORSIT made this choice even better. At first I was anxious of the unknown and the difficult challenges that I would have to encounter. In the end I can only say I loved every part of the thesis, starting from the fieldwork, to gathering knowledge, to critically thinking, to eventually writing. I have always preferred to work independently and to carry out my own research in my field of interest, and this thesis provided just that.

This thesis could not be realised without the support of Marie-Leen Verdonck, who has helped me from the beginning to the very end with her feedback, help and proofreading. Hence a big thanks to her. I would also like to thank my promotors Frieke Van Coillie and Rob De Wulf for giving me the opportunity to carry out this thesis. Also a special thanks to Prof. Ming Zhiming Zhang for the guidance in Kunming and to my boyfriend Mike for the proofreading, some tips and tricks, for joining me in Kunming and of course for the emotional support in general. Finally, I want to thank my cats for all their love and warmth while writing this thesis.

Table of contents

SUMMARY.....	VII
SAMENVATTING	VIII
1. INTRODUCTION	1
2. LITERATURE STUDY.....	2
2.1 Urbanisation	2
2.1.1 General.....	2
2.1.2 China	2
2.1.3 Kunming	3
2.1.4 Drivers of urbanisation.....	4
General drivers in China.....	4
Additional drivers in Kunming.....	5
2.1.5 Consequences of urbanisation	7
Environmental and health issues related to urbanisation	7
Land use/cover changes	9
Urban Heat Island	9
2.2 Local Climate Zone (LCZ)-mapping.....	11
2.2.1 Background	11
2.2.2 WUDAPT Protocol	13
2.2.3 Data: Landsat	14
2.2.4 Classification algorithm: random forest classifier	16
2.3 Land Surface Temperature	17
2.3.1 Definition.....	17
2.3.2 Relationship LCZ and LST.....	17
2.3.3 LST estimation	18
2.3.4 Land Surface Emissivity (LSE)	19
3. MATERIAL AND METHODS.....	20
3.1 Study area	20
3.2 Data and methods.....	20
3.2.1 LCZ mapping	20
Landsat images	20
ROI and training areas	21
.....	22
Classification and its adaptations.....	23
3.2.2 Land Surface Temperature retrieval	24
Images.....	24
LST estimation.....	24
3.2.3 Surface Urban Heat Island assessment	27
Evolution of the sUHII during 2004 -2017.....	27
sUHII classification in 2017	27
4. RESULTS	29
4.1 LCZ mapping.....	29

4.1.1	Accuracies	29
4.1.2	LCZ localisation.....	30
4.1.3	LUCC between 2005 and 2017	32
4.2	Land surface retrieval.....	34
4.2.1	Evolution of LST during 2004 -2017	34
4.2.2	Thermal behaviour of the different LCZs	35
4.3	Surface urban heat island intensity	35
4.3.1	Evolution of the sUHI during 2004 - 2017	35
	General sUHII intensity of Kunming.....	35
	sUHII of the different LCZs over the different time periods	36
4.3.2	sUHI classification	37
5.	DISCUSSION.....	38
5.1	LCZ classification	38
5.2	Thermal behaviour of the different LCZs	39
5.3	Urban development	40
5.3.1	Urban expansion and densification.....	40
	Period between 2005 and 2011.....	40
	Period between 2011 and 2017	41
	Changes in LST	42
5.4	sUHII assessment	42
5.4.1	sUHII of the different LCZs	43
5.4.2	sUHII for 2017 in general.....	44
6.	CONCLUSION.....	45
7.	FURTHER RESEARCH.....	46
	BIBLIOGRAPHY.....	47
	APPENDIX.....	59

Abbreviations

ART	Anomaly Response Team
LUCC	Land Use/Cover Changes
KEPB	Kunming Environmental Protection Bureau
(s)UHI(I)	(surface) Urban Heat Island (Intensity)
UHII	Urban heat Island Intensity
IPCC	Intergovernmental Panel on Climate Change
LCZ	Local Climate Zone
WUDAPT	World Urban Database and Access Portal Tools
USGS	United States Geological Survey
ASTER	Advanced Spaceborne Thermal Emission and Reflection radiometer
HUMINEX	The Human Influence Experiment
RFC	Random Forest Classifier
ETM+	Enhanced Thematic Mapper Plus
SCL	Scan Line Corrector
SHE	Stedelijk Hitte Eiland
ART	Anomaly Response Team
GLS	Global Land Survey
NASA	National Aeronautics and Space Administration
WRS-2	Worldwide Reference System-2
LST	Land Surface Temperature
MODIS	Moderate-resolution Imaging Spectroradiometer
MWA	Mono-Window Algorithm
TIRS	Thermal Infrared Sensor
OLI	Operational Land Imager
LSE	Land Surface Emissivity
NASA	National Aeronautics and Space Administration
NDVI	Normalized Difference Vegetation Index
NBEM	NDVI - Based Emissivity Method
NDVI	Normalized difference vegetation index
ROI	Region Of Interest
OA	Overall Accuracy
UA	User's Accuracy
PA	Producer's Accuracy
TOA	Top Of Atmosphere
DN	Digital Number
PV	Proportion of Vegetation
BT	Brightness Temperatures
NIR	Near InfraRed
SIUHI	Surface Intra UHI
TCZ	Thermal Climate Zones

List of Figures

Figure 1. Location of Kunming, situated in the Yunnan province in China (China highlights, 2018; Google Earth, 2018; modified).	4
Figure 2. China's urban area expansion from 1990 to 2010 (Lancet, 2012).	5
Figure 3. The proportions of each landcover class from 2000 to 2015 in Kunming (Gao et al., 2018)...	6
Figure 4. The development of the urbanisation of Kunming since 2005 (Gao et al., 2018; modified)..	6
Figure 5. Prediction of built-up areas in 2025 and the comparison with the built-up areas in 2015 (Gao et al., 2018).	7
Figure 6. Overview Urban Heat Island mechanism (Chen et al., 2006; modified).	10
Figure 7. Local climate zone scheme (Steward & Oke, 2012).	12
Figure 8. WUDAPT's different levels of data gathering (Bechtel et al., 2015).	13
Figure 9. Differences between a working and non-working SLC (USGS)	15
Figure 10. Simplified Random Forest (Malekipirbazari & Aksakalli, 2015; modified)	17
Figure 11: Overview LCZ classification. Workflow A is the WUDAPT based method, while workflow B is the modified workflow that uses a moving window to include neighbourhood information (Verdonck et al., 2017).	23
Figure 12. Overall method for LST estimation.	25
Figure 13. LCZ -maps from 2005 with kernel size 9x9 (A), 2011 with kernel size 7x7 (B) and 2017 with kernel size 5x5 (C).....	31
Figure 14. Histogram of the LCZs with their corresponding percentage of the total area from 2005, 2011 and 2017.....	33
Figure 15. Histogram of the LCZs with their corresponding percentage of the total urban area.....	33
Figure 16. Normalised LST of Kunming from May 2004 (A), June 2012 (B) and May 2017 (C).....	34
Figure 17. sUHI intensity of each LCZ of the three different years.	35
Figure 18. Difference in sUHII of each LCZ for 2004-2012 and 2012-2017.	36
Figure 19. sUHI classification of Kunming for May 2017.....	37

List of tables

Table 1. Landsat images information for the LCZ mapping.....	20
Table 2. Overview of LCZs in Kunming	22
Table 3. Landsat images information for the LST calculation.	24
Table 4. Threshold values for sUHI classification based on the LST, whereas μ and SD are the mean and standard deviation values of the LST respectively (Zhang et al., 2013).....	28
Table 5. OAs of the LCZ maps with kernel size 7x7, 9x9 or 11x11 from 2005, 2011 and 2017.....	29
Table 6. Total occupied area of each LCZ for the different years.	32
Table 7. The mean LST ($^{\circ}$ C) for each LCZ in the month May 2017.	35
Table 8. sUHI intensity of each LCZ of the three different years.	36

Summary

During the last 10 years, there has been a strong urbanisation in Kunming, which is the result of economic growth and population growth in the city. It is expected that this urbanisation will only increase as the population will see a strong increase in the future. The rapid economic growth and the associated urbanisation has a major impact on the environment and the social and cultural aspects of the society. The city life has an impact on the air, water and soil pollution. In addition, the land use/cover changes that need to happen for the urban areas to expand cause a great impact. Because of these consequences, it is necessary to study the development of the city, in order to have better regulation on the urbanisation in the future.

In this study, the driving forces of urbanisation in Kunming are determined. In addition, the development of the city will be investigated between 2005 and 2017, based on local climate zones. The trend, land surface temperatures and surface urban heat island intensities (SUHII) of the different local climate zones are determined based on remote sensing data and methods. This results in maps and tables for 2005, 2011 and 2017, showing the distribution of the different local climate zones and land surface temperatures.

The analysis of the motives shows that the urban development in Kunming is led by economic growth, urban population increase and socio-economic, topographical and proximity factors. The results of the surveys on urban development show that between 2005 and 2011, there was mainly a spatial expansion of the city, whereas between 2011 and 2017, there was mainly a densification of the city. The most common local climate zone of 2005, 2011 and 2017 is compact mid-rise (LCZ 2), which mainly occurs in the centre of the city. Between 2005 and 2017, there was a sharp increase in open local climate zones, with the largest increase taking place between 2011 and 2017. In addition, large low-rise (LCZ 8) also experienced a strong increase between 2005 and 2017. The largest decrease can be seen in low-plants (LCZ D) and agricultural greenhouse (LCZ H), which is due to the transformation of agricultural areas into urban areas. For the land surface temperatures, the highest temperatures are found in zones with heavy industry (LCZ 10), large low-rise (LCZ 8), compact mid-rise (LCZ 2) and compact low-rise (LCZ 3). From the values of the different surface urban heat island intensities, for both the entire city and the separate local climate zones, there is a general increase between 2005 and 2017.

It can be concluded that Kunming is subject to strong urbanisation and the associated consequences. Over the years, there has been a change in development with more focus on creating higher buildings that are located in a more open and green space. Despite the greater awareness of the consequences of the strong urbanisation and the adjustments that the policy wants to implement to reduce the consequences, the expected population increase and climate change will require a greener and more elaborated city policy.

Samenvatting

Gedurende de laatste 10 jaar wordt Kunming gekarakteriseerd door een sterke verstedelijking, ten gevolge van de economische groei en de bevolkingstoename in de stad. Aangezien de bevolking nog een sterke stijging zal kennen in de toekomst, zal deze verstedelijking enkel maar toenemen. De snelle economische groei en de daarbij horende verstedelijking heeft een grote impact op het milieu en de sociale en culturele aspecten van de samenleving, zoals lucht-, water- en bodemvervuiling, maar ook aan de omvormingen in het landgebruik en landbedekking. Daarom is het aangewezen om de ontwikkeling van de stad te bestuderen, zodat deze kennis gebruikt kan worden om de verstedelijking beter te reguleren.

In deze studie worden de drijfveren van de verstedelijking in Kunming bepaald. Daarnaast zal de stadsontwikkeling onderzocht worden tussen 2005 en 2017 op basis van lokale klimaatzones, waarbij de trend, de temperaturen van de landoppervlakte en de oppervlakte stedelijke hitte eiland (SHE) intensiteiten van de verschillende lokale klimaatzones bepaald worden op basis van teledetectiegegevens en -methodes. Dit resulteert in kaarten en tabellen voor 2005, 2011 en 2017, waarbij de verdeling van de verschillende lokale klimaatzones en landoppervlakte temperaturen weergegeven worden.

De analyse van de drijfveren toont aan dat de stadsontwikkeling in Kunming geleid wordt door de economische groei, stedelijke populatiestijging en de sociaaleconomische, topografische en nabijheidsfactoren. De resultaten van de onderzoeken naar de stadsontwikkeling geven weer dat er tussen 2005 en 2011 vooral een spatiale expansie van de stad is, terwijl er tussen 2011 en 2017 voornamelijk een verdichting van de stad gebeurde. De meest voorkomende lokale klimaatzone doorheen alle jaren in Kunming is *compact mid-rise* (LCZ 2), welke voornamelijk in het centrum van de stad voorkomt. Tussen 2005 en 2017 was er een sterke toename van open lokale klimaatzones, waarbij de grootste stijging plaatsvond tussen 2011 en 2017. Daarnaast kende *large low-rise* (LCZ 8) ook een sterke stijging tussen 2005 en 2017. De grootste daling is te zien in *low-plants* (LCZ D) en *agricultural greenhouse* (LCZ H), die te wijten is aan de omvorming van landbouwgebieden naar urbane gebieden. Voor de landoppervlakte temperaturen kan er in het algemeen vastgesteld worden dat de hoogste temperaturen gevonden worden in zones met *heavy industry* (LCZ 10), *large low-rise* (LCZ 8), *compact mid-rise* (LCZ 2) en *compact low-rise* (LCZ 3). Uit de waarden van de verschillende oppervlakte *Urban Heat Island* Intensiteiten, voor zowel de ganse stad als de aparte lokale klimaatzones, is er een algemene stijging te zien tussen 2005 en 2017.

Er kan geconcludeerd worden dat Kunming onderhevig is aan een sterke verstedelijking en de gevolgen die hieraan verbonden zijn. Doorheen de jaren is er een verandering in de ontwikkeling te zien waarbij er meer focus gelegd wordt op het creëren van hogere gebouwen die zich in een meer open en groene ruimte bevinden. Ondanks het grotere bewustzijn van de gevolgen van de sterke verstedelijking en de aanpassingen die het beleid wil uitvoeren om de gevolgen te verkleinen, zal door de verwachte populatiestijging en klimaatverandering, een groener en meer uitgewerkt stadsbeleid noodzakelijk zijn.

1. Introduction

The past century has been characterised by rapid urbanisation, whereby cities are formed and grow larger as more people are living and working in the central areas. Population is still increasing and natural resources are continuously exploited. Urbanisation leads to land use/cover changes (LUCC), where natural and agricultural land are replaced by urban areas (Nyambod, 2010).

In this thesis, the development of the urbanisation of Kunming, located in Southwest China, will be investigated. In order to do this, five objectives are conducted:

- (1) Investigate the drivers of the urbanisation in Kunming between 2005 and 2017;
- (2) Develop Local Climate Zone-maps for Kunming in 2005, 2011 and 2017;
- (3) Evaluate the thermal behaviour of the different LCZs, based on the LST and LCZ maps;
- (4) Study the urbanisation in Kunming using Land Surface Temperature (LST) maps;
- (5) Assess the surface Urban Heat Island (sUHI) in Kunming.

In the first objective, the drivers of the urbanisation in Kunming are investigated, so knowledge can be gained about the causes of the rapid urbanisation and how it may be regulated. In the second, Kunming is divided into LCZs for 2005, 2011 and 2017. In the third objective, the LST is used to evaluate the thermal behaviour of the LCZs. These LST maps are subsequently used for the fourth objective, where the LUCC and urban development is studied using LST and LCZ maps. In the fifth objective, the LST is used to investigate the sUHI of Kunming. This can be helpful to divide the city according to their capacity to cause heat stress. This division is especially important for the future urbanisation plans since the expected increase in population and climate change can cause more problems with heat stress in the city.

The thesis is made up by a literature study, material and methods, results, discussion and conclusion. The literature study focusses on the urbanisation in China and Kunming, whereby drivers (objective 1) and the consequences are discussed. Furthermore, there is information given, necessary to complete the second to fifth objective. This includes information about the definition, background, mechanism and the calculation or mapping of the LCZ scheme, (s)UHI and LST. The climate zone mapping is used to study the changes in building patterns between 2005 and 2017, which are driven by the drivers of urbanisation. This spatial pattern has an impact on the LST distribution and sUHI of Kunming, due to the different thermal characteristics of the local climate zones. In material and methods, the used data and methods that are necessary to carry out the researches of objectives (2) to (5) are written down. In the results, the results of the research are given. These results are discussed in the discussion and links with the literature study and other studies are made. Finally, a general answer on the objectives (2 to 5) is given in the conclusion.

2. Literature study

2.1 Urbanisation

2.1.1 General

Urbanisation is characterised by a raising population in the city and a decreasing population in rural areas (Li et al., 2009). In 2008, more than half of the world's human population lived in urban areas (Gutman et al., 2008; Fund, 2007). The current worldwide urbanisation is related to the fast economic development and to the profound changes in social organisation, land use, and patterns of human behaviour (Crane & Kinzig, 2005; Un, 2004), and can occur in two ways (Tisdale, 1942). The first one is when the amount of areas with a high population concentration increases and the second one is when an area with a high population concentration expands.

Urbanisation has an impact on the three pillars of sustainable development; (1) environmental protection, (2) economic and (3) social development (United Nations, 2014). During the past century, population has been rapidly growing in combination with a continuous exploitation of natural resources. As a result, there have been Land use/cover changes (LUCC) worldwide (Li et al., 2009), whereby natural vegetation and agricultural land are often replaced by impervious surfaces, such as buildings and roads (Thi Van & Xuan Bao, 2010). This Land use change comes with an environmental impact, such as negative effects on biodiversity, local climate and hydrologic processes (Nyambod, 2010; Streutker, 2002). Due to increasing population, research of the urban environment is required in order for cities to remain or become sustainable (Zhao et al., 2008). In general, a sustainable city is characterised by supplying sustainable welfare to its people, while maintaining and improving its ecosystem services (Zhao et al., 2009).

Consequences of urbanisation are global environmental changes and socio-economic development (Grimm et al., 2008; Wu et al., 2010). The demographic scale of these changes is unprecedented (Angel & Sheppard, 2005; Un, 2004) and causes consequences for the global environment that are still poorly understood (Bettencourt et al., 2010).

2.1.2 China

China is characterised by a rapid urbanisation. The launch of economic reforms since the late 1970's has contributed largely to this process (Luo & Wei, 2009) and helped half a billion people out of poverty in the past 30 years. This is because the urbanisation provided labour, cheap land and good infrastructure for the people (The world bank, 2014).

The urbanisation in China distinguishes itself from other developing countries due to the absence of widespread proliferation of urban slums. This is partly the result of China's governmental commitment to the expansion of housing and basic infrastructure in urban places (Practices, 2010), and is achieved by investing in housing for urban workers and private enterprises, such as large factories and construction companies (Qu et al., 2010; Un-Habitat, 2003). Besides newbuild houses, the rural-turned-urban people sublet their property as an alternative source of income, which provide extra housing options for migrant populations (Liu et al., 2010). Although these activities restrict the growth of urban and peri urban slums, substandard housing is still a problem in China.

Because of the predicted urban population rise to 70% of the current country's population by 2030, a better coordinated urbanisation process is needed in order to have sustainable cities (The world bank, 2014). In 2012, China has asked the World Bank Group to conduct a joint study on the urbanisation challenges of China. This partnership has led to the a model of urbanisation that consists of the following aspects (The world bank, 2014):

(1) Reforming land management and institutions

Most of the urban expansion happens on converted rural land. This has caused the current available amount of farmland to be close to the 'red line' of 120 million hectares, which is considered the amount of farmland that is necessary to ensure food security. In order to implement more efficient land use, stronger property rights for farmers are required.

(2) Reforming the hukou household-registration system to provide equal access to quality services for all citizens

The current barriers to labour mobility from rural to urban areas and between cities, should be removed in order to stimulate the wages of the workers.

(3) Reforming urban planning and design

Industrial zones should be moved to smaller, secondary cities. To do so, government prices for industrial land should be based on market value. The transport infrastructure should be linked with the urban centres and the coordination between cities should be promoted to ensure better management of congestion and pollution The cities should also make better use of the existing urban land through flexible zoning. This includes smaller plots and more mixed land use and would lead to denser and more efficient urban development.

(4) Managing environmental pressures

Several environmental laws, regulations and standards are already chosen, but in order to achieve greener urbanisation, enforcement is needed. This can be done by introducing taxes and trading systems for carbon, air and water pollution, and energy.

2.1.3 Kunming

Kunming is the capital city of the province Yunnan, which is situated in the southwest of China, Figure 1. In 2015, Kunming had a population of 6.68 million people, with a resident population of 5 million people. Of the resident population 64% lived in the city and 36% lived in rural areas. Kunming counts 1.98 million immigrants from other provinces or from other cities in Yunnan. According to the United Nations, Kunming is an aging society because more than 10% of its population is older than 60 (Kanmei & Minqi, 2017). In the last two decades, Kunming had a fast economic development, which was in general supported by local and central governments (Li et al., 2013; Wu et al., 2014). For example, in the past years, the Yunnan provincial government made several urbanisation development plans to promote economic growth of the province (Gao et al., 2018). This economic growth, in combination with land reforms and housing commercialisation, has led to development of Kunming into a regional mega city (Qiyang et al., 2015).



Figure 1. Location of Kunming, situated in the Yunnan province in China (China highlights, 2018; Google Earth, 2018; modified).

The urbanisation in Kunming has caused a great loss of green space in the suburban areas and an increase of built up area in general. Spatial trend surface analysis showed that the annual urban expansion was 20.8% in 2000-2005, 7.1% in 2005-2010 and 0.7% in 2010-2015. The urban expansion in 2000-2005 mainly occurred around Kunming itself, while in 2010-2015, the greatest urbanisation was in the South of Kunming (Gao et al., 2018).

2.1.4 Drivers of urbanisation

General drivers in China

The main drivers of urbanisation vary for different regions. In China, the most important driver is the annual GDP growth per capita, which is responsible for almost half of the urban land expansion, whereas in India and Africa, the urban population growth has the most effect on urbanisation. However, much of the urban expansion is difficult to observe at global scale, such as international capital flows, informal economy, local land use policy and generalised transport costs (Seto et al., 2012). The speed and scale of China's urban growth has been driven by many important factors such as economic reforms in the late 1970s, within-country migration policies, increasing urban and/or rural income disparities, surplus agricultural labourers, and conversion of farmland for urban use (Yeh et al., 2011).

The most important driver in China is the economic growth. Since the beginning of the market reforms in 1978, the economy of China has switched from centrally-planned to market-based, which has caused a rapid economic and social development in China (Chow, 2004). Together with the global financial crisis of 2008, China has become the largest contributor to the economic growth worldwide (Haacke, 2015). Nevertheless, because of China's lower capita income (in comparison with advanced countries), China is still a developing country with incomplete market reforms.

The rapid economic growth in China has brought many challenges, such as inequality, challenges in environmental sustainability, external imbalances and demographic pressures due to the ageing population and the internal migration (Haacke, 2015).

Besides the economic growth, the migration in China also affects urbanisation. The growth of the urban population in China is mostly due to rural-to-urban migration and not so much due to in-situ urbanisation of rural areas and natural population growth. Between 2010 and 2020, more than 150 million Chinese farmers will move to cities (Gong et al., 2012). To accommodate all the migrants and the natural population growth in cities, the urban area needs to increase quickly (Figure 2). This causes the conversion of large areas of farmland to urban land (in-situ urbanisation; Gong et al., 2012).

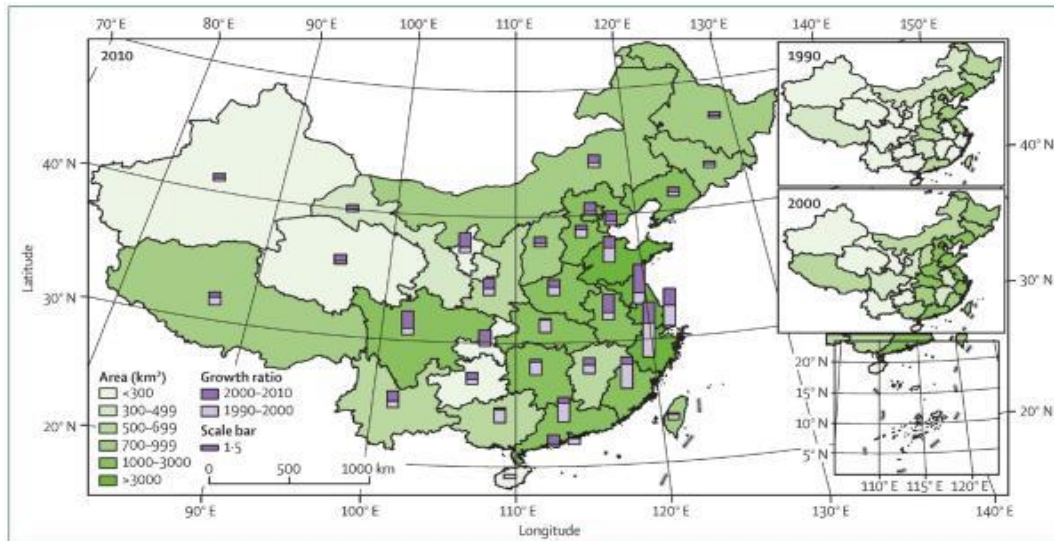


Figure 2. China's urban area expansion from 1990 to 2010 (Gong et al., 2012).

Additional drivers in Kunming

In addition to the general drivers of urbanisation in China, Kunming is led by urbanisation plans and social-economic, topographic and proximity factors.

Between 1999 and 2010, the urbanisation was speeded up due to two factors. The first one is the World Horticultural Expo in 1999, which improved the urban infrastructure, road, tree and air projects because of its successful organising. As a result, the planning and construction of main road networks were completed 10 years earlier than expected and the image of Kunming was improved. It also stimulated the attraction of foreign investment, modifications to the industrial structure and the rapid development of the tourism-centred tertiary industry. Kunming is now a preferred tourism site in China and migration destination (Qiyang et al., 2015). The second important factor is the new planning framework that was approved in 2003 and will shape the urbanisation between 2008 and 2030. This framework had an important influence on the increasing urbanisation level, and has helped the increase in built-up area from 185 km² in 2003 to 275 km² in 2010 (National Bureau of Statistics of China, 2004). In addition, the new framework promotes the agglomeration of Kunming with neighbouring cities (e.g. Yuxi, Qujing and Chuxiong). This is the so called Kunming centred Dianzhong urban agglomeration that started on 2009 and will end in 2030 (Su et al., 2011). Urban agglomeration is the result of the integration and interaction of regional central cities with their surrounding cities and leads to changes in spatial organisation (Gottmann, 1957; Kipnis, 1997; Haggett et al., 1977). It merges independent cities and it is the sum of all their interurban relationships (Baigent, 2004; Chen, 2017; Fang & Yu, 2017; Gottmann, 1957). An important agglomeration is the Kunming-Yuxi integration. In 2011, the Yunnan Provincial government made an agreement for the integration of Kunming and

Yuxi, which was an agreement of five years. Since then, the government stimulates the urbanisation between the two big cities and tries to accelerate the economic development of Yunnan. This urbanisation has caused a dramatical decline in agricultural land and forest between 2005 and 2015, while shrub and grass land has increased (Figure 3). In addition, the gap between the southern part of Kunming and the North of Yuxi is almost completely filled up by urban areas between 2010 and 2015 (Figure 4 ; Gao et al., 2018).

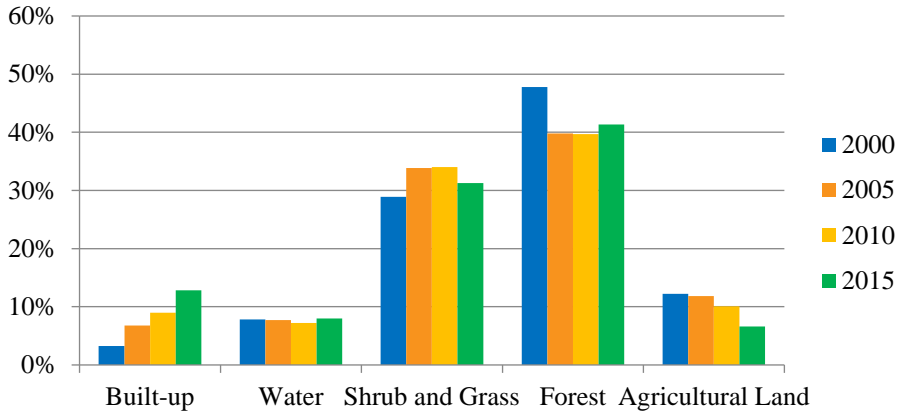


Figure 3. The proportions of each landcover class from 2000 to 2015 in Kunming (Gao et al., 2018).

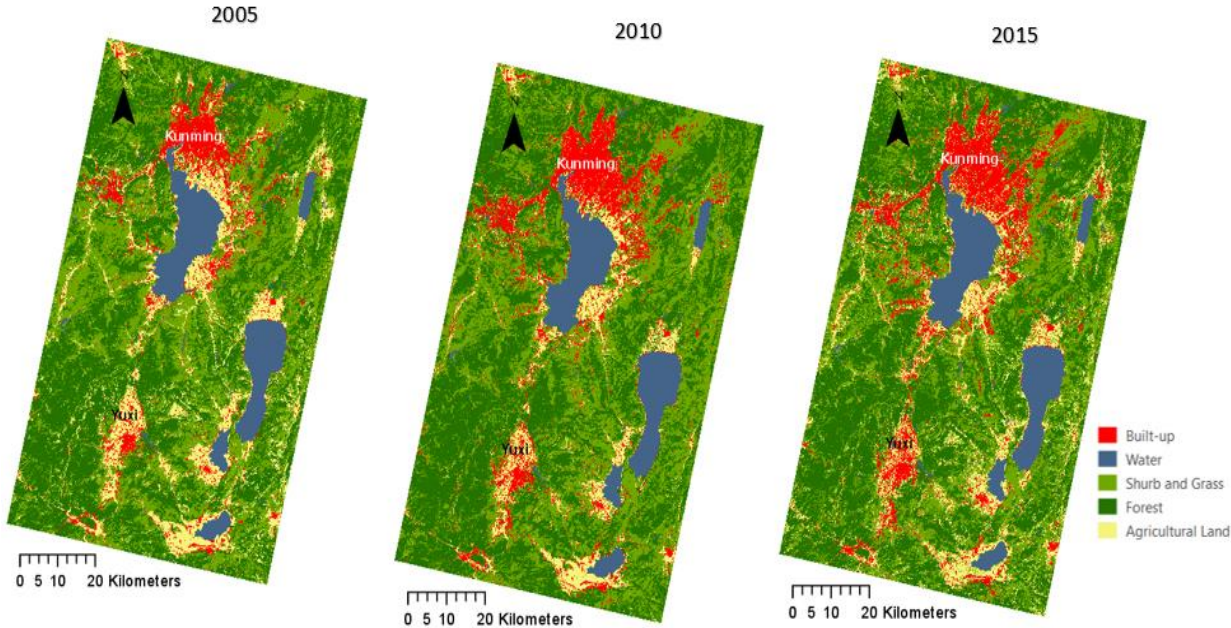


Figure 4. The development of the urbanisation of Kunming since 2005 (Gao et al., 2018; modified).

With the knowledge of the current urbanisation patterns, it is expected by 2025 to have a better connection between Kunming and Yuxi and the two cities would experience a further expansion (Gao

et al., 2018). A prediction for 2025 and the comparison of this prediction with 2015 can be seen on Figure 5.

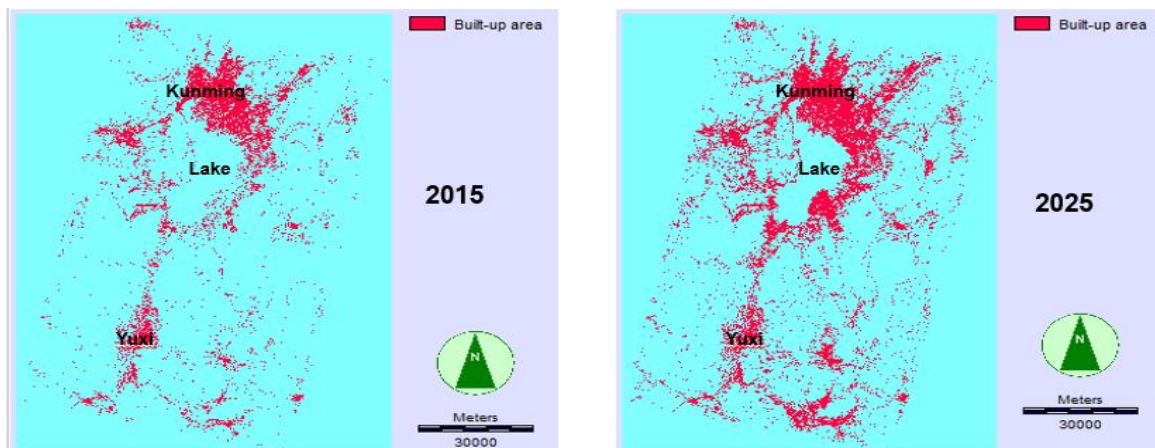


Figure 5. Prediction of built-up areas in 2025 and the comparison with the built-up areas in 2015 (Gao et al., 2018).

In the new planning framework, the North District will be a core city area and the centre of banking, commerce and trade, tourism and service. The East District will contain new industry, scientific, cultural and educational zones and a modern centre of urban logistics. The South District will form a new model of tourism and holiday town, with clustering development. The West District will become an industrial place of phosphorus chemical industry, electronic devices, mechanic manufacturing and tourism and service (Qiyang et al., 2015). By 2030, this new planning framework will transform Kunming into a regional centre and a land hub that connects China with Southeast Asian countries.

Besides the political factors, the topographic factors are also one of the main drivers of urbanisation. For example, the agreement of Kunming-Yuxi integration in 2011 is greatly affected by the topography of the landscape and the morphology of the Dianchi Lake. Before 2010, the urbanisation mostly occurred in the flat agricultural areas with a concentric growth pattern. Flat areas or areas with a slope less than 15° are preferred for urban expansion and more than 90% of the urbanisation is situated in these regions. Since 2010, Kunming mostly expanded to the South and is shaped by the topographic pattern (Figure 4). Most of the urban expansion is located around the lake, since this is a more attractive place to live (Gao et al., 2018).

2.1.5 Consequences of urbanisation

Environmental and health issues related to urbanisation

China

Since the 1970s, economic growth in China has induced rapid industrialisation and high pollutant emissions, which cause dramatic environmental degradation, including water and air pollution. The strong need for energy and raw materials is putting a big pressure on the environment and results in health problems for people (Chan & Yao, 2008; Huang et al., 2014; Mao et al., 2014; Qu et al., 2010; Yang et al., 2011). Eventually, due to the rising costs of environmental degradation, Chinese leaders gradually changed their conventional view of realising economic growth at the expense of environment (Wang et al., 2012).

In the last years, there have been frequent severe air pollution episodes in China causing huge health issues and social losses (Li, 2016). High emissions, from coal burning and industry processes, are a

primary cause for the increasing pollutant concentrations (Petäjä et al., 2016). In addition, vehicle emissions are an increasing concern, especially in megacities (Yang et al., 2013). China has the highest lung cancer burden of the world (Guo et al., 2016) and it is estimated that the amount of premature deaths due to the poor air quality is 1.27 million a year (Yang et al., 2013). Since 2016, after the environmental figures of China were published, the environment is a key factor in the local governments performance evaluation and national-controlled monitoring sections for the air quality has been introduced

Due to pollutant discharges in water bodies, eutrophication is high. Organic and toxic pollution is widespread trough China, together with severe ecological devastation (Miao et al., 2012). The increasing health concern and environmental awareness has led to stricter regulation, so various industries are challenged to change their wastewater treatment technologies (Teh et al., 2016). By 2020, the numbers of severely polluted water bodies and groundwater overdraft should be reduced, the pollution of the groundwater should be preliminarily controlled and the quality of the aquatic ecosystems in the Beijing-Tianjin-Hebei region and the drinking water should be improved (The state council, 2016). Also by 2030, the quality of the ecological environment should be improved and by the middle of the 21st century the ecological environment should be fully recovered and the ecosystem should have a virtuous cycle (Teh et al., 2016).

Kunming

Kunming has one of the best air qualities of the Chinese big cities, but the airborne pollution is getting worse (Sally, 2013). Reliable data about the air pollution is however not easy to find. Daily smog readings published by the Kunming Environmental Protection Bureau (KEPB) are mostly half those reported by independent sources. According to the head of KEBP, the contradictions between the bureau and the national reporting agencies are due to differences in sample durations and calculations. The constant construction and the daily addition of hundreds of new cars play an important role in Kunming's air quality (Sally, 2013).

Problems with the water quality of the Dianchi lake began when the city grew and farmers started using big amounts of industrial fertilisers to grow more crops (Yang et al., 2010). The situation was aggravated by the continuous discharge of Kunming's untreated sewage directly into the lake. By the late 1980s, a film of algae began to spread across the lake, eventually growing so large and pervasive that by the early 2000s, almost the entire surface was green and fetid. In addition, natural cleansing buffers, such as shoreline wetlands, withered and died (Huang et al., 2013). Efforts to restore lake water quality were postponed for a long time. The local government began a series of costly and unsuccessful attempts to rebalance the lake's oxygen levels and to get rid of algae. The projects included wetland restoration, planting hundreds of tons of invasive water hyacinths, banning all new construction near the lakeshore and injecting ozone directly into the lake. Still, water quality stayed low. Much of the water that leaves the Dianchi lake will eventually flow into the Jinsha river. If the leaving water is not treated well, pollution will enter again into the source of China's largest river (Yangtze), which could cause a far-reaching impact on the Jinsha and upper reaches of the Yangtze (Sally, 2016).

The amount of green parks is scarce in Kunming, but since March 2017, plans for building 37 new parks are included in the thirteenth five-year plan. There would be an effort to turn the 'Spring City' into a 'Garden City'. The goal is to make 45% of Kunming's total land area green space by 2020. It is estimated

that probably they will not succeed to reach the 45% due to the continuous building of urban areas that occupy large amounts of land. For 16 of the 37 new parks there would only be a restoration and protection of already forested areas. The other 21 public areas will be completely new (Scally, 2017).

Land use/cover changes

Urbanisation causes the city to expand in area and causes land use changes, which lead to an increasing average temperature (Kim, 1992). For example, the expansion of the impervious surface area changes the heat capacity and radiative properties of the land surface, which can lead to a reduction of evapotranspiration in urban areas (Streutker, 2002). Each land cover type has unique thermal, moisture and optical spectral properties, so changes in land use/cover will result in a different local thermal environment (Oke, 1982). LUCC can range from the modification of the landscape character without affecting the overall classification to the complete replacement of one land cover type. Land cover modification can be anthropogenic, as deforestation, or naturally caused, as flooding. In both cases, the replaced spatial entities can fall into a different land cover category (Mölders, 2012).

The outward expansion of cities is responsible for the decreasing area of agricultural land and forests. This urban sprawl is accompanied by many temperature rising factors, which change the urban heat budget. Examples of these factors are concretisation, industrial growth, traffic congestion, air pollution and emission of volatile organic compounds (Lo & Quattrochi, 2003; Roy, 2011; Singh et al., 2014; Yang & Lo, 2002). For this reason, land cover changes play a big role in the increasing urban heat island (UHI), which is characterised by higher temperatures in urban areas compare to its surrounding temperatures (EPA, 2008; Solecki et al., 2005).

Urban Heat Island

Definition

Urban heat islands have already been a concern for over 40 years. It changes the processes of energy and water balance and influences the dynamics of air movements (Oke, 1987). As mentioned above, an urban heat island is an urban or metropolitan area characterised by significantly warmer air temperatures in the urban areas compared to the temperatures in the surrounding rural areas. The difference in temperature is larger at night than during the day, when winds are weak and when sky is cloud free (EPA, 2008; Solecki et al., 2005). The main contributors to the UHI-effect are the LUCC (EPA, 2008; Solecki et al., 2005) and the waste heat that is generated by energy usage (Li et al., 2013).

The UHI can be divided in two types. The first is the atmospheric UHI, that consists of canopy Layer UHI and Boundary Layer UHI. This type can be calculated from weather station networks (Chow & Roth, 2006; Fast et al., 2005; Karl & Quayle, 1988; Peterson, 2003). The second one is the surface UHI (sUHI) that is estimated by using thermal infrared remote sensing techniques (Imhoff et al., 2010; Jin et al., 2005; Peng et al., 2012; Voogt & Oke, 2003). sUHIs are largest at day, while atmospheric UHIs are largest at night (Lo & Quattrochi, 2003). Due to easy access of satellite images, the sUHI has been getting more interests in studies in areas where air temperature is difficult to obtain (Clinton & Gong, 2013; Imhoff et al., 2010; Jin et al., 2005; Peng et al., 2012; Tran et al., 2006; Zhang et al., 2010).

Drivers of an UHI

An UHI emergences due to the additional input of heat in urban areas in the form of power automobiles, air-conditioners and other sources of anthropogenic heat, in combination with the ability of the urban structures to keep the heat inside the city. The exchange of heat is influenced by

conduction, convection and radiation and arises due to the mutual response of multiple factors that can be divided in two categories, controllable and uncontrollable factors (Chen et al., 2006). These factors can be further categorized as temporary effect variables, such as air speed and cloud cover, permanent effect variables, such as green areas, building material and sky view factor, and cyclic effect variables, such as solar radiation and anthropogenic heat sources (Figure 6, Chen et al., 2006). In general, surfaces consisting of building, asphalt, bare-soil and short grasses are urban surfaces that heat up rapidly and contribute to the UHI-effect (Taha, 1997).

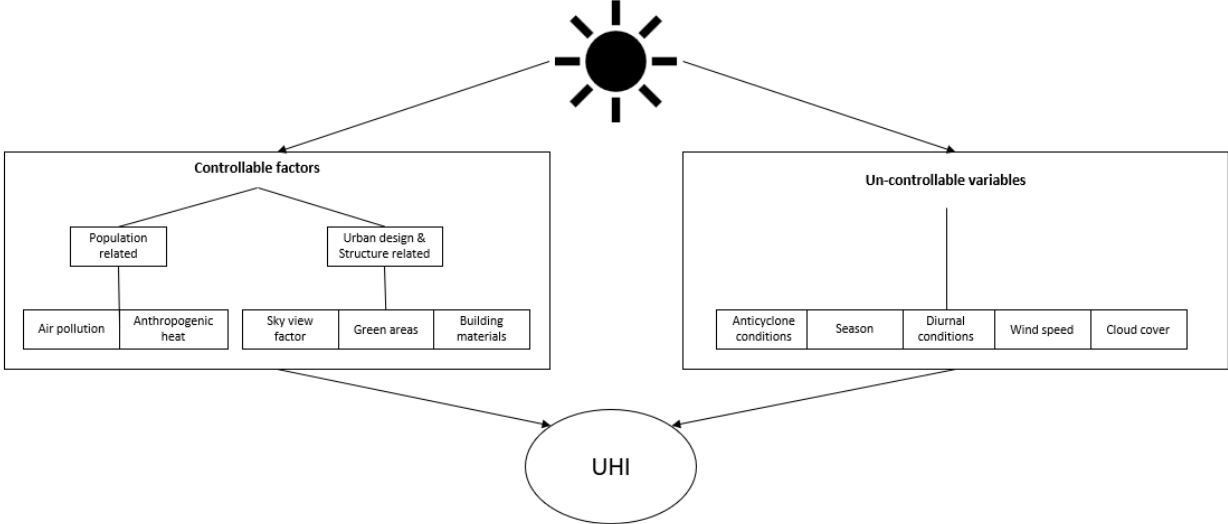


Figure 6. Overview Urban Heat Island mechanism (Chen et al., 2006; modified).

In urban areas, the ground level consists of specific structures such as walls, roof facets, irrigated gardens, non-irrigated spaces, lawns and paved areas. These structures capture and absorb solar radiation and store it as heat energy. The process goes on from sunrise until late afternoon. After the sun sets, the environment starts to cool down and the stored heat energy is released to the environment. The amount of heat that is released by the urban structures depends on controllable factors like sky view factor and the materials of the building. Due to the city building and thus the low sky view factor, the release of longwave radiation to the atmosphere is low. This has as consequence that a lot of heat is stored in building structures (Chen et al., 2006). In addition, one of the main causes of high air temperatures in cities is due to the typical street canyon configuration that causes a low albedo effect (Chen et al., 2006).

Other factors that causes heat storage are the lack of vegetation, the high roughness of the urban structures and air pollution. Due to the lack of vegetation, there is almost no latent heat flux and the high roughness is responsible for a reduction of convective heat removal and transfer by wind (Taha, 1997). The aerosols in air polluted areas absorb and re-radiate longwave radiation and can inhibit the corresponding radiative surface cooling. This causes a pseudo-greenhouse effect that strengthens the UHI (Phelan et al., 2015). As for the uncontrollable factors, the Urban Heat Island Intensity (UHII) can be increased by anticyclone conditions (Chen et al., 2006). These are large-scale wind circulations around a central region of high atmospheric pressure that goes clockwise in the Northern Hemisphere and counter clockwise in the Southern Hemisphere (Hakim et al., 2002). Furthermore a negative correlation can be found between the wind speed and the cloud cover, and the UHI (Kim & Baik, 2002; Oke, 1982; Pongracz et al., 2006). Concerning the effect of the population, there is a positive correlation between a higher city population and the UHI-effect (Tran et al., 2006). This effect can be direct as well as indirect. The direct effect is due to more metabolisms and thus human heat production and the indirect effect is due to the higher amount of buildings, vehicles and factories. However a

higher population does not necessarily mean a higher heat storage since variables such as sky view factor, anthropogenic heat, building design and albedo play a more important role (Memon et al., 2008).

Consequences of an UHI

Urban heat islands have many adverse effects such as the deterioration of living environment, increasing energy consumption (Konopacki & Akbari, 2002), elevation in ground-level ozone (Rosenfeld et al., 1998) and an increase in mortality rates (Changnon et al., 1996). The higher temperature influences the regional climate, eco-environment, such as net primary production (Imhoff et al., 2010), biodiversity (Reid, 1998), water and air quality, (Grimm et al., 2008) and socio-economic development (Chen et al., 2006).

The higher temperatures in the city can lead to periods with extreme heat on warm summer days (Clarke, 1972; Rooney et al., 1998). During these hot-weather events, the UHIs strengthen the thermal stress on vulnerable and at-risk people (Kovats & Hajat, 2008; Smargiassi et al., 2009). Because of this, it is important to know the hotspots within the city or the surface intra-UHI (SIUHI), so certain problems due to this extreme heat can be avoided (Martin et al., 2015).

2.2 Local Climate Zone (LCZ)-mapping

2.2.1 Background

The impact of urbanisation on the local environment has been studied for almost 185 years and is influenced by city form and function. For example, the controllable factors from the UHI mechanism, such as the sky view factor and other morphological parameters, have an important influence on the thermal behaviour of a city. Because of this, the city can be divided into thermal zones based on its morphological characteristics, which gives an idea of the intensity of the UHI (Stewart & Oke, 2006). These thermal zones, i.e. Local Climate Zones (LCZs), are very useful to evaluate the combined effect of land use change and fast urban growth. LCZs can be described as areas with uniform surface coverage, material, structure and human activity that covers hundreds of meters to several kilometres on a horizontal scale. The zones are determined by physical and functional information of the area, including the urban structure, urban coverage, urban fabric and urban metabolism. Each zone features a typical screen-height temperature that is most clearly seen on dry surfaces, on quiet, clear nights and on simple relief (Stewart & Oke, 2012).

The LCZ scheme (Figure 7) was initially introduced for the classification of urban and rural field sites for observational studies about UHI and was intended to facilitate objective measurements of UHI intensity worldwide (i.e. to measure the difference in temperature between two LCZ types; Bechtel et al., 2015; Stewart et al., 2015). But since the labelling of landscapes into urban or rural areas causes a high variability (Stewart, 2011), the LCZ scheme can help to obtain standardised measurements of the UHI (Bechtel et al., 2015). Furthermore, LCZs contain physical and functional information, which makes the LCZ scheme useful to discretise the landscape and is therefore suitable for mapping purposes. It can contribute to the World Urban Database and Access Portal Tools (WUDAPT; Bechtel et al., 2015). WUDAPT was conceived to gather and spread data on the physical geographies of cities worldwide by using the Local Climate Zone scheme in order to overcome the shortcoming of useful information about the form and function of cities at a detailed spatial resolution (Bechtel et al., 2015; Stewart et al., 2015). This data is necessary in global urban climate science to simulate urban

trajectories, so mitigation and adaption policies could be supported. The necessity of information about the urban landscapes is recognised in the Intergovernmental Panel on Climate Change (IPCC) assessment reports on both adaptation and mitigation (Pachauri et al., 2014). At present, most of the available global data consist only of the urban mask, which just shows the boundaries that separate the urban from the ‘natural’ landscape (Esch et al., 2013).








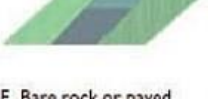

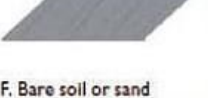
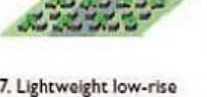

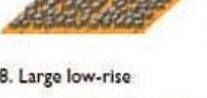



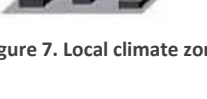
Built types	Definition	Land cover types	Definition
1. Compact high-rise 	Dense mix of tall buildings to tens of stories. Few or no trees. Land cover mostly paved. Concrete, steel, stone, and glass construction materials.	A. Dense trees 	Heavily wooded landscape of deciduous and/or evergreen trees. Land cover mostly pervious (low plants). Zone function is natural forest, tree cultivation, or urban park.
2. Compact midrise 	Dense mix of midrise buildings (3–9 stories). Few or no trees. Land cover mostly paved. Stone, brick, tile, and concrete construction materials.	B. Scattered trees 	Lightly wooded landscape of deciduous and/or evergreen trees. Land cover mostly pervious (low plants). Zone function is natural forest, tree cultivation, or urban park.
3. Compact low-rise 	Dense mix of low-rise buildings (1–3 stories). Few or no trees. Land cover mostly paved. Stone, brick, tile, and concrete construction materials.	C. Bush, scrub 	Open arrangement of bushes, shrubs, and short, woody trees. Land cover mostly pervious (bare soil or sand). Zone function is natural scrubland or agriculture.
4. Open high-rise 	Open arrangement of tall buildings to tens of stories. Abundance of pervious land cover (low plants, scattered trees). Concrete, steel, stone, and glass construction materials.	D. Low plants 	Featureless landscape of grass or herbaceous plants/crops. Few or no trees. Zone function is natural grassland, agriculture, or urban park.
5. Open midrise 	Open arrangement of midrise buildings (3–9 stories). Abundance of pervious land cover (low plants, scattered trees). Concrete, steel, stone, and glass construction materials.	E. Bare rock or paved 	Featureless landscape of rock or paved cover. Few or no trees or plants. Zone function is natural desert (rock) or urban transportation.
6. Open low-rise 	Open arrangement of low-rise buildings (1–3 stories). Abundance of pervious land cover (low plants, scattered trees). Wood, brick, stone, tile, and concrete construction materials.	F. Bare soil or sand 	Featureless landscape of soil or sand cover. Few or no trees or plants. Zone function is natural desert or agriculture.
7. Lightweight low-rise 	Dense mix of single-story buildings. Few or no trees. Land cover mostly hard-packed. Lightweight construction materials (e.g., wood, thatch, corrugated metal).	G. Water 	Large, open water bodies such as seas and lakes, or small bodies such as rivers, reservoirs, and lagoons.
8. Large low-rise 	Open arrangement of large low-rise buildings (1–3 stories). Few or no trees. Land cover mostly paved. Steel, concrete, metal, and stone construction materials.	VARIABLE LAND COVER PROPERTIES	
9. Sparsely built 	Sparse arrangement of small or medium-sized buildings in a natural setting. Abundance of pervious land cover (low plants, scattered trees).	b. bare trees	Leafless deciduous trees (e.g., winter). Increased sky view factor. Reduced albedo.
10. Heavy industry 	Low-rise and midrise industrial structures (towers, tanks, stacks). Few or no trees. Land cover mostly paved or hard-packed. Metal, steel, and concrete construction materials.	s. snow cover	Snow cover >10 cm in depth. Low admittance. High albedo.
		d. dry ground	Parched soil. Low admittance. Large Bowen ratio. Increased albedo.
		w. wet ground	Waterlogged soil. High admittance. Small Bowen ratio. Reduced albedo.

Figure 7. Local climate zone scheme (Steward & Oke, 2012).

2.2.2 WUDAPT Protocol

Since the spectral features of the LCZ are not the same for different parts of the world, a semi-automated method has to be used for mapping. A common used and promising approach is based on multi-temporal multi spectral and thermal remote sensing data and modern machine learning methods. For this, an universal, objective and simple LCZ mapping method was introduced, which is based on free data and free software (Bechtel et al., 2015), in order to conduct and validate LCZ classifications by local experts of their cities. This method was developed by WUDAPT in order to fill the gap between urban development and local climate conditions (Cai et al., 2017). It is designed to be an universal, simple and objective way to gather data about the form and function of cities (Bechtel et al., 2015).

The method uses free satellite images from USGS Earth Explorer and free software including SAGA-GIS and Google Earth (See et al., 2015). The data gathering can be categorised into different levels that each represent a certain level of detail. An overview of these levels is shown on Figure 8.



Figure 8. WUDAPT's different levels of data gathering (Bechtel et al., 2015).

The level 0 method can be used to give global and culturally neutral information about the urban morphology and is based on the Local Climate Zone scheme (Stewart & Oke, 2012; Kaloustian & Bechtel, 2016). The protocol for the collection of level 0 data consists of six steps (Bechtel et al., 2015):

- (1) Demark the city.
- (2) Training areas of the respective LCZs are digitised using Google Earth and are subsequently imported into SAGA software.
- (3) Satellite images for the urban domain are downloaded and imported into SAGA software. The satellite images consist of multiple spectral bands at a 30 m resolution, which can be used to distinguish the surface covers. More explanation can be found in section 2.2.3.
- (4) The LCZ map is made by using the random forest classifier in SAGA where the training areas are necessary to classify the study area into local climate zones. More explanation can be found in section 2.2.4.

- (5) The resulting map is evaluated based on visual interpretation and is compared to Google Earth, whereby the LCZ training areas are added or modified, in order to reduce the amount of misclassifications.
- (6) Step (4) and (5) is repeated until the executor is satisfied about the map, based on its visual interpretation.

Despite the benefits that this method has to offer, there are some disadvantages. Firstly, this method is a time consuming process due to the image pre-processing steps and the selection of training samples. Moreover, it only applies on city level and not on a global level. Because of this, it will take a long time before all the cities are classified (Cai et al., 2017).

Secondly, the conventional method only uses freely available Landsat images. This causes a lower accuracy compared to the use of Advanced Spaceborne Thermal Emission and Reflection radiometer (ASTER) satellite data (Xu et al., 2017).

Thirdly, the conventional method can cause problems with the horizontal heterogeneity or the mixture of different LCZs on small surfaces. In the original method, the spectral Landsat data is classified on a per-pixel basis, but these individual pixels do not include the horizontal heterogeneity of the urban landscape of cities areas (Verdonck et al., 2017). This causes problems in cities where no systematic planning is present and in fast growing cities located in less developed regions (Seto et al., 2012). These cities contain most of the time a high mixture of functions and structures at small horizontal scales (Verdonck et al., 2017).

Finally, in the conventional method, no accuracy assessment is available. The maps are only compared with Google Earth, and the quality of the LCZ maps is consequently not ensured (Verdonck et al., 2017). The Human Influence Experiment (HUMINEX) from Bechtel et al., 2017 investigated the quality of 94 crowdsourced training datasets for ten cities, which were generated by 119 students and concluded that most of the resulting LCZ maps were of poor to moderate quality. In general, this is due to difficulties in the interpretation of the (urban) landscape and due to a lack of knowledge of the LCZ scheme. They also concluded that the quality of the LCZ maps could improve up to 20 % in overall accuracy when multiple training datasets are used to create a single LCZ map.

2.2.3 Data: Landsat

In General

In July 1972, the Earth resources technology satellite was launched and has eventually been renamed to Landsat (Short, 2011). Landsat has currently launched eight satellites and has provided satellite images of the Earth since 1972. The images are archived in the United States and in Landsat receiving stations around the world. The images are used in multiple disciplines, for example in geology, cartography and forestry. Each Landsat image can be accessed through the U.S. Geological Survey (USGS) 'EarthExplorer' website (Wulder et al., 2011).

Landsat 7

The seventh satellite of the Landsat program was launched on April 15 in 1999 and was built by Lockheed Martin Space Systems Company. The main purpose of this satellite was to refresh the global archive of satellite photos, in order to provide cloud free and up-to-date images. The satellite goes in a polar, sun-synchronous orbit, so it can scan the entire earth surface and has an altitude of 705 km at the equator (Lillesand et al., 2015). Landsat 7 is capable to collect and transmit 532 images per day. These images contain eight spectral bands, 1-7 plus a panchromatic band, with a spatial resolution

between 15 and 60 m and with a temporal resolution of 16 days or 232 orbits (Chander et al., 2005). Unlike the previous Landsat satellites, Landsat 7 makes use of the Enhanced Thematic Mapper Plus (ETM+). This ETM+ instrument has a Scan Line Corrector (SCL), that compensates the forward motion (along track) of the sensor, in order to have scans that are aligned parallel to each other (Storey et al., 2005)

Scan line error

In May 2003, the Scan Line Corrector (SLC) in the ETM+ instrument failed, which gave errors in the image. When there is no working SCL present, the ETM+ line of sight gives a zig-zag pattern along the satellite ground track, see Figure 9.

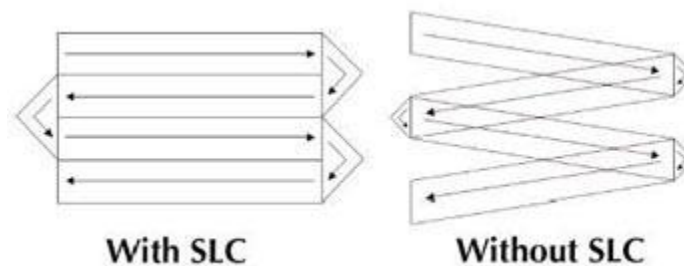


Figure 9. Differences between a working and non-working SLC (USGS)

This gives images where some areas are missing and others are imaged twice, which results in a total loss of 22 % of the data. The gaps along the edge of the images have a maximum width that is equivalent to one full scan line (390 to 450 m) and the precise location varies from scene to scene (Katzschner et al., 2015). The raw images still have a high geometric and radiometric fidelity, but the information is missing for the wedges varying in size from one 30 m pixel near the centre of the image to fourteen 30 m pixels along the eastern and western edges of the image (Storey et al., 2005). There have been efforts to repair the SCL, but without success. It has been concluded by the Anomaly Response Team (ART) that the SCL problem was mechanical and permanent (Katzschner et al., 2015). Due to the SCL failure, the use of the SLC-off is confined, which limits the applicability of the system since it is impossible to produce images for the entire swath (Hossain et al., 2015)

To minimise the effects of the SCL-failure, several approaches have been developed to improve the utility of the 'SLC-off' images. Examples are image segmentation (Maxwell et al., 2007) and multi-date (same season) image compositing (Gutman, 2008). The image segmentation is more designated for certain land cover applications (Bédard et al., 2008), while the multi-date approach is used for the NASA/USGS Global Land Survey product suite (Gutman et al., 2008). Another approach to fill the gaps is based on interpolating from neighbouring scan lines or using pixel values extracted from one or more images of the same area that has been taken before the SCL-failure (Lillesand et al., 2015). To fill the scan gap, precise knowledge is required about what pixels are valid in an image and which need to be filled. For this, a scan gap mask can be created for each band in order to mark the existing data as 1 and the missing data in the scan gap as 0. After locating the gaps, a linear histogram matching methodology attempts to find a linear transformation between one image and another. When the transformation is applied on the entire scene, a global linear histogram match is made. The pixel values

of the SLC-Off image can be generated by applying a corrective gain and bias to the pixel values of an SLC-On image, using the mean and standard deviation of the data (Potić, 2015).

However, this global histogram match is not always optimal. In scenes with transient object such as clouds, visible errors can be created. To minimise this, high saturated pixels are excluded before the corrective gain and bias are calculated. But in general, when a better precision and product is required, corrective gains and biases should better be calculated in a moving window around each pixel in the scene (Scaramuzza et al., 2004).

Landsat 8

In February 2013, Landsat 8 joined Landsat 7 and has as main purpose to extend the collection of Landsat data on an operational basis into the future. The satellite was launched into a repetitive, near-circular, sun-synchronous, near polar orbit. This orbit has a nominal altitude of 705 km at the equator and has an inclination angle of 98.2°. The satellite can do 14.5 orbits a day and the time interval between the adjacent coverage tracks of the satellite is seven days. The images have an East-West width of 185 km and a North-South width of 180 km. The images are archived in the Worldwide Reference System-2 (WRS-2), according to their location (Lillesand et al., 2015).

The mission of Landsat 8 has multiple objectives, including:

- (1) to collect and archive moderate resolution (30 m GSD) reflective, multispectral image data permitting seasonal coverage of the Earth for less than five years;
- (2) to collect and archive moderate to low resolution (120 m) thermal multispectral image data, permitting seasonal coverage of the Earth in a period less than three years;
- (3) to ensure that the resulting data is sufficiently consistent with the data from the previous Landsat data, so land cover and land use changes can be seen and
- (4) to make standard data products available for general public (Lillesand et al., 2015).

Landsat 8 has two sensors, the Operational Land Imager (OLI) and the Thermal Infrared Sensor (TIRS). These sensors give 12-bit data, that is processed to produce a 'Level 1T' GeoTIFF that is corrected to the terrain. This GeoTiff image product is radiometrically corrected and the non-polar scenes are co-registered to an UTM cartographic projection, while the polar scenes are co-registered to Polar Stereographic projection (Lillesand et al., 2015).

2.2.4 Classification algorithm: random forest classifier

The Random Forest Classifier (RFC), used to classify the Landsat images, is a statistical ensemble algorithm created by Leo Breiman and consists of multiple tree-structured classifiers, see Figure 10. The main principle of an ensemble approach is that a group of 'weak learners' can come together to form a 'strong learner'. In the RFC, the trees are weak learners and the random forest is the strong learner. Each decision tree considers a random subset of features from the full training set and makes a prediction for the outcome (LCZ), based on its available data. The decision tree consists of three kinds of nodes, the root node, internal nodes and the leaf nodes. The root and internal nodes are a set of features that describes the data, while the leaf nodes denote an output or LCZ. In case of LCZ mapping the feature sets include spectral information about each LCZ, determined based on the training (sub)set. The final prediction is ultimately made by taking the majority vote for the predicted class from all the decision trees (Breiman, 1999; Malekipirbazari & Aksakalli, 2015).

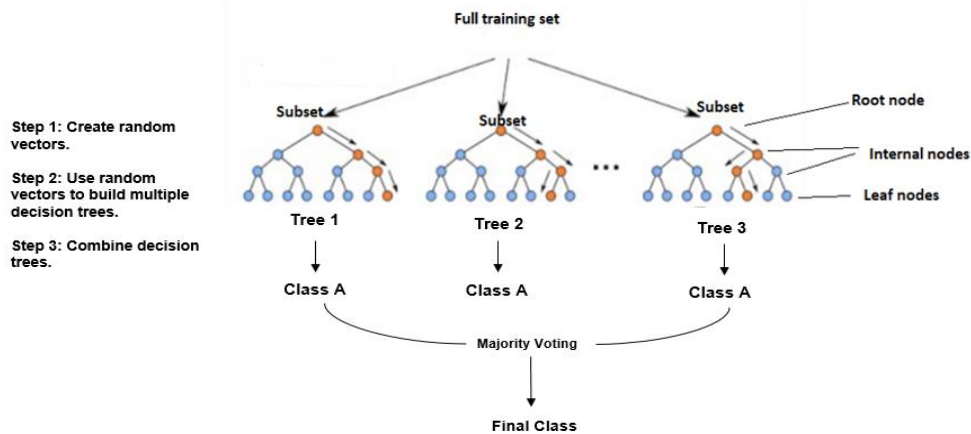


Figure 10. Simplified Random Forest (Malekipirbazari & Aksakalli, 2015; modified)

Advantages of the RFC are fast runtimes and the ability to deal with unbalanced and missing data. The RFC makes use of randomly chosen trees, which increases the diversity in the forest and leads to more robust overall predictions. The classifier gives a good classification performance and computing efficiency and is capable to handle large data- and feature sets. Furthermore, the classifier can be used for unsupervised learning and can detect outliers by using proximity analysis.

Weaknesses of the RFC include the absence of the potential, when used for regression, to predict beyond the range in the training data and the fact that the classifier could over-fit data sets that are quite noisy (Malekipirbazari & Aksakalli, 2015; Mingers, 1989; Pal & Mather, 2003).

2.3 Land Surface Temperature

2.3.1 Definition

The Land Surface Temperature (LST) is the radiative skin temperature of the land that is derived from solar radiation (ESA, 2017) and is not the same as air temperature. It is a key parameter of the Earth surface energy budget and is used in applications of hydrology, meteorology and climatology. It is an important indicator of the greenhouse effect and of the energy flux between the atmosphere and the land surface (Li et al., 2013). The LST is furthermore useful to study urbanisation. It is an indicator for the direction and degree of urbanisation due to the higher LST in built-up areas and lower LST in vegetation and water bodies (Linh & Van Chuong, 2015).

Like other geophysical parameters, LST is dynamic, both spatially and temporally, which makes the conventional measurement techniques complex and not practical. Because of this, the use of remote sensing satellites to estimate the LST is preferred, due to its synoptic and repeated coverage, which makes the estimation more easy (Rozenstein et al., 2014).

2.3.2 Relationship LCZ and LST

For analysing the temperature differences among LCZ classes, air temperature is the most suitable meteorological parameter. Since the amount of observational meteorological stations are in general limited, alternative temperature data is required to assess the effect of the urban morphology on local climate conditions (Geletič et al., 2016). Although the LCZ classification is based on measurements of the air temperature, LST was also found to be associated with LCZ classes. This is because satellite

images, especially acquired during night-time, have a strong relationship between the land surface and the adjacent air (Cai et al., 2017). In addition, surface temperature and land use/cover are positive related to each other due to land characteristics like albedo and moisture content of the different surface types (Lo & Quattrochi, 2003). Because of this correlation, (surface)UHIs can be identified based on the differences in surface temperature (Lo & Quattrochi, 2003; Oke, 1982).

Geletič et al. (2016) found that, among most of the LCZs the LST differ significantly. The LST from large low-rise buildings (LCZ8), heavy industry (LCZ 10) and LCZ D (low plants) are most distinguishable, while the LST from compact midrise (LCZ 2), open high-rise (LCZ 4) and sparsely built-up (LCZ 9) are less distinguishable. It is found that the LST of built-up LCZ classes are in general higher than the LCZ from natural land cover classes. Heavy industry (LCZ 10), compact mid-rise (LCZ 2) and compact low-rise buildings (LCZ 3) have the warmest LST, while water bodies (LCZ G) and dense forest (LCZ A) have the coldest LST (Geletič et al., 2016). To know whether the LCZs differ significantly, the LST of two European cities were statistically tested with ANOVA. Cai et al. (2017) found that at night the highest LST in the built-up areas are found in zones with compact high-rise (LCZ 1). While as for the natural land cover types, the highest LST was detected in areas covered with water (LCZ G), which is due to its high heat capacity. Vegetation zones (LCZ A-D) have the lowest LST among all classes. Nevertheless there are also inconsistencies in the LST variations, especially in sparsely built (LCZ 9), dense trees (LCZ A), scattered trees (LCZ B) and bush, scrub (LCZ C), due to its highly variable urban morphology and temporal variation in vegetation.

2.3.3 LST estimation

The estimation of LST from satellite data knows several difficulties, such as atmospheric correction, the quantity expression of thermal infra process, the difficult separation of temperature and emissivity, the seasonal and dynamic states of surfaces and the uncertainty of land classification (Li et al., 2013). For the estimation of the LST, multiple algorithms have been developed and can be grouped into different categories, whereas the most popular algorithms are the single channel and the split-window algorithm. In general the two algorithms differ more or less 3 K from each other, whereas the split-window algorithm is more correlated to the MODIS LST (Nikam et al., 2016). The single channel method is a commonly used approach to estimate LST based on thermal-infrared remote sensing image data (Jimenez-Munoz et al., 2009). The algorithm only requires one thermal-infrared channel and uses the same equation and coefficients for different sensors while the split-window algorithm requires simultaneous data from at least two sensor channels (Galve et al., 2008). In addition, it only requires atmospheric moisture content and land surface emissivity as parameters, making it widely applied in UHI studies. The two most used algorithms are described below.

(1) Single Channel

The single channel method or the mono-window algorithm (MWA) is a practical algorithm when in situ atmospheric radiosonde profiles are unavailable. Only a few parameters are required to generate LST with high accuracy (Li et al., 2013).

The estimation of the LST using this method requires information regarding the atmospheric parameters, such as down-welling path radiance, up-welling path radiance, atmospheric transmittance and surface emissivity for each band, along with the radiance observed by each band of TIRS. In the single channel method, the atmospheric upwelling and downward radiance are simplified, while the

other atmospheric parameters are usually estimated by solving atmospheric transmittance/radiance codes (Jimenez-Munoz et al., 2009).

The most important error source of this LST estimation is due to atmospheric effects, which can lead to an error between 0.2 K and 0.7 K on the LST, and an error between 0.2 K and 0.7 K on the surface emissivity uncertainty. Since typical uncertainties for remote sensing measurements can be assumed, a total error for the LST using the single channel method is estimated between 0.3 K and 0.8 K. Unless more accurate in situ values for emissivity and atmospheric parameters are available, an accuracy lower than this total error cannot be expected (Jiménez-Muñoz & Sobrino, 2006).

(2) Split-Window

The split-window algorithm was developed to improve the accuracy of the LST retrieved from remote sensing data (Sobrino et al., 1993). The majority of the LST products are obtained from various sensors by using this algorithm (Wan, 1996). This algorithm requires data from two spectrally adjacent thermal bands, typically located in the atmospheric window between 10 and 12 μm . The basic principle of the split window algorithm is that the radiance attenuation for the atmospheric absorption is proportional to the radiance difference of simultaneous measurements at two different wavelengths, which are each subjected to different quantities of atmospheric absorption (Sobrino et al., 2008). Despite the fact that this method is seen as the most widely used algorithm for LST estimation, there are still limitations regarding techniques for the estimation of land surface emissivity (LSE) and atmospheric water vapor content (Nikam et al., 2016).

2.3.4 Land Surface Emissivity (LSE)

The LSE is one of the most essential parameter for the estimation of LST, and can be estimated by using the single channel or the split-window method (Yu et al., 2014). Emissivity at a certain wavelength can be theoretically defined as the ratio of the radiance emitted by a body at temperature T to the radiance emitted by a black body at the same temperature. The emissivity of the land surface is dependent on the water content, surface roughness, vegetation condition and viewing angles (Salisbury & D'Aria, 1994). There are several techniques for the estimation of the LSE since the direct estimation of LSE from satellite measurements is complex. One of the techniques is the NDVI-based emissivity method (NBEM; Li et al., 2013), which estimates the LST based on the Normal Difference Vegetation Index (NDVI). This method is easy to use but has limitations for areas with low NDVI and can cause a deviation of -0.038 to 0.032 in these areas (Dash et al., 2005).

3. Material and methods

3.1 Study area

Kunming is the capital and largest city of Yunnan province and is located in southwest China, see Figure 1, page 4. In the last three decades, the city has known a large economic growth, due to its remote location, which resulted in a rapid urbanisation. Because of this, Kunming is an interesting area to study the fast urbanisation in China.

Kunming is located on a plateau with an elevation from 1500 m to 2800 m and is surrounded by mountain scenery in the North, East and West. The metropolitan area of Kunming is found in the Dianchi basin (Zhou & Wang, 2011). The city has a subtropical monsoon climate with humid and warmer summers and dry and colder winters. Kunming has a mean annual precipitation between 788 and 1000 mm and the rain is mostly falling in May to October. Because of the various landscapes, the amount of rainfall is dependent on the location. In general, mountainous regions will have more rainfall than flat regions. The annual average air temperature is between 15.4°C and 24.2°C, with a minimum of -3°C and a maximum of 32.2°C (Gao et al., 2018). The climate is one of the mildest of China due to its surrounding landscape (Zhou & Wang, 2011). The landscape causes a more or less all year round spring climate, this is why the city is also called the 'City of Eternal Spring'.

3.2 Data and methods

3.2.1 LCZ mapping

Landsat images

In relation to the second objective of this study, cloudless to almost cloudless Landsat images of the study area with a resolution of 30 m are downloaded from USGS for the different years. For the LCZ classification of 2017, 2011 and 2005, respectively four (Landsat 8 level 1), three and three (Landsat 7 level 1) images are selected. Within the specific year, images are chosen from different seasons, and thus with different climate characteristics. For Landsat 8, only the bands 1, 2, 3, 4, 5, 6, 7, 10 and 11 are used, and for the Landsat 7 images only the bands 1, 2, 3, 4, 5, 6 and 7. More information about the images can be found in Table 1.

Table 1. Landsat images information for the LCZ mapping.

Mapping period	Landsat Entity ID	Date
2005	LE07_L1TP_129043_20050406_20170116_01_T1	06/04/2005
	LE07_L1TP_129043_20050201_20170116_01_T1	01/02/2005
	LE07_L1TP_129043_20060103_20170111_01_T1	03/01/2006
2011	LE07_L1TP_129043_20110306_20161209_01_T1	6/03/2011
	LE07_L1TP_129043_20120120_20161203_01_T1	20/01/2012
	LE07_L1TP_129043_20111117_20161205_01_T1	17/11/2011
2017	LC08_L1TP_129043_20170109_20170311_01_T1	01/09/2017
	LC08_L1TP_129043_20170314_20170328_01_T1	14/03/2017
	LC08_L1TP_129043_20170501_20170515_01_T1	01/05/2017
	LC08_L1TP_129043_20170109_20170311_01_T1	09/01/2017

Due to the failure of the Scan Line Corrector from the Landsat 7 Enhanced Thematic Mapper (ETM) sensor, the satellite images need to be corrected before they can be used in the LCZ mapping or LST calculation. This problem can be solved by multiple methods. The method used in this research is based on the application of a linear transform to the 'filling' image in order to adjust it on the standard deviation and mean values of each band (Scaramuzza et al., 2004). This method will fill the gaps in one scene with data from another Landsat scene, using ENVI software and the 'landsat_gapfill.sav' plugin.

ROI and training areas

According to the WUDAPT method, the first step in the LCZ classification is to select the region of interest (ROI, Appendix 1) in Google Earth. Within this ROI, multiple training areas are selected for the different LCZs. The sampling of the training areas is based on making representative and correct areas for the different local climate zones, in order to minimise the amount of misclassifications. Examples of the different LCZs are presented in Table 2.

To select the training areas for the situation in 2017, a first impression of the city is made by walking and driving through the streets. After this first step, initial training areas are chosen based on both baidu maps top view and street view. Baidu maps is a mapping service application that offers satellite imagery, street maps, street view and indoor view perspectives of the entire world. These initial training areas are then checked in real life and are modified if necessary. This method was chosen because of its efficiency and because it gives a more accurate insight in the size and the composition of the different areas. The final training areas are visualised in Appendix 2. The training areas for 2005 and 2010 are collected using only the timeline of Google Earth pro and baidu maps. To do so, the training areas of 2017 are reviewed and used, changed or omitted, and clear and new training areas are added. These training areas are shown in Appendices 3 and 4.

In the sampling for 2017, almost no lightweight low-rise (LCZ 7), sparsely built (LCZ 9), bare rock or paved (LCZ E) and bare soil and sand (LCZ F) areas are found with an acceptable size. These LCZs were thus left out of the classification. For 2005 and 2010, some extra LCZs are left out of the classification due to the absence of (enough) representative areas. For 2011, compact high-rise (LCZ 1) is further not included and for 2005, compact high-rise (LCZ 1), open high-rise (LCZ 4) and heavy industry (LCZ 10) are not included in the classification.

Despite the attempt to have optimal training areas, there are some uncertainties. Leaving out bare soil and sand (LCZ F) causes the disadvantage of misclassification due to the construction sites that contain bare soil. In most of the training areas, spectral information of bare soil and sand (LCZ F) is present, so construction sites can be mapped as a combination of multiple LCZs.

Another difficulty lies in the usage of plastic foils that cover rose plantations. Because of the uncertainty of the spectral response of this foil, a new zone was added, which is called 'agriculture-greenhouse' (LCZ H). A last uncertainty is found in the sampling for 2010 and 2005, because the chosen training areas could not be checked in real life or with street view.

Table 2. Examples of the different LCZs in Kunming.



- LCZ 1 Compact high-rise
- LCZ 2 Compact mid-rise
- LCZ 3 Compact low-rise
- LCZ 4 Open high-rise
- LCZ 5 Open mid-rise
- LCZ 6 Open low-rise
- LCZ 8 Large low-rise
- LCZ 10 Heavy industry
- LCZ A Dense trees
- LCZ B Scattered trees
- LCZ C Bush, scrub
- LCZ D Low plants
- LCZ G Water
- LCZ H Agricultural greenhouse

Classification and its adaptations

For the LCZ classification, the WUDAPT-protocol, with certain adaptations (Verdonck et al., 2017), is followed. A general overview of both the conventional and the modified method can be seen in Figure 11.

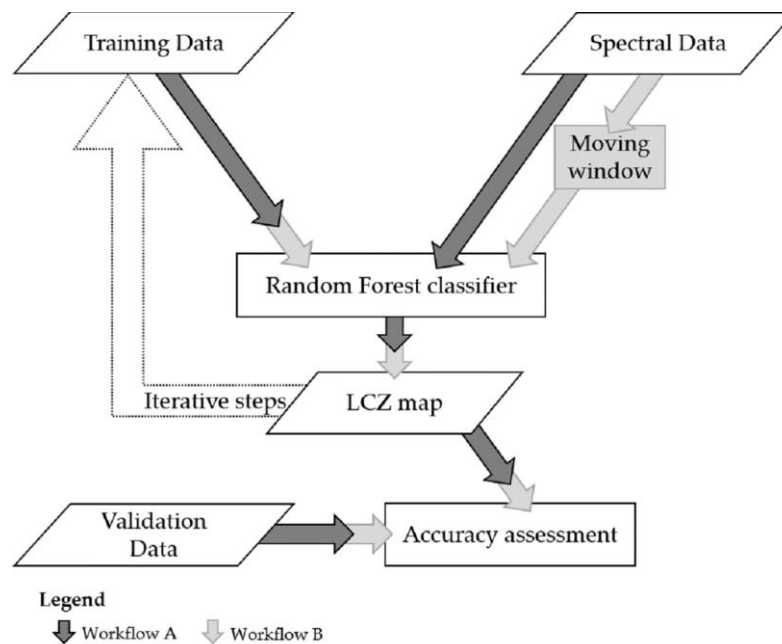


Figure 11: Overview LCZ classification. Workflow A is the WUDAPT based method, while workflow B is the modified workflow that uses a moving window to include neighbourhood information (Verdonck et al., 2017).

The development of the LCZ maps requires adaptations (workflow B, Figure 11) to the original method presented by WUDAPT (workflow A, Figure 11). In workflow A, the Landsat images are resampled from a resolution of 30 m to 100 m. After this step, a random forest classification in SAGA is carried out and the LCZ maps are validated visually using Google Earth. Since this method is not optimal for a city characterised by small heterogeneous areas, like Kunming, workflow B is preferred. In workflow B some adaptations are made:

1. A first adaptation is applied on the first condition of the WUDAPT protocol, where the training areas should be homogeneous polygons with a minimum surface area of 1 km², because smaller surface areas would not be large enough to establish a local climate zone (Bechtel et al., 2015). Since Kunming is characterised by heterogeneous areas, training areas of at least 1 km² are difficult to find, therefore many smaller, homogeneous areas were selected.
2. The second adaptation is taking into account the neighbourhood information. This is not included into the original WUDAPT method and causes spectral variability to be lost due to the resampling of Landsat images to a 100 m resolution. Because of this, a contextual classifier is used, which uses information from neighbouring 30 m pixels through a moving window (Verdonck et al., 2017). This is a way to include horizontal heterogeneity. Multiple moving windows with different kernel sizes are used in order to select the most appropriate moving window per year.
3. The second adaptation is assessing a validation. For each kernel size, 10 random forest classifications are performed. These runs are evaluated by assessing the map accuracies on the pixels of the independent validation polygon set, using an error matrix. Independent validation polygons are selected on randomly selected pixels from training areas, in order to

avoid a positive bias of neighbouring training and validation samples (Verdonck et al., 2017). The error matrix computes the overall accuracy (OA) and provides an estimation of the accuracy of the classification result. The OA is the division of the correctly allocated validation pixels by the total amount of validation pixels. In addition to the OA, F1-scores are computed. The F1-score is the arithmetic mean of the class-wise F1 scores. These F1- values are the weighted averages of the user's (UA) and producer's accuracies (PA). The UA gives an idea about how often the LCZ on the map is actually the LCZ in real life, while the PA is the probability that a certain LCZ in real life is correctly classified. The class-wise F1-score for class i is calculated as followed (Sokolova & Lapalme, 2009):

$$F1_i = \frac{2 UA_i PA_i}{UA_i + PA_i}$$

In order to assess the robustness of the different classification methods, standard deviations (SD) on the OA and F1 are calculated.

3.2.2 Land Surface Temperature retrieval

Images

For the LST calculation, cloudless Landsat images from the warm season are taken because of their ability to give a better visibility of the urban structures. The selected Landsat images are shown in Table 3. For 2005 and 2011, no cloudless Landsat images are found in the warm season. As a result, cloudless images from 2004 and 2012 are taken. The bands of Landsat 8, which are used for making the LST map, are bands 4, 5 and 10, while for Landsat 7, bands 3, 4 and 6.1 are used.

Table 3. Landsat images information for the LST calculation.

Mapping period	Landsat Entity ID	Date
2005	LE07_L1TP_129043_20040521_20170121_01_T1	21/05/2004
2011	LE07_L1TP_129043_20120615_20161123_01_T1	15/06/2012
2017	LC08_L1TP_129043_20170501_20170515_01_T1	01/05/2017

In the satellite image of 2004 some clouds are present in the mountainous areas. To overcome a disturbed result because of these clouds, due to its notable lower LST, the clouds are left out of the image. To do so, the clouds are first separated in another raster and their pixel values are subsequently reclassified to NoData-value. In the final step, this reclassified raster is added with the original LST map.

LST estimation

LST is estimated using the single channel algorithm because of its relatively simple data requirements and high accuracy. In addition, the National Aeronautics and Space Administration (NASA) suggests not to use band 11 for surface temperature retrieval when problems with data from one of the Landsat 8 thermal bands (band 11) are considered (Vlassova et al., 2014). An overview of the method is visualised on Figure 12 and will be explained in more detail in the following paragraphs.

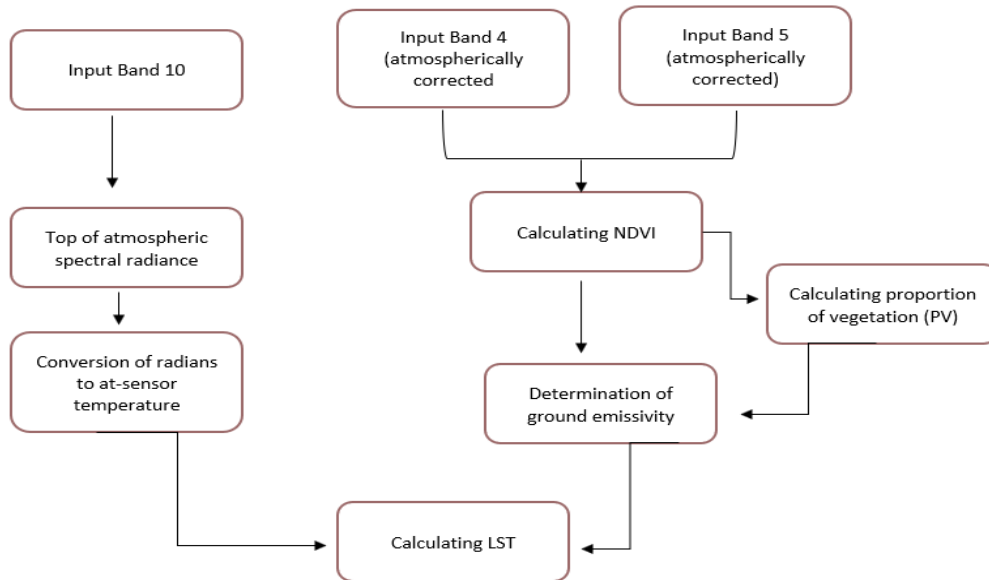


Figure 12. Overall method for LST estimation.

Conversion digital numbers to top of atmosphere reflectance

At-sensor radiances measured at a certain wavelength region is converted into Digital Numbers (DNs), using a quantification system. These DN values have no physical connotation and no unit. DNs can be converted to radiance, thereafter to Top Of Atmosphere (TOA, at-sensor) brightness temperature and finally into land surface temperatures, so a quantitative analysis can be done from thermal remote sensing data.

The first step is to convert the Digital Numbers (DN) of band 10 to Top Of Atmosphere (TOA) reflectance, using the radiance rescaling factors that are provided in the metadata file. For this conversion, the equation below is used.

$$L_{\lambda} = M_L Q_{cal} + A_L$$

With M_L the band-specific multiplicative rescaling factor, Q_{cal} the Band 10 image and A_L the band-specific rescaling factor. The M_L -and A_L -value are provided in the metadata file and are respectively 3.3420×10^{-4} and 0.1.

Conversion of reflectance values into satellite brightness temperature

The second step is to convert the reflectance values into satellite brightness temperature. Therefore, the thermal constants are used that are found in the metadata file. This results in at-satellite brightness temperatures expressed in Kelvin (Li et al., 2013). Since values in degrees Celsius are desired, a conversion from Kelvin to Celsius is added.

After the digital numbers are converted to reflection, the TIRS band data should be converted from spectral radiance to brightness temperature at sensor (BT) using the thermal constants (K1 and K2)

that are provided in the metadata file. The following equation is used to convert the reflectance to BT in Celsius degrees:

$$BT = \frac{K_2}{\ln\left(\frac{K_1}{L_\lambda} + 1\right)} - 273.15$$

K_1 , K_2 = band-specific thermal conversion constants from the metadata with $K_1=774.8853$ and $K_2=1321.0781$

LSE calculation

The third step is to calculate the Land Surface Emissivity (LSE), based on the NDVI emissivity method. To do so, the Normalized Difference Vegetation Index (NDVI) is calculated using band 4 and 5. These bands did first undergo an atmospheric correction. This NDVI is then used to calculate the Proportion of Vegetation (PV), which is subsequently used to calculate the LSE. For the calculation of the NDVI and the PV, equation below are used.

$$NDVI = \frac{NIR(band\ 5) - Red(band\ 4)}{NIR(band\ 5) + Red(band\ 4)}$$

Thereafter the PV is calculated with the following equation:

$$PV = \left(\frac{NDVI - NDVI_{min}}{NDVI_{max} - NDVI_{min}}\right)^2$$

With $NDVI_{min}$ and $NDVI_{max}$ the minimum and maximum value of the NDVI interval.

To calculate the Land Surface emissivity (LSE), the Normalized Difference Vegetation Index (NDVI) and the Proportion of Vegetation (PV) are needed. The LSE is an important factor for the estimation of LST, since the LSE is a proportionality factor that scales blackbody radiance (Planck's law) to predict emitted radiance. It is the efficiency of transmitting thermal energy across the surface into the atmosphere. The LSE can be estimated using the error correction:

$$LSE = 0.004PV + 0.986$$

LST calculation

The final step is the calculation of the LST, using the at-satellite brightness temperature of band 10, the wavelength of emitted radiance at 11.5 μm and the LSE (Cai et al., 2017).

Finally, the LST or the emissivity-corrected land surface temperature is calculated using the following formula:

$$LST = \frac{BT}{1 + \left(\lambda \frac{BT}{\rho}\right) \ln(LSE)}$$

With

$$\rho = h \frac{c}{\sigma} = 1.438 \cdot 10^{-2} mK$$

Where BT is the at-sensor brightness temperature ($^{\circ}\text{C}$) of band 10, λ is the wavelength of the emitted radiance of band 10, LSE is the estimated land surface emissivity, σ is the Boltzmann constant ($= 1.38 \cdot 10^{-23} \text{ J/K}$), h is Planck's constant ($= 6.262 \cdot 10^{-34} \text{ Js}$) and c is the velocity of light ($= 2.998 \cdot 10^8 \text{ m/s}$).

In order to compare the LSTs from the different years, the maps are normalised. To do so, the equation below is used.

$$\text{Normalised LST} = \frac{\text{pixel value} - \min(\text{pixel value})}{\max(\text{pixel value}) - \min(\text{pixel value})}$$

With pixel value the pixel value of the raster, $\min(\text{pixel value})$ the minimum value and $\max(\text{pixel value})$ the maximum pixel value of the raster image.

3.2.3 Surface Urban Heat Island assessment

Evolution of the sUHII during 2004 -2017

Urbanisation has many consequences, as discussed in section 2.1.5. One of them is the sUHI, which means that the surface temperature in the city is higher than the surface temperature in the areas surrounding it. The evolution of the sUHII between 2005 and 2017 can give information about the development of the city in that period. For example, there is a significant correlation between sUHII and population as well as GDP (Cui et al., 2016).

The sUHII of each LCZ as well as Kunming in general, based on the LCZs, is calculated. The sUHII is calculated to assess the surface heating effects in urban areas as well as in each LCZ. To obtain the overall mean sUHII, the difference in mean land surface temperature between the urban (LST_{urban}) and natural (LST_{natural}) LCZ are calculated according to the following formula (Bonafoni et al., 2017):

$$sUHII = \text{mean } LST_{\text{urban}} - \text{mean } LST_{\text{natural}} \quad (8)$$

To obtain the sUHII of each LCZ, the difference between the mean LST of LCZ i and the mean LST of all the natural LCZs covered with vegetation is calculated according to the formula below (Bechtel et al., 2015):

$$sUHII(i) = \text{mean } LST_{LCZ(i)} - \text{mean } LST_{\text{natural}} \quad (9)$$

This will give both positive and negative values for the sUHII, as such both the Urban Heat (UHI) and Urban Cool Islands (UCI) can be determined. The determination of the urban and natural zones are done according to the characterisations of the LCZs, because the urban LCZ (LCZ 1-10) have normally the highest LST and are linked to the city, while the natural LCZ (LCZ A-H) have normally colder LST and are linked to rural and natural areas.

sUHII classification in 2017

Besides the information about the development, it is useful to know which parts of the city can have the ability to cause problems with extreme heat. The urban LCZs of Oke (2004) can be used to classify the zones by their thermal climate zones (TCZs) and redefining the UHI magnitude by inter-zone temperature difference. However, these TCZs are not easy to use in operational modes and to be incorporated in risk management since more practical thermal references are needed. Because of this, the characterisation of a sUHI in terms of a temperature exceedance level or threshold is eligible. The

thermal references of these surface intra-urban heat islands (SIUHIs) are based on multiple temperature thresholds that are related to the spatial average of the LSTs (Martin et al., 2015). The comparison of LSTs in LCZs is based on the assumption that every LCZ is characterised by a unique LST regime (Geletič et al., 2016). Because of this, an overlay analysis was applied whereby the mean LST (μ) and its standard deviation (SD) is calculated for each LCZ using zonal statistics in ArcGIS. The advantage of using mean values and standard deviations of the LSTs is because it shows better the spatial differentials regardless of the temporal variation of the actual LST values (Zhang et al., 2013). For Kunming, the sUHI is classified into five levels according to the standard deviation from the mean LST. The threshold values for the classification is represented in Table 4 (Zhang et al., 2013).

Table 4. Threshold values for sUHI classification based on the LST, whereas μ and SD are the mean and standard deviation values of the LST respectively (Zhang et al., 2013).

LST category	RANGE
Very low	$T_s < \mu - 1 \text{ SD}$
Low	$\mu - 1 \text{ SD} \leq T_s < \mu - \text{SD}/3$
Medium	$\mu - \text{SD}/3 \leq T_s < \mu + \text{SD}/3$
High	$\mu + \text{SD}/3 \leq T_s < \mu + 1 \text{ SD}$
Very high	$T_s \geq \mu + 1 \text{ SD}$

4. Results

4.1 LCZ mapping

4.1.1 Accuracies

To select the best LCZ classification for the different years, the appropriate kernel size is chosen based on the classification accuracies and F1-scores. The first mapping process was done for 2017, which explains the greater amount of kernel sizes for that time period. For 2011 and 2005, the choice of the tested kernel sizes was more focused. The OAs and F1-scores of the LCZ maps with different kernel sizes (workflow B) are shown in Table 5.

Table 5. OAs of the LCZ maps with kernel size 7x7, 9x9 or 11x11 from 2005, 2011 and 2017.

		5x5	7x7	9x9	11x11
2017					
	OA (%)	95.8 ± 0.1	95.8 ± 0.1	95.7 ± 0.1	95.4 ± 0.2
F1 Measure (%)	LCZ 1 Compact high-rise	74.8 ± 1.2	78.0 ± 0.8	78.0 ± 0.7	71.8 ± 2.2
	LCZ 2 Compact mid-rise	86.6 ± 0.4	84.4 ± 0.6	84.1 ± 0.5	83.0 ± 0.9
	LCZ 3 Compact low-rise	61.3 ± 0.8	67.8 ± 2.3	50.5 ± 3.1	56.9 ± 4.0
	LCZ 4 Open high-rise	77.4 ± 0.3	76.7 ± 0.8	74.4 ± 0.6	69.9 ± 0.7
	LCZ 5 Open mid-rise	45.1 ± 1.0	45.3 ± 2.5	48.1 ± 2.1	43.0 ± 3.6
	LCZ 6 Open low-rise	56.7 ± 1.3	50.6 ± 1.5	49.9 ± 1.8	49.1 ± 1.2
	LCZ 8 Large low-rise	90.7 ± 0.9	93.8 ± 0.4	92.4 ± 0.6	88.8 ± 0.8
	LCZ 10 Heavy industry	75.8 ± 3.5	63.2 ± 1.2	63.7 ± 9.4	50.7 ± 5.1
	LCZ A Dense trees	97.3 ± 0.2	98.2 ± 0.3	97.0 ± 0.5	96.0 ± 0.4
	LCZ B Scattered trees	60.8 ± 1.9	61.6 ± 4.5	52.8 ± 4.6	46.7 ± 4.8
	LCZ C Bush, scrub	80.9 ± 4.5	74.2 ± 3.8	60.6 ± 4.1	74.1 ± 4.9
	LCZ D Low plants	85.6 ± 2.6	83.5 ± 1.3	78.0 ± 2.4	72.1 ± 3.2
	LCZ G Water	100.0 ± 0.0	100.0 ± 0.0	100.0 ± 0.0	100.0 ± 0.0
LCZ H Agricultural greenhouse	96.7 ± 0.4	96.3 ± 0.3	96.9 ± 0.2	96.4 ± 0.1	
2011					
	OA (%)	96.8 ± 0.1	96.7 ± 0.1		
F1 Measure (%)	LCZ 2 Compact mid-rise	73.2 ± 1.0	77.6 ± 0.7		
	LCZ 3 Compact low-rise	54.5 ± 2.5	55.8 ± 1.2		
	LCZ 4 Open high-rise	75.4 ± 0.9	77.2 ± 0.7		
	LCZ 5 Open mid-rise	57.6 ± 0.7	56.4 ± 1.1		
	LCZ 6 Open low-rise	60.8 ± 2.4	56.8 ± 1.7		
	LCZ 8 Large low-rise	89.0 ± 1.4	91.4 ± 0.4		
	LCZ 10 Heavy industry	68.8 ± 0.4	60 ± 0.2		
	LCZ A Dense trees	98.9 ± 0.2	99.4 ± 0.1		
	LCZ B Scattered trees	60.4 ± 1.4	68.2 ± 2.0		
	LCZ C Bush, scrub	70.0 ± 3.3	72.5 ± 1.4		
	LCZ D Low plants	86.6 ± 2.2	83.2 ± 2.8		
	LCZ G Water	100.0 ± 0.0	100.0 ± 0.0		
	LCZ H Agricultural greenhouse	96.9 ± 0.7	95.5 ± 0.9		
2005					
	OA (%)		97.4 ± 0.1	97.7 ± 0.1	97.3 ± 0.1
F1 Measure (%)	LCZ 2 Compact mid-rise		75.6 ± 1.8	79.0 ± 2.0	74.6 ± 1.5
	LCZ 3 Compact low-rise		47.6 ± 2.8	48.3 ± 4.1	40.2 ± 5.3
	LCZ 4 Open high-rise		62.9 ± 2.2	61.1 ± 2.1	56.4 ± 2.4
	LCZ 5 Open mid-rise		63.9 ± 3.8	67.4 ± 2.1	72.4 ± 4.3
	LCZ 6 Open low-rise		85.1 ± 1.6	85.7 ± 2.7	81.4 ± 2.1
	LCZ A Dense trees		99.3 ± 0.0	99.4 ± 0.1	99.5 ± 0.0
	LCZ B Scattered trees		75.8 ± 2.8	80.5 ± 2.1	74 ± 3.6
	LCZ C Bush, scrub		62.3 ± 0.8	67.0 ± 3.4	66.2 ± 5.2
	LCZ D Low plants		67.1 ± 3.3	75.1 ± 2.5	73.4 ± 1.6
	LCZ G Water		99.9 ± 0.0	99.9 ± 0.0	99.9 ± 0.0
	LCZ H Agricultural greenhouse		93.0 ± 1.0	95.7 ± 0.7	94.6 ± 0.4

The confusion matrix of the LCZ map obtained by using workflow A is shown in Appendix 5 and the confusion matrices of the different years with an appropriate kernel size is shown in Appendix 6 to Appendix 8. For the LCZ map of 2005, the highest OA with the lowest SD is achieved using a kernel size of 9x9, while for the maps of 2011 and 2017 this was achieved using a kernel size of 5x5 or 7x7. The F1-scores for the LCZ map of 2005 with kernel size 9x9 gave the best results. For the LCZ map of 2011 with kernel size 7x7, the best F1-scores with the lowest SD were achieved for the urban zones. Because of this, a kernel size of 7x7 is preferred over a kernel size of 5x5 for 2011, despite the little higher OA of the LCZ map with kernel size 5x5. Kernel size 9x9 was not tested due to the high possibility of having both a higher OA and F1 scores of the urban zones. For 2017, the LCZ maps with kernel size 5x5 gave the highest F1-scores and the lowest SD for the urban zones. For this reason, a kernel size of 5x5 is preferred for 2017. For all the different years and all the different kernel sizes, it can be noticed that compact low-rise (LCZ 3) has the lowest F1-score of the urban LCZs, and a higher SD, this is especially the case for 2005 and 2011. Also LCZ 5 and LCZ 6 have a lower F1-score and a somewhat higher SD. The natural LCZs gave in general better F1-scores.

4.1.2 LCZ localisation

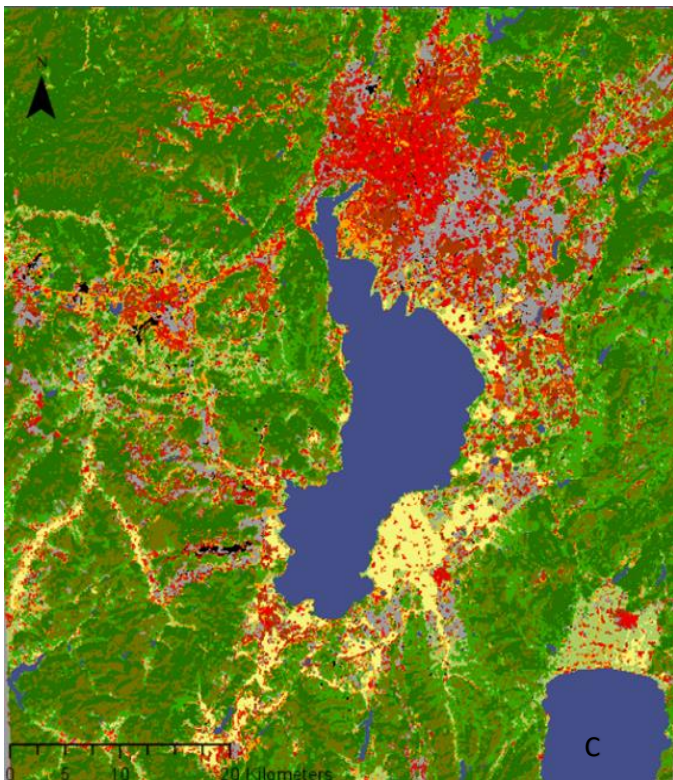
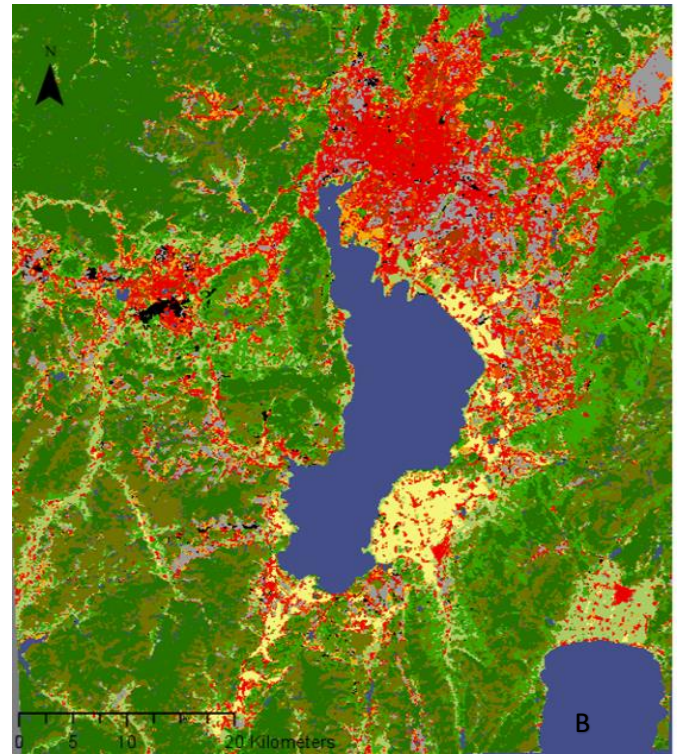
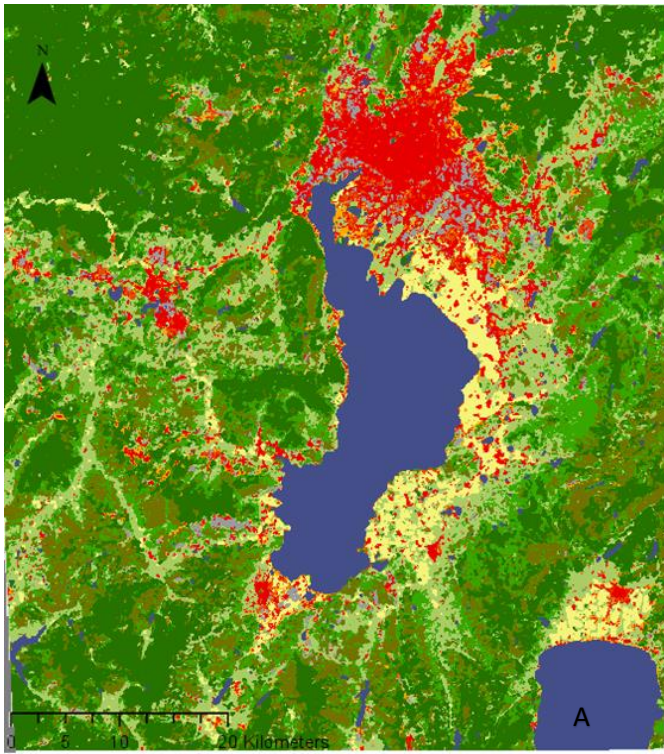
The final LCZ maps of 2005, 2011 and 2017 with their appropriate kernel sizes are shown in Figure 13. In Table 6, the area of every LCZ is shown for the different years. In Figure 14 and 15 the LCZs are expressed relative to respectively the total area and the total urban area.

The LCZ maps (Figure 13) show the landcover pattern of Kunming between 2005 and 2017. For all the different years, the centre of Kunming is mostly covered with compact mid-rise (LCZ 2), the Southwest of the Dianchi lake has the most agricultural land (LCZ D and LCZ H) and the mountainous areas are mostly covered with dense trees (LCZ A), scattered trees (LCZ B) and bush, scrubs (LCZ C).

In 2005 (Figure 13A), the presence of compact high rise (LCZ 1), open high rise (LCZ 4), lightweight (LCZ 7), sparsely built (LCZ9), heavy industry (LCZ 10), bare rock or paved (LCZ E) and bare soil or sand (LCZ F) is negligible. Small villages of compact low-rise (LCZ 3) and compact mid-rise (LCZ 2) are located between zones of low plants (LCZ D) or agricultural greenhouse (LCZ H).

In 2011 (Figure 13B), compared to 2005, the presence of open high-rise (LCZ 4) and open mid-rise (LCZ 5) is more pronounced in the outskirts of the city and large low-rise (LCZ 8) is present in greater abundance in the South of the centre. Due to the construction of the airport in the Eastern part of Kunming in 2012, open mid-rise (LCZ 5) and large low-rise (LCZ 8) is present in this region and in the direction to it. In the East-side of the Dianchi Lake, a mixture of compact mid-rise (LCZ 2), open mid-rise (LCZ 5) and large low-rise (LCZ 8) is found. Areas with agricultural LCZ are less dominant compared to 2005. Heavy industry (LCZ 10) has increased a little and is visible in the Northwest of the Dianchi lake and in the Northern direction of the city centre. Areas with compact high-rise (LCZ 1), lightweight (LCZ 7), sparsely built (LCZ 9), bare rock or paved (LCZ E) bare soil or sand (LCZ F) are still not present or are too small to be mapped.

In 2017 (Figure 13C), the presence of open high-rise (LCZ 5) has increased and the presence of compact mid-rise (LCZ 2) has decreased in the outskirts of the city. The South of Kunming is getting more urbanised by open high-rise (LCZ 5) and open mid-rise (LCZ 4). In the East side of the Dianchi lake the presence of open mid-rise (LCZ 4) has also increased, while the amount of compact mid-rise has decreased. Zones of compact high-rise (LCZ 1) are now more present but still occupy a small area of the urban area of Kunming (1.1%; Figure 15).



LCZ

- LCZ 1 Compact high-rise
- LCZ 2 Compact mid-rise
- LCZ 3 Compact low-rise
- LCZ 4 Open high-rise
- LCZ 5 Open mid-rise
- LCZ 6 Open low-rise
- LCZ 8 Large low-rise
- LCZ 10 Heavy industry
- LCZ A Dense trees
- LCZ B Scattered trees
- LCZ C Bush, scrub
- LCZ D Low plants
- LCZ G Water
- LCZ H Agricultural greenhouse

Figure 13. LCZ -maps from 2005 with kernel size 9x9 (A), 2011 with kernel size 7x7 (B) and 2017 with kernel size 5x5 (C).

Table 6. Total occupied area of each LCZ for the different years.

		2005 (km ²)	2011 (km ²)	2017 (km ²)
Urban LCZ	LCZ 1	/	/	13.6
	LCZ 2	197.50	256.59	150.63
	LCZ 3	50.64	34.88	30.77
	LCZ 4	/	82.55	264.70
	LCZ 5	60.54	73.53	105.34
	LCZ 6	63.74	131.41	215.07
	LCZ 8	71.80	221.22	444.53
	LCZ 10	/	46.23	20.85
Total urban area		444.20	846.41	1245.49
Natural LCZ	LCZ A	1 402.35	1 248.04	1 260.49
	LCZ B	608.19	582.26	628.60
	LCZ C	590.39	779.08	696.58
	LCZ D	736.1	402.61	295.40
	LCZ G	467.26	470.98	475.37
	LCZ H	155.30	119.20	136.15

4.1.3 LUCC between 2005 and 2017

The landcover changes that occurred between 2005 and 2017 can be seen on the LCZ- maps in Figure 13 and on the histograms in Figures 14 and 15. The urban growth between 2005 and 2011 (Figures 13A, 13B), is seen in both Northern, Eastern and Southern direction of the centre where natural LCZ are replaced by urban LCZ. In addition, the West side of the Dianchi Lake is more urbanised. Between 2011 and 2017 (Figures 13B, 13C), most of the LUCC consists of the conversion of urban LCZs to other urban LCZs. In addition, the urbanisation to the South is more pronounced.

The biggest LUCC is the conversion of low plants (LCZ D) to urban zones, whereas LCZ D decreases from 16.7 % of the total area in 2005, to 9.1 % in 2011 and to 6.2 % in 2017 (Figure 14). Other important changes are the increasing areas of open high-rise (LCZ 4), open low-rise (LCZ 6) and large low-rise (LCZ 8), whereas open high-rise (LCZ 4) and large low-rise (LCZ 8) had a spectacular growth. Open high-rise (LCZ 4) increased from 16.7 % of the urban area in 2011 to 21.1 % in 2017 and large low-rise (LCZ 8) went from 16.2 % of the urban area in 2005, to 26.1 % in 2011 and to 35.7 % in 2017 (Figure 15). Furthermore, the presence of compact high-rise (LCZ 1) has become noticeable, but is still fairly low (1.1 % of the urban area; Figure 15).

Besides the big decrease of areas with low plants (LCZ D), other notable decreases in area are found in zones with compact low-rise (LCZ 3) and dense trees (LCZ A). Of the total urban area, compact low-rise (LCZ 3) decreased from 11.4 % in 2005, to 4.1 % in 2011, to 2.5 % in 2017 (Figure 15) and dense trees (LCZ A) decreased from 31.8 % of the total area in 2005 to 28.1 % in 2011 to 26.6 % in 2017 (Figure 14). Open mid-rise (LCZ 5) increased in total area over the period 2005-2017 (Figure 14), but decreased in percentage relative to the total urban area (Figure 16), which means that the total area of the LCZ does have a smaller increase compared to the increase of the total urban area. For compact mid-rise (LCZ 2), a big reduction in percentage relative to the total urban area is seen (from 44.5 % in 2005 to 30.3 % in 2011 to 12.1 % in 2017; Figure 15), while the percentage relative to the total area knows an

increase between 2005 and 2011 (4.6 % to 5.8 %; Figure 14) and a decrease between 2011 and 2017 (5.8 % to 3.2 %; Figure 14). This means that between 2005 and 2011, the total area of LCZ 2 increased, but not to the same extent as the urban area.

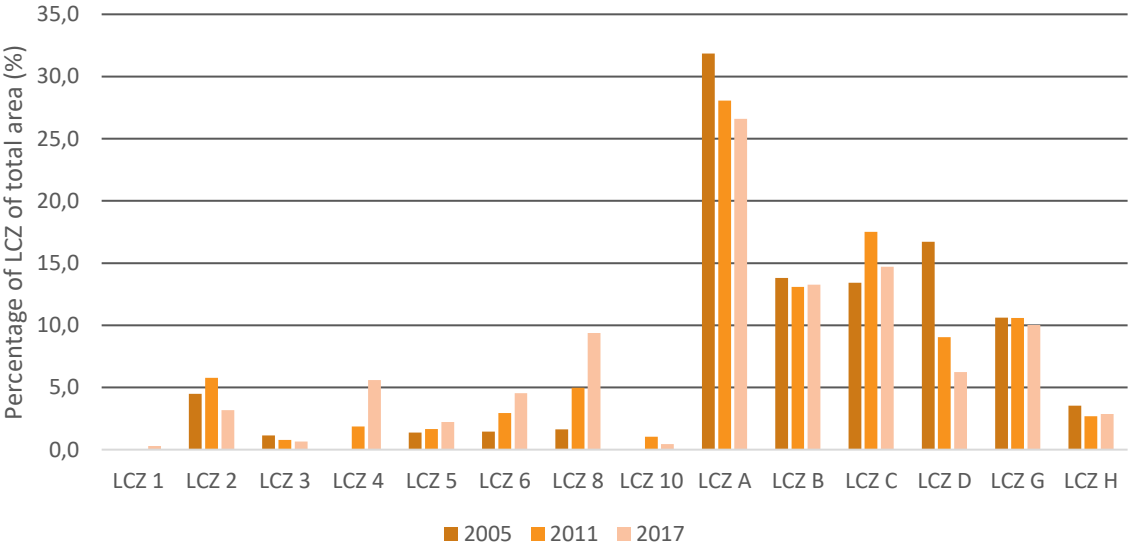


Figure 14. Histogram of the LCZs with their corresponding percentage of the total area from 2005, 2011 and 2017.

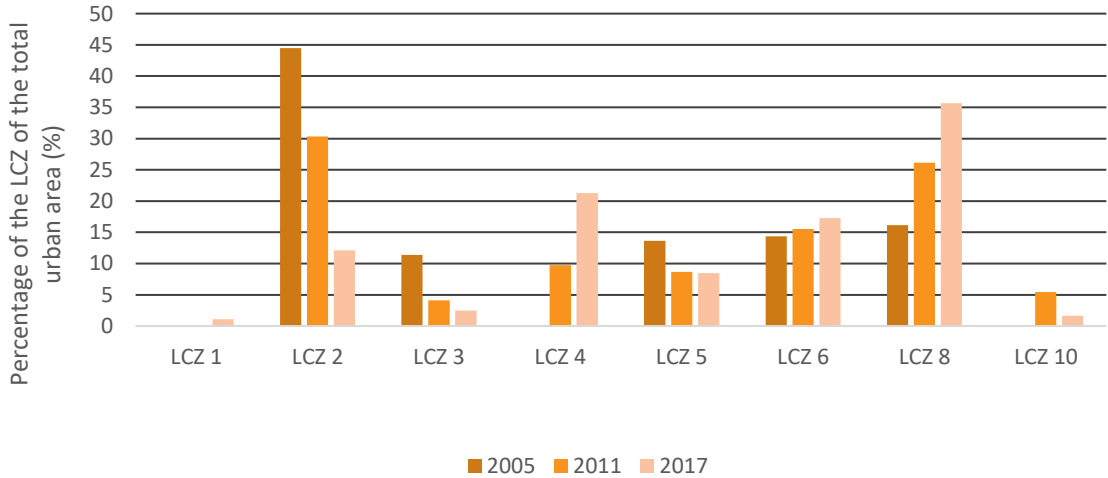


Figure 15. Histogram of the LCZs with their corresponding percentage of the total urban area.

4.2 Land surface retrieval

4.2.1 Evolution of LST during 2004 -2017

The LST of 2004, 2012 and 2017 is calculated and normalised and is shown on Figure 16. For May 2004 (Figure 16A), the highest temperatures are found in the centre of the city and in some mountainous areas. The warmer regions are mostly located on more natural landscape around the lake and in the mountains. In the Dianchi lake, there are also some warm zones, which can be due to algae. The colder areas are found in water bodies and in the mountains. The white dots represent the clouds, which contain no data. For 2012 (Figure 16B), the areas in the South, the West and the East of the city have more hot areas in comparison to 2004. The warmer and colder areas stay more or less the same, except for the warmer regions in the lake, which are absent in 2012. In 2017 (Figure 16C), compared to 2012, the hot areas are more densified, the warmer regions have expanded and the colder areas are less cold.

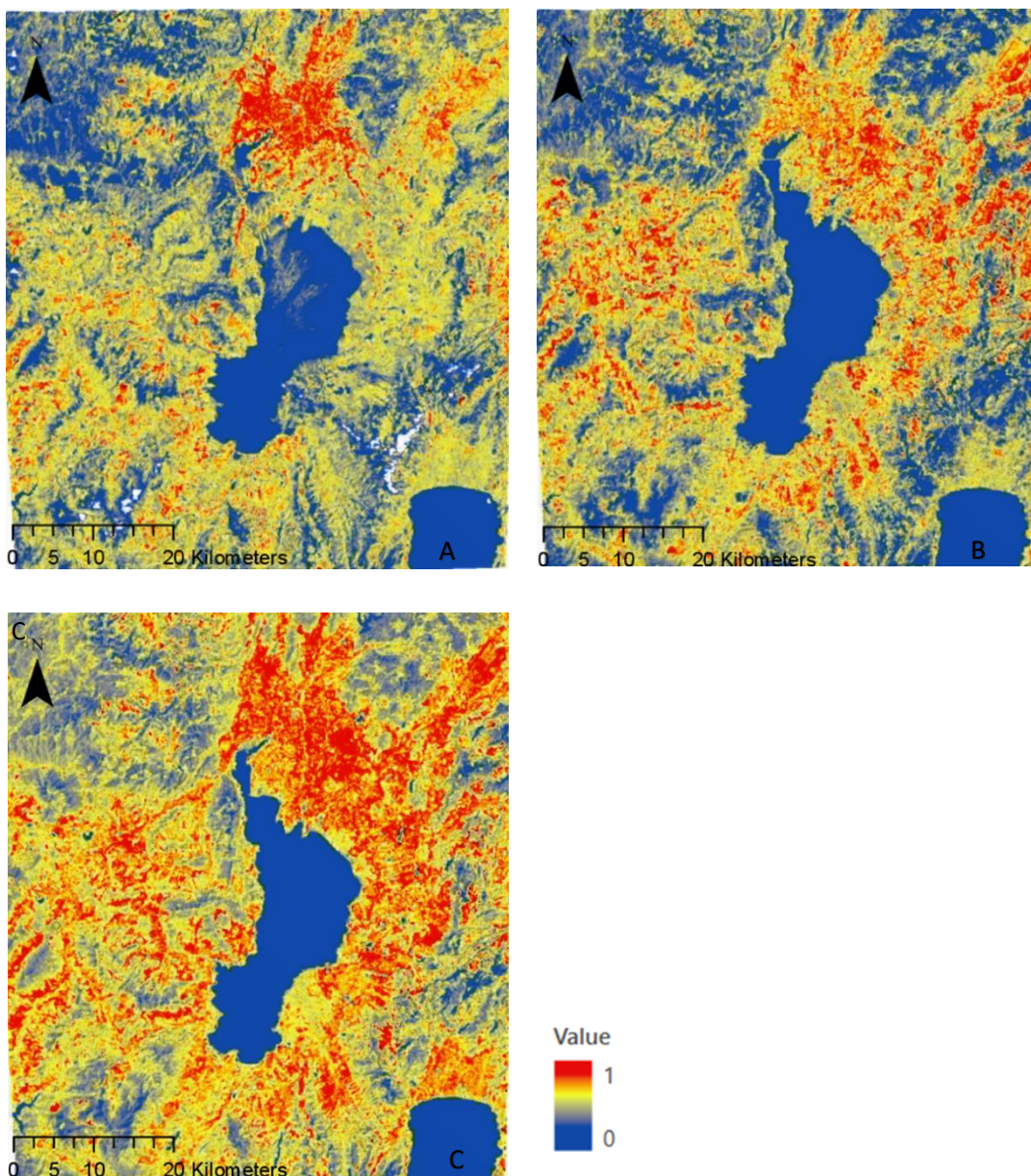


Figure 16. Normalised LST of Kunming from May 2004 (A), June 2012 (B) and May 2017 (C).

4.2.2 Thermal behaviour of the different LCZs

In Table 7, the mean LSTs of the different LCZs with their SDs are calculated for 2004, 2012 and 2017. The highest LSTs are found in compact mid-rise (LCZ 2), compact low-rise (LCZ 3), large low-rise (LCZ 8) and heavy industry (LCZ 10), whereas the lowest LST is found in water (LCZ G). The largest SD on the mean LST is for all the different years found in heavy industry (LCZ 10) and large low-rise (LCZ 8). For the other LCZs, the SD differs over the LCZs, which is due to the different time of taking the satellite image.

Table 7. The mean LST (°C) for each LCZ in the month May 2017.

	Mean LST May 2004 ± SD (°C)	Mean LST June 2012 ± SD (°C)	Mean LST May 2017 ± SD (°C)
LCZ 1 Compact high-rise	/	/	29,64 ± 1.11
LCZ 2 Compact mid-rise	26.07 ± 2.18	33.48 ± 2.04	31.28 ± 2.9
LCZ 3 Compact low-rise	24.94 ± 1.79	32.95 ± 1.96	30.92 ± 1.98
LCZ 4 Open high-rise	/	31.81 ± 2.20	29.61 ± 1.57
LCZ 5 Open mid-rise	24.28 ± 1.80	32.52 ± 1.92	29.44 ± 2.35
LCZ 6 Open low-rise	23.72 ± 1.66	31.81 ± 2.56	29.31 ± 1.36
LCZ 8 Large low-rise	26.48 ± 2.74	33.97 ± 2.51	31.96 ± 3.31
LCZ 10 Heavy industry	/	34.29 ± 3.33	32.35 ± 3.38
LCZ A Dense trees	21.54 ± 1.71	27.31 ± 2.17	25.31 ± 1.22
LCZ B Scattered trees	23.92 ± 1.68	31.12 ± 3.02	28.32 ± 1.22
LCZ C Bush, scrub	23.73 ± 1.95	30.83 ± 2.87	29.78 ± 1.43
LCZ D Low plants	24.23 ± 1.48	31.52 ± 2.68	29.81 ± 1.75
LCZ G Water	19.31 ± 1.53	23.71 ± 3.08	18.54 ± 1.56
LCZ H Agricultural greenhouse	23.34 ± 1.34	31.32 ± 2.01	28.59 ± 1.21

4.3 Surface urban heat island intensity

4.3.1 Evolution of the sUHI during 2004 - 2017

General sUHI intensity of Kunming

The sUHI intensities of 2004, 2012 and 2017 are shown in Figure 17. The sUHI increases from 2.31°C in 2004 to 3.7°C in 2012 to 3.84 °C in 2017.

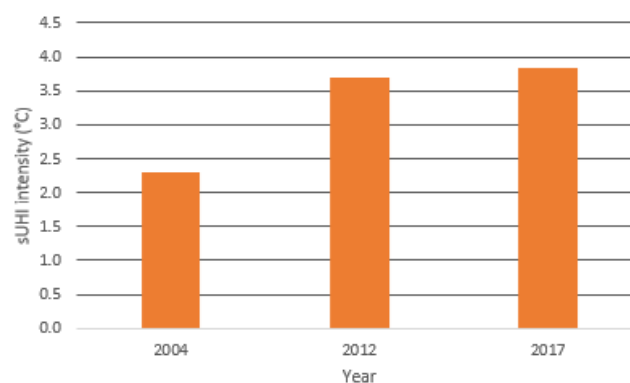


Figure 17. sUHI intensity of each LCZ of the three different years.

sUHI of the different LCZs over the different time periods

The sUHIs of each LCZ of 2004, 2012 and 2017 can be found in Table 8. Positive values indicate an intensifying effect on the sUHI, while the negative values indicate an UCI. In general, the sUHI for each LCZ increases between 2004 and 2017, except for open mid-rise (LCZ 5), dense trees (LCZ A) and scattered trees (LCZ B) where the sUHI for 2012 is larger than the sUHI for 2017. The highest positive sUHI are seen in heavy industry (LCZ 10) and large low-rise (LCZ 8), followed by compact mid-rise (LCZ 2) and compact low-rise (LCZ 3). The lowest positive sUHIs are found in scattered trees (LCZ B) and agricultural greenhouse (LCZ H). The only UCIs are found in areas with dense trees (LCZ A) and water (LCZ G).

Table 8. sUHI intensity of each LCZ of the three different years.

LCZ-type	sUHI intensity 2004 (°C)	sUHI intensity 2012 (°C)	sUHI intensity 2017 (°C)
LCZ 1 Compact high-rise	/	/	2.9
LCZ 2 Compact mid-rise	3.4	4.2	4.6
LCZ 3 Compact low-rise	2.3	3.7	4.2
LCZ 4 Open high-rise	/	2.6	2.9
LCZ 5 Open mid-rise	1.4	3.3	2.7
LCZ 6 Open low-rise	1.1	2.6	2.6
LCZ 8 Large low-rise	3.4	4.7	5.2
LCZ 10 Heavy industry	/	5.0	5.6
LCZ A Dense trees	-1.1	-1.9	-1.4
LCZ B Scattered trees	1.3	1.8	1.6
LCZ C Bush, scrub	1.1	1.6	3.1
LCZ D Low plants	1.4	2.3	3.1
LCZ G Water	-3.3	-5.5	-8.2
LCZ H Agricultural greenhouse	0.7	1.8	1.9

In Figure 18, the difference in sUHI of each LCZ is shown for 2004-2012 and 2012-2017. Between 2004-2012, the sUHI-intensifying effects increased the most for compact low-rise (LCZ 3), open mid-rise (LCZ 5), open low-rise (LCZ 6) and large low-rise (LCZ 8). For period 2012-2017, the largest increase in sUHI-intensifying effects are seen in bush and scrub (LCZ C) and low plants (LCZ D). The difference in sUHI of open low-rise is zero for the period 2012-2017. For the sUHI-mitigating effects, the zones with water (LCZ G) know a large increase in both periods 2004-2012 and 2012-2017.

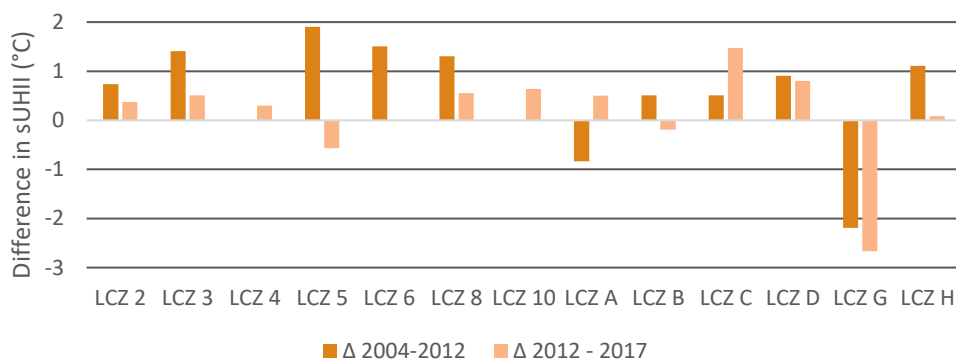


Figure 18. Difference in sUHI of each LCZ for 2004-2012 and 2012-2017.

4.3.2 sUHI classification

The sUHI classification with its 5 classes is shown in Figure 19. Very high LST temperatures and thus high sUHI (class 5) are found in most of the urban regions of Kunming, while very low and low LSTs (class 1 and 2) are found in the most of the natural and agricultural areas. Moderate LSTs (class 3) are present in the urban and the agricultural areas, and high LSTs (class 4) are only visible in some parts of the city.

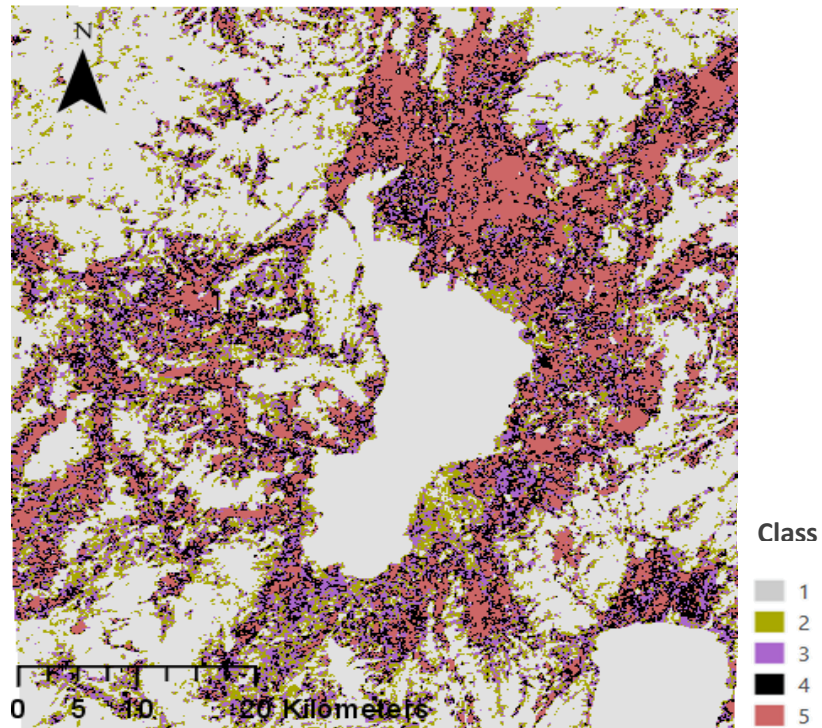


Figure 19. sUHI classification of Kunming for May 2017.

5. Discussion

5.1 LCZ classification

Different kernel sizes are used for the LCZ classifications of 2005, 2011 and 2017 in order to generate the best classification for that time period (Verdonck et al., 2017). For 2005, kernel sizes 9x9 and 11x11 give the best classification, while for 2011 and 2017, kernel sizes 7x7 and 5x5 give a better result. The reason why higher kernel sizes are better for 2005, while smaller kernel sizes are better for 2011 and 2017 is due to the urbanisation trend in Kunming. This trend causes the city to have more heterogeneous areas and smaller plots with mixed land uses. This is the result of the new model of urbanisation, which has as purpose to be more efficient, inclusive and sustainable (The world bank, 2014). It should be noted that the difference in OA between the LCZ maps obtained by using a moving window and the LCZ maps without a moving window is bigger than the difference in OA between the LCZ maps with a moving window themselves. This has already been concluded in the study by Verdonck et al. (2017).

For the three different years, the lowest F1-scores occur at compact low-rise (LCZ 3), open mid-rise (LCZ 5) and open low-rise (LCZ 6). For compact low-rise (LCZ 3), this lower F1-score is due to errors of commission (misclassification of LCZ 2 into LCZ 3) of compact mid-rise (LCZ 2). These misclassifications can have three causes. The first one is because of small difference between the characteristics of compact mid-rise (LCZ 2) and compact low-rise (LCZ 3), which are not always well distinguishable on the Landsat image. For instance, Landsat images give spectral information and are not useful to measure height levels and consequently cause misclassifications (Cai et al., 2017). The second reason is because of the mix of compact mid-rise (LCZ 2) and compact low-rise (LCZ 3) in the rural villages, which can cause errors of commission and omission of compact mid- and low-rise (LCZ 2 and LCZ 3). The reason why the misclassification due to these rural villages do not have much effect on the F1 - score of compact mid-rise (LCZ 2) is because of the high occurrence of compact mid-rise (LCZ 2) in the centre of the city, while compact low-rise (LCZ 3) mostly only occur in the rural villages. The third and final cause for the lower F1-score of compact low-rise (LCZ 3) are the building constructions that change during the year. The appearance of these building constructions can change from bare soil to constructions of some height. Since the training areas of all the different LCZs can have spectral information of bare soil, misclassifications of these areas can easily be made. In addition, the height and the surface material of the construction can change during the year and alter the spectral information. The lower F1-score of open mid-rise (LCZ 5) and open low-rise (LCZ 6) is mostly due to errors of commission and omission of open mid- and low-rise (LCZ 5 and LCZ 6). The reason for these misclassification can be due to the combination of similar characteristics of the two LCZs and the limited information of the Landsat images on the height. This is especially the case for the suburbs areas containing open mid-rise (LCZ 5) buildings that only consist of four or five floors. A second reason are the construction sites that change during the year.

5.2 Thermal behaviour of the different LCZs

The obtained results for the LST is based on satellite observations (Landsat 8) and thus ignore thermal responses of the vertical surfaces. Only the surface temperatures of the satellite subpoint on the surface of the Earth that is centred below the satellite, are analysed. Because of this, the results are not the same as the general thermal responses of any particular LCZ (Dobrovolný & Krahula, 2015). Therefore, the results only provide a partial, but nevertheless coherent, insight into the nature of the LSTs of the LCZs. In addition, the LSTs of the different years are obtained by only one moment in time and can therefore not give a general LST regime for the different LCZs.

The highest LST of the LCZs is found in heavy industry (LCZ 10), which is the result of the industrial activities and the material from which the factories are built. This causes high LSTs in industrial areas during daytime, which has been confirmed in many other studies (e.g. Geletič et al. (2016) and Roth et al. (1989)). The land surface temperature in the perimeter of factories also increases and may cause a buffer zone. This buffer zone can affect the surface temperatures of other areas (Abdelnasser & El Shirbeny, 2016). The second highest LST is found in large low-rise (LCZ 8). This can be due to the presence of LCZ 8 in the buffer zone of heavy industry (LCZ 10). Large low-rise (LCZ 8) has also a higher variability. This higher statistical variability of the LST in this zone can be due to the location of large low-rise (LCZ 8), since not all the LCZ 8 are located near industrial area. Another explanation for the higher statistical variability can be due to the different thermal properties associated with the large roof surfaces (Akbari & Levinson, 2008). Compact mid- and low-rise (LCZ 2 and LCZ 3) do have a similar LST as large low-rise (LCZ 8) and heavy industry (LCZ 10). The typical LST for compact mid-rise (LCZ 2) and compact low-rise (LCZ 3) can be the result of the central location of the zones, the sky view factor (Scarano & Sobrino, 2015), anthropogenic heat flux and the absence of green elements (Chakraborty et al., 2015; Meng, 2017).

The sky view factor has a positive correlation with LST, which means higher sky view factors are associated with higher LST during daytime (Scarano & Sobrino, 2015). This is because of the larger contact between solar radiation and surfaces. Because compact mid-rise (LCZ 2) has a lower sky view factor as well as a higher LST, other factors need to be included. Compact mid-rise (LCZ 2) is mostly located in the city centre and contain a lot of anthropogenic heat sources, including vehicle engines, domestic combustion processes and human metabolism due to the higher population density in the centre (Kotthaus & Grimmond, 2012) These heat sources have an impact on the surface temperature by means of the surface-energy balance that channels the anthropogenic heat into heating the urban surfaces (Bohnenstengel et al., 2014). The speed of this process is depend on the material (heat capacity), of the urban surface. In addition, the absence of the green elements inhibit the possibility to cool down the area by increasing the latent heat flux.

Compact low-rise (LCZ 3) has a similar LST as compact mid-rise (LCZ 2), but a fraction smaller. Compact low-rise (LCZ 3) has a larger sky view factor than compact mid-rise (LCZ 2), which means a larger surface area can be reached by solar radiation and can be heat up during daytime, compared to compact mid-rise (LCZ 2). Nevertheless, due to the location (rural villages) of compact low-rise (LCZ 3) and smaller patch size and lower anthropogenic activity of the zone, the LST is little smaller than compact mid-rise (LCZ 2).

Despite the high anthropogenic heat flux and absence of green elements in zones with compact high-rise (LCZ 1), the LST is lower in these areas, compared to compact mid- and low-rise (LCZ 2 and LCZ 3). This could be due to the presence of more shadowy areas on the surface of the buildings because of lower contact with solar radiation and/or due the result of other and better building material since

these zones are quite recent. Nevertheless, areas with compact high-rise (LCZ 1) are rather limited in Kunming and are also smaller than other LCZs. This can cause a less accurate mean LST for this LCZ.

The lowest LST is found in areas with dense trees (LCZ A) and water (LCZ G). The lower LST for dense trees (LCZ A) can be due to the positive relation between sky view factor and LST. Areas with dense trees have a low sky view factor due to the dense crowns. These dense crowns inhibit solar radiation and prevent surface heating of the trees. Furthermore, the crown evaporates water, which causes the latent heat flux to increase. The presence of dense crowns is depended on multiple factors, such as the season and diseases. But since Kunming has a special climate ('Spring City'), the trees contain leaves throughout the year. The low LST for water bodies is the result of the small heat capacity, which causes a slow heating and cooling of the water. This is especially the case for large and deep water basins, such as the Dianchi lake.

5.3 Urban development

5.3.1 Urban expansion and densification

Period between 2005 and 2011

Between 2005 and 2011, urban growth with regard to the centre of Kunming was established in the north-western, eastern and southern part, which are led by both urbanisation plans and social-economic, topographic and proximity factors (Gao et al., 2017). Several LUCC occurred between 2005 and 2017, but the biggest change happened between 2005 and 2011 and consisted of the conversion of agricultural land to urban zones. This can be explained by rural-to-urban migration where Chinese farmers move to the city which in effect causes the agricultural land to decrease. Since accommodation is needed for these migrants, urban area increases at the expense of rural area. This LUCC confirms the study of Gong et al. (2012), which concluded that rural-to-urban migration occurs in the whole of China.

Urbanisation in the north-western part could have been the result of the World Expo in 1999, which stimulated the progress of suburbanisation of residential housing (Qiyang et al., 2015) and due to the agglomeration of Anning with Kunming. In 2005, the west of the Dianchi lake (Anning) is mostly covered with agricultural land (LCZ D and LCZ H), compact mid-rise (LCZ 2) and compact low-rise (LCZ 3). By 2011, the agglomeration with Kunming city is visible and most of the farmland has been converted into urban LCZ, such as compact mid-rise (LCZ 2) and open mid-rise (LCZ 5).

In the south-eastern part of the city, the settlement of the Changshui airport in 2012 has led to the conversion of agricultural land to urban areas. Before the settlement of the airport, the region in the south-eastern part of the city centre was mostly covered with rural villages (LCZ 2 and LCZ 3) and agricultural land (low plants; LCZ D). In 2011, the airport was under construction and is classified as large low-rise (LCZ 8) and the direction to the airport was densified with mostly large low-rise (LCZ 8) and building constructions of open mid-rise (LCZ 5). The occurrence of large low-rise (LCZ 8) and open mid-rise in that area can be respectively due to the presence of a wood factory and establishment of (touristic) residences.

For all the regions, the percentage of compact mid-rise (LCZ 2) relative to the total urban area decreased (Figure 15, page 34), while the total area of compact mid-rise (LCZ 2) increased (Table 6, page 33). This is probably due to insufficient new areas with compact mid-rise (LCZ 2), compared to the total new areas with urban LCZs. Another possible factor is the absence of open high-rise (LCZ 4)

in the classification of 2005. This can cause open high-rise (LCZ 4) zones to be misclassified as compact mid-rise (LCZ 2) and can lead to a higher total area of compact mid-rise (LCZ 2), compared to the reality. Nevertheless, this amount should be relative small or even neglectable.

Period between 2011 and 2017

Between 2011 and 2017, there has both been an expansion and densification, as seen in Figures 13B and 13C, page 32. The expansion is most commonly noticed in the eastern and southern part relative to the centre of Kunming and is a result of both agglomeration and the settlement of the airport. The expansion causes areas with agricultural land (LCZ D and LCZ H), compact low-rise (LCZ 3) and compact mid-rise (LCZ 2) to decrease because of the removal of rural villages for apartment buildings (LCZ 1, LCZ 4, LCZ 5) or suburbs (LCZ 6). New areas with compact low-rise (LCZ 3) are rare since these zones cannot provide plentiful residences compared to higher LCZs. Aside from the expansion, there is densification in the already existing urban areas, for example in the western region where open high-rise (LCZ 4) and open mid-rise (LCZ 5) have replaced or were added to the already existing compact mid-rise (LCZ 2). This densification is the result of the new model of urbanisation in China. Through densification and compact building, the 'compact city' approach of the urbanisation model wants to counteract the negative effects of urban sprawl, such as ineffective land use and environmental problems (Haaland & van den Bosch, 2015). It also spares farmland, which is getting more important in China since the current available amount of farmland is close to the 'red line' of 120 million hectares. This red line is considered to be the minimum area necessary to ensure food security. The decreased reduction of agricultural land is noticeable in Kunming, as shown in Figure 14 and in Table 6. Densification of the urban areas also enhances the efficiency, reduces carbon emissions and infrastructural costs (The world bank, 2014).

The urbanisation in the eastern part of Kunming is mostly the result of the establishment of the new airport Changshui, that was officially opened in 2012. The Changshui Airport is the fourth largest airport in China and connects Kunming to the primary cities in Asia (Qiyang et al., 2015). Because of this, the airport has significantly promoted the development of the urbanisation and tourism in the Yunnan Province (Jian et al., 2017). The urbanisation to the south can mostly be explained by the Kunming-Yuxi integration in 2011, which is affected by topographic factors, such as the Dianchi lake and the mountains. The biggest LUCC that happened in the south is the conversion of agricultural land into urban LCZs. Especially open high-rise (LCZ 4), open mid-rise (LCZ 5) and large low-rise (LCZ 8) have been built there. The establishment of areas with open high-rise (LCZ 4) and open mid-rise (LCZ 5) to the south of the centre is probably due to the combination of the Kunming-Yuxi integration (Gao et al., 2017), the new planning framework (Qiyang et al., 2015) and the need for more compact and green residences. The increase of large low-rise (LCZ 8) to the south of the centre can be the result of the establishment of new businesses (e.g. flower plantation and horticulture in the south) as a result of industrialisation and economic growth.

Especially for 2017, areas with open high-rise (LCZ 4) are more commonly seen in the centre. This can be due to the combination of expansion, densification and the desire to create a greener environment. The expansion and densification is necessary because of increasing population and less available land. Because of this, apartment buildings with more floors can be desired. The choice for LCZs with more green is the result of the bigger awareness of the need for a better living environment (Wang et al., 2012), especially in terms of air quality. Trees in streets are important for improving the urban environment (Wang et al., 2018) and have multiple advantages. The trees provide ecosystem services

that improve the quality of the environment and human life. The trees can conserve energy, remove air pollutants, sequester CO₂ and reduce storm water runoff (Armson et al., 2013; McPherson et al., 2016; Soares et al., 2011). Nevertheless, the trees also produce volatile organic compounds (VOC) and can disturb the upward airflow when streets are narrow and trees are close to each other (Nowak et al., 2000). In case of the open LCZs, there is more open space and these negative effects should not be a problem. In terms of human life, it creates a more pleasant living environment and can increase real estate values by increasing the attractiveness and recreational opportunities (Wang et al., 2018).

Changes in LST

The urban expansion is also visible on the LST maps. The rapid urbanisation in Kunming has altered the local thermal environment, especially by increasing the LST in the zones surrounding the urban core. This confirms the study of Zhou & Wang (2010). Between 2005 and 2017, the areas with higher LSTs have increased sharply. The LST increased mostly in areas that were converted from vegetated land, such as forests and agricultural land, to built-up land. This change consists of multiple stages. In the first stage, vegetation is removed and the surface energy balance changed. This increases the sensible heat flux at the cost of the latent heat flux, due to the loss of evapotranspiration (Owen et al., 1998). The second stage is the conversion of bare soil into impervious surface, which changes the moisture balance. This reduces the water storage of the land and further strengthens the sensible heat flux. In addition, the thermal environment gets warmer due to the modifications in the thermal properties of the land surface, such as heat capacity and thermal conductivity (Li et al., 2009). In the last stage, the impervious surface is developed and the resulting built-up areas facilitate the absorption of solar radiation. This whole process causes the increase of areas with higher LSTs from 2005 to 2017. Besides the Land use change, the increased human population and industrial activities also contribute to the changing urban thermal environment by rising the anthropogenic heat discharge.

5.4 sUHI assessment

The sUHI has an increasing trend between 2004 and 2017 and increased with 1.53 °C. This is due to the positive relationship between sUHI and urban area size, where a doubling of urban area can result in an increase in sUHI of 0.7 °C (Zhou et al., 2017). The size of the urban area can explain almost 87% of the sUHI, but with large spatial and temporal variations. The positive correlation between sUHI and the urban area size is higher in regions where the thermal characteristics of the surrounding landcover is more homogeneous. This is the case in Kunming where the urban areas are surrounded by large areas of homogeneous forest and agricultural land (Li et al., 2017). The urban area in 2005 (444.20 km²) has almost tripled in 2017 (1245.49 km²), which lead to even a higher increase in sUHI than expected according to Li et al. (2017).

The reason why the sUHI increases with increasing size of urban area is due to the lower albedo, higher thermal conductivity and larger heat capacity, which result in a higher surface heat storage that comes along with the implementation of impervious surfaces. Other sUHI-induced factors are population, energy consumption and air pollution, due to the effect on the surface-energy balance, that leads to the heating of the urban surfaces (Bohnenstengel et al., 2014). Several studies, focusing on big cities in China, have found that a higher LST is linked with an increase of patch density, aggregation and irregularity of the built-up class (Li et al., 2011; Zhou et al., 2011).

5.4.1 sUHII of the different LCZs

Whether LCZs can mitigate or intensify the sUHII is self-evidently depended on their LST regime. Different land cover types cause different feedbacks to LST, and thus to the sUHII, due to the variation of their physical and biochemical characteristics (Du et al., 2016; Jin et al., 2011; Wang et al., 2016). Besides the properties of the land cover of the LCZ, local climatic conditions, such as precipitation, temperature, soil moisture and air humidity, have influence on the correlation between urban landscapes and the UHI-effect (Peng et al., 2014; Zhao et al., 2014). These local climatic conditions are not included in this study.

The intensities of the sUHIs are different in the LCZs. The LCZs that intensify the sUHII of Kunming the most are heavy industry (LCZ 10), large low-rise (LCZ 8), compact mid-rise (LCZ 2) and compact low-rise (LCZ 3). The LCZs that mitigate the sUHII are dense trees (LCZ A) and water (LCZ G). This is the case for all the three different years and is due to the characteristics of the land cover type in these zones, which are already discussed in the section of the LST regime in the LCZ.

For most of the LCZs, the sUHII increases between 2004 and 2017, except for open mid-rise (LCZ 5), dense trees (LCZ A) and scattered trees (LCZ B), where the sUHII is the highest in 2012 instead of 2017. This can be due to more bare soil in 2012 for dense trees (LCZ A) and scattered trees (LCZ B), which will lead to a higher LST than normally is expected since the LST of bare soil or sand (LCZ F) is higher than the land cover in these zones. For open mid-rise (LCZ 5), the higher sUHII in 2012 can be due to higher accuracy of the classification of the zone, compared to 2004 and 2017.

In general, the biggest increase in sUHII of the LCZs is seen between 2004 and 2012. This is because of the amount of converted land in that time period, which is larger than between 2012 and 2017, due to the greater urban expansion and due to the larger time period in between. These two reason are evidently correlated with each other.

Between 2004 and 2012, compact mid-rise (LCZ 3), open mid-rise (LCZ 5), open low-rise (LCZ 6) and large low-rise (LCZ 8) zones have the largest difference in sUHII. This is probably due to densification and land cover changes where natural LCZs are converted into urban LCZs, f.e. in 2004 zones with compact low-rise (LCZ 3) are mostly surrounded by agricultural land, while in 2012, some of the compact low-rise (LCZ 3) will be surrounded by other built-up area. This will result in less heat that can escape due to the surrounding buildings. For large low-rise (LCZ 8), an additional reason can be due to the increasing area of neighbouring heavy industry (LCZ 10). This causes a warmer LST for large low-rise (LCZ 8) than when it would be surrounded by other built-up area or natural land cover.

Between 2012 and 2017, the biggest difference in sUHII is seen in heavy industry (LCZ 10), bush and scrub (LCZ C) and low plants (LCZ D). For heavy industry (LCZ 10), it can be the result of densification in its surrounding areas. For bush and scrub (LCZ C) and low plants (LCZ D), this can be due to the amount of bare soil or sand (LCZ F), which has a larger LST than the LST in these LCZs. The presence of bare soil in bush and scrub (LCZ C) can be due to natural open spaces. For low plants (LCZ D), it can be due to fallow farmland or conversion to other built-up area since the LCZ map is from 2011 and conversion could be missed in the overlay with the LST map of 2012.

5.4.2 sUHI for 2017 in general

For the situation in 2017, high sUHI are found in most of the urban regions of Kunming. Especially compact LCZs, large low-rise (LCZ 8) and heavy industry (LCZ 10) have a higher LST and have thus a higher UHI intensity. Compact LCZs have a higher sUHI because of its urban topography, also known as the 'canyon effect' (Oke, 1982), the population density and the absence of green elements. These results confirm the study of Cai et al. (2017). While urban LCZs can increase the sUHI intensity, water (LCZ G) and natural LCZs are important to mitigate the sUHI-effect. Due to the plan to incorporate more green parks in the city, the urban thermal environment could be moderated and can help to decrease the sUHI intensity in these urban zones.

6. Conclusion

Drivers of urbanisation in Kunming are a combination of general drivers in China on the one hand and specific drivers in Kunming on the other hand. In China, urbanisation is mostly driven by economic growth (Chow, 2004) and rural to urban migration, whereby the latter is due to in-situ urbanisation of rural areas and natural population growth (Gong et al., 2012). In addition, Kunming is led by urbanisation plans (e.g. world horticultural expo in 1999, the new planning framework in 2003 and the new model of urbanisation in 2012; Qiyan et al., 2015) and social-economic, topographic (e.g. mountains, flat regions) and proximity factors (Gao et al., 2018).

Accurate LCZ maps of 2005, 2011 and 2017 can be generated using a moving window with respectively a kernel size of 9x9, 7x7 and 5x5. The need for smaller kernel sizes of the later years can be explained by the urban development in Kunming. Kunming is characterised by a rapid urbanisation between 2005 and 2017. In the period between 2005 and 2011, there was mostly a conversion of agricultural land into urban LCZs in order to expand the city for residences or industrial zones. Starting from 2011 onwards, expansion decreased and focus changed to densification, where smaller plots with mix land uses are built over larger homogeneous areas with only one land use or one built up type (The world bank, 2014). In addition, there is a slow conversion of low and compact building zones to higher and more open building zones. This is an approach to have a more compact and green city. This trend is visible on the LCZ maps looking at the increasing areas with open high-rise (LCZ 4) and open mid-rise (LCZ 5). Next to the more compact and green residences, areas with large low-rise (LCZ 8) increased due to industrialisation of the city. As a result of land cover changes, urban expansion and densification, changes in the thermal climate of the city is inevitable. The urban expansion is in general responsible for higher surface temperatures due to concretisation, increasing anthropogenic heat and building areas, which is visible on the LST maps of 2004, 2012 and 2017. Nevertheless, the impact of urbanisation can be influenced by building type, density, greenery and location. Higher LSTs are found in areas with heavy industry (LCZ 10), large low-rise (LCZ 8), compact mid-rise (LCZ 2) and compact low-rise (LCZ 3). The higher surface temperature in heavy industry (LCZ 10) is caused by industrial activities and building materials of the factories. Furthermore, zones located around heavy industry are prone to having a higher surface temperature as a result of thermal buffer around these areas (Abdelnasser & El Shirbeny, 2016). Since areas with large low-rise (LCZ 8) are often located near heavy industry (LCZ 10), the thermal buffer can be a reason for the higher mean LST in these zones. The LST of compact mid- and low-rise (LCZ 2 and LCZ 3) is somewhat lower than the LST of large low-rise (LCZ 8) and heavy industry (LCZ 10). The reason for higher surface temperatures in these zones can be due to the central location, sky view factor (Scarano & Sobrino, 2015), anthropogenic heat flux, high population density and the absence of green elements (Chakraborty et al., 2015; Meng, 2017). Areas with higher LSTs have the possibility to increase sUHI, while areas with lower LSTs can lower the sUHI. In Kunming, only areas with dense trees (LCZ A) and water (LCZ G) can mitigate the sUHI-effect. Between 2005 and 2017, an increase is seen in sUHI, which is, among others, the result of the strong urbanisation. This increase in sUHI can cause heat stress in specific locations at certain points of time. Especially the centre of Kunming is prone to heat stress. Knowledge of the sUHI of the different LCZs, and its characteristics is therefore important for future urbanisation plans.

In the current plans, attempts will be made to limit further increase of (s)UHI and to achieve a more sustainable urbanisation (e.g. the 37 new green parks in Kunming, Scally 2011). In addition, promoting electric cars (Shirouzu & Jourdan, 2017), greenroofs (Xiao et al., 2014) and decreasing polluting

industry (Nace, 2017) is raising in China. Other measurements that can help mitigate the sUHI are sprinkling and watering surfaces of buildings, using building materials with lower albedo, reducing anthropogenic heat and using more pervious surfaces (Meng, 2017).

7. Further Research

With the expectation of a further population increase and climate change challenges, Kunming is still in a developing phase, especially since its current environmental goals are not yet achieved. Because of this, further research can be conducted on the following up of the urbanisation in Kunming, with emphasis on future urbanisation plans, the feasibility of the plans and their impact on social, cultural, economic and environmental level.

Bibliography

- Abdelnasser, R., & El Shirbeny, M. (2016). Impact of Industrial Activities on Land Surface Temperature Using Remote Sensing and GIS Techniques - A Case Study in Jubail, Saudi Arabia. *Journal of Geography & Natural Disasters*, *s6*. <https://doi.org/10.4172/2167-0587.S6-002>
- Akbari, H., & Levinson, R. (2008). Evolution of cool-roof standards in the US. *Advances in Building Energy Research*, *2*(1), 1–32. <https://doi.org/10.3763/aber.2008.0201>
- Angel, S., & Sheppard, S. (2005). *The dynamics of global urban expansion. Transport and Urban ...* <https://doi.org/10.1038/nature09440>
- Armson, D., Stringer, P., & Ennos, A. R. (2013). The effect of street trees and amenity grass on urban surface water runoff in Manchester, UK. *Urban Forestry and Urban Greening*, *12*(3), 282–286. <https://doi.org/10.1016/j.ufug.2013.04.001>
- Baigent, E. (2004). Patrick Geddes, Lewis Mumford and Jean Gottmann: divisions over “megalopolis.” *Progress in Human Geography*, *28*, 687–700. <https://doi.org/10.1191/0309132504ph514oa>
- Bechtel, B., Alexander, P., Böhner, J., Ching, J., Conrad, O., Feddema, J., ... Stewart, I. (2015). Mapping Local Climate Zones for a Worldwide Database of the Form and Function of Cities. *ISPRS International Journal of Geo-Information*, *4*(1), 199–219. <https://doi.org/10.3390/ijgi4010199>
- Bechtel, B., Demuzere, M., Sismanidis, P., Fenner, D., Brousse, O., Beck, C., ... Verdonck, M.-L. (2017). Quality of Crowdsourced Data on Urban Morphology—The Human Influence Experiment (HUMINEX). *Urban Science*, *1*(2), 15. <https://doi.org/10.3390/urbansci1020015>
- Bédard, F., Reichert, G., Dobbins, R., & Trépanier, I. (2008). Evaluation of segment-based gap-filled Landsat ETM+ SLC-off satellite data for land cover classification in southern Saskatchewan, Canada. *International Journal of Remote Sensing*, *29*(7), 2041–2054. <https://doi.org/10.1080/01431160701281064>
- Bettencourt, L. M. A., Lobo, J., Strumsky, D., & West, G. B. (2010). Urban scaling and its deviations: Revealing the structure of wealth, innovation and crime across cities. *PLoS ONE*, *5*(11). <https://doi.org/10.1371/journal.pone.0013541>
- Bohnenstengel, S. I., Hamilton, I., Davies, M., & Belcher, S. E. (2014). Impact of anthropogenic heat emissions on London’s temperatures. *Quarterly Journal of the Royal Meteorological Society*, *140*(679), 687–698. <https://doi.org/10.1002/qj.2144>
- Bonafoni, S., Baldinelli, G., Verducci, P., & Presciutti, A. (2017). Remote sensing techniques for urban heating analysis: A case study of sustainable construction at district level. *Sustainability (Switzerland)*, *9*(8). <https://doi.org/10.3390/su9081308>
- Breiman, L. (1999). Random Forests. *Machine Learning*, *45*(5), 1–35. <https://doi.org/10.1023/A:1010933404324>
- Cai, M., Ren, C., Xu, Y., Lau, K. K.-L., & Wang, R. (2017). Investigating the relationship between local climate zone and land surface temperature using an improved WUDAPT methodology – A case study of Yangtze River Delta, China. *Urban Climate*. <https://doi.org/10.1016/j.uclim.2017.05.010>
- Chakraborty, S. D., Kant, Y., & Mitra, D. (2015). Assessment of land surface temperature and heat fluxes over Delhi using remote sensing data. *Journal of Environmental Management*, *148*, 143–152. <https://doi.org/10.1016/j.jenvman.2013.11.034>

- Chan, C. K., & Yao, X. (2008). Air pollution in mega cities in China. *Atmospheric Environment*.
<https://doi.org/10.1016/j.atmosenv.2007.09.003>
- Chander, G., Markham, B. L., Micijevic, E., Teillet, P. M., & Helder, D. L. (2005). Improvement in absolute calibration accuracy of Landsat-5 TM with Landsat-7 ETM+ data, 5882, 588209.
<https://doi.org/10.1117/12.620136>
- Changnon, S. A., Kunkel, K. E., & Reinke, B. C. (1996). Impacts and responses to the 1995 heat wave: A call to action. *Bulletin of the American Meteorological Society*, 77(7), 1497–1506.
[https://doi.org/10.1175/1520-0477\(1996\)077<1497:IARTTH>2.0.CO;2](https://doi.org/10.1175/1520-0477(1996)077<1497:IARTTH>2.0.CO;2)
- Chen, X. L., Zhao, H. M., Li, P. X., & Yin, Z. Y. (2006). Remote sensing image-based analysis of the relationship between urban heat island and land use/cover changes. *Remote Sensing of Environment*, 104(2), 133–146. <https://doi.org/10.1016/j.rse.2005.11.016>
- Chow, G. C. (2004). Economic reform and growth in China. *Annals of Economics and Finance.*, 152, 127–152. Retrieved from <http://down.aefweb.net/AefArticles/aef050107.pdf>
- Chow, W. T. L., & Roth, M. (2006). Temporal dynamics of the urban heat island o Singapore. *International Journal of Climatology*, 26(26), 2243–2260. <https://doi.org/10.1002/joc>
- Clarke, J. F. (1972). Some effects of the urban structure on heat mortality. *Environmental Research*, 5(1), 93–104. [https://doi.org/10.1016/0013-9351\(72\)90023-0](https://doi.org/10.1016/0013-9351(72)90023-0)
- Clinton, N., & Gong, P. (2013). MODIS detected surface urban heat islands and sinks: Global locations and controls. *Remote Sensing of Environment*, 134, 294–304.
<https://doi.org/10.1016/j.rse.2013.03.008>
- Crane, P., & Kinzig, A. (2005). Nature in the metropolis. *Science (New York, N.Y.)*, 308(5726), 1225.
<https://doi.org/10.1126/science.1114165>
- Cui, Y., Xu, X., Dong, J., & Qin, Y. (2016). Influence of urbanization factors on surface urban heat island intensity: A comparison of countries at different developmental phases. *Sustainability (Switzerland)*, 8(8). <https://doi.org/10.3390/su8080706>
- Dash, P., Göttsche, F. M., Olesen, F. S., & Fischer, H. (2005). Separating surface emissivity and temperature using two-channel spectral indices and emissivity composites and comparison with a vegetation fraction method. *Remote Sensing of Environment*, 96(1), 1–17.
<https://doi.org/10.1016/j.rse.2004.12.023>
- Dobrovolný, P., & Krahula, L. (2015). The spatial variability of air temperature and nocturnal urban heat island intensity in the city of Brno, Czech Republic. *Moravian Geographical Reports*, 23(3), 8–16. <https://doi.org/10.1515/mgr-2015-0013>
- Du, H., Wang, D., Wang, Y., Zhao, X., Qin, F., Jiang, H., & Cai, Y. (2016). Influences of land cover types, meteorological conditions, anthropogenic heat and urban area on surface urban heat island in the Yangtze River Delta Urban Agglomeration. *Science of the Total Environment*, 571, 461–470.
<https://doi.org/10.1016/j.scitotenv.2016.07.012>
- EPA. (2008). Urban heat island basics. In *Reducing Urban Heat Islands: Compendium of Strategies / Heat Island Effect / US EPA* (p. 22). Retrieved from <http://www.epa.gov/heatisland/resources/compendium.htm>
- ESA. (2017). Land Surface Temperature. Retrieved from <https://sentinel.esa.int/web/sentinel/user-guides/sentinel-3-slstr/overview/geophysical-measurements/land-surface-temperature>
- Esch, T., Marconcini, M., Felbier, A., Roth, A., Heldens, W., Huber, M., ... Dech, S. (2013). Urban footprint processor-Fully automated processing chain generating settlement masks from global

- data of the TanDEM-X mission. *IEEE Geoscience and Remote Sensing Letters*, 10(6), 1617–1621. <https://doi.org/10.1109/LGRS.2013.2272953>
- Fang, C., & Yu, D. (2017). Urban agglomeration: An evolving concept of an emerging phenomenon. *Landscape and Urban Planning*, 162, 126–136. <https://doi.org/10.1016/j.landurbplan.2017.02.014>
- Fast, J. D., Torcolini, J. C., & Redman, R. (2005). Pseudovertical Temperature Profiles and the Urban Heat Island Measured by a Temperature Datalogger Network in Phoenix, Arizona. *Journal of Applied Meteorology*, 44, 3–13. <https://doi.org/10.1175/JAM-2176.1>
- Fund, U. N. P. (2007). UNFPA state of world population 2007: unleashing the potential of urban growth. *United Nations Population Fund*.
- Galve, J. M., Coll, C., Caselles, V., Valor, E., & Mira, M. (2008). Comparison of split-window and single-channel methods for land surface temperature retrieval from MODIS and aatsr data. In *International Geoscience and Remote Sensing Symposium (IGARSS) (Vol. 3)*. <https://doi.org/10.1109/IGARSS.2008.4779341>
- Gao, W., Wang, Y., Wang, B., Yang, Z., & Zhiming, Z. (2018). The urban agglomeration processes of Kunming and Yuxi cities driving by political driving forces in plateau of Yunnan, Southwest of China.
- Geletič, J., Lehnert, M., & Dobrovolný, P. (2016). Land surface temperature differences within local climate zones, Based on two central European cities. *Remote Sensing*, 8(10). <https://doi.org/10.3390/rs8100788>
- Gong, P., Liang, S., Carlton, E. J., Jiang, Q., Wu, J., Wang, L., & Remais, J. V. (2012). Urbanisation and health in China. *The Lancet*. [https://doi.org/10.1016/S0140-6736\(11\)61878-3](https://doi.org/10.1016/S0140-6736(11)61878-3)
- Gottmann, J. (1957). Megalopolis or the urbanization of the northeastern seaboard. *Economic Geography*, 33(3), 189–200. <https://doi.org/10.1126/science.11.277.620>
- Grimm, N. B., Faeth, S. H., Golubiewski, N. E., Redman, C. L., Wu, J., Bai, X., & Briggs, J. M. (2008). Global Change and the Ecology of Cities. *Science*, 319(5864), 756–760. <https://doi.org/10.1126/science.1150195>
- Guo, Y., Zeng, H., Zheng, R., Li, S., Barnett, A. G., Zhang, S., ... Williams, G. (2016). The association between lung cancer incidence and ambient air pollution in China: A spatiotemporal analysis. *Environmental Research*, 144, 60–65. <https://doi.org/10.1016/j.envres.2015.11.004>
- Gutman, G., Byrnes, R., Masek, J. G., Covington, S., Justice, C. O., Franks, S., & Headley, R. (2008). Towards monitoring land-cover and land-use changes at a global scale: The Global Land Survey 2005. *Photogrammetric Engineering and Remote Sensing*, 75(1), 6–10.
- Haacke, O. (2015). Understanding China's 13th five-year plan. *China Business Review*.
- Haaland, C., & van den Bosch, C. K. (2015). Challenges and strategies for urban green-space planning in cities undergoing densification: A review. *Urban Forestry and Urban Greening*. <https://doi.org/10.1016/j.ufug.2015.07.009>
- Hakim, G. J., Snyder, C., & Muraki, D. J. (2002). A New Surface Model for Cyclone – Anticyclone Asymmetry. *Journal of the Atmospheric Sciences*, 59(16), 2405–2420.
- Hossain, M. S., Bujang, J. S., Zakaria, M. H., & Hashim, M. (2015). Assessment of the impact of Landsat 7 Scan Line Corrector data gaps on Sungai Pulai Estuary seagrass mapping. *Applied Geomatics*, 7(3), 189–202. <https://doi.org/10.1007/s12518-015-0162-3>

- Huang, B., Wang, B., Ren, D., Jin, W., Liu, J., Peng, J., & Pan, X. (2013). Occurrence, removal and bioaccumulation of steroid estrogens in Dianchi Lake catchment, China. *Environment International*, *59*, 262–273. <https://doi.org/10.1016/j.envint.2013.06.018>
- Huang, R.-J., Zhang, Y., Bozzetti, C., Ho, K.-F., Cao, J.-J., Han, Y., ... Prévôt, A. S. H. (2014). High secondary aerosol contribution to particulate pollution during haze events in China. *Nature*. <https://doi.org/10.1038/nature13774>
- Imhoff, M. L., Zhang, P., Wolfe, R. E., & Bounoua, L. (2010). Remote sensing of the urban heat island effect across biomes in the continental USA. *Remote Sensing of Environment*, *114*(3), 504–513. <https://doi.org/10.1016/j.rse.2009.10.008>
- Jian, H., Pan, H., Xiong, G., & Lin, X. (2017). The Impacts of Civil Airport layout to Yunnan Local Tourism Industry. In *Transportation Research Procedia* (Vol. 25, pp. 77–91). <https://doi.org/10.1016/j.trpro.2017.05.383>
- Jimenez-Munoz, J. C., Cristobal, J., Sobrino, J. A., Sòria, G., Ninyerola, M., & Pons, X. (2009). Revision of the single-channel algorithm for land surface temperature retrieval from landsat thermal-infrared data. *IEEE Transactions on Geoscience and Remote Sensing*, *47*(1), 339–349. <https://doi.org/10.1109/TGRS.2008.2007125>
- Jiménez-Muñoz, J. C., & Sobrino, J. A. (2006). Error sources on the land surface temperature retrieved from thermal infrared single channel remote sensing data. *International Journal of Remote Sensing*, *27*(5), 999–1014. <https://doi.org/10.1080/01431160500075907>
- Jin, M., Dickinson, R. E., & Zhang, D. L. (2005). The footprint of urban areas on global climate as characterized by MODIS. *Journal of Climate*, *18*(10), 1551–1565. <https://doi.org/10.1175/JCLI3334.1>
- Jin, M. S., Kessomkiat, W., & Pereira, G. (2011). Satellite-observed urbanization characters in Shanghai, China: Aerosols, urban heat Island effect, and land-atmosphere interactions. *Remote Sensing*, *3*(1), 83–99. <https://doi.org/10.3390/rs3010083>
- Kaloustian, N., & Bechtel, B. (2016). Local Climatic Zoning and Urban Heat Island in Beirut. In *Procedia Engineering* (Vol. 169, pp. 216–223). <https://doi.org/10.1016/j.proeng.2016.10.026>
- Kanmei, H., & Minqi, S. (2017). The Investigation and Analysis about the Problem of the House for the Elderly — Taking the Evergreen Apartment in Kunming for Example Huang Kanmei and Shen Minqi, *48*, 481–488.
- Karl, T. R., & Quayle, R. G. (1988). Climate change in fact and in theory: Are we collecting the facts? *Climatic Change*, *13*(1), 5–17. <https://doi.org/10.1007/BF00140159>
- Katzschner, A., Waibel, M., Schwede, D., Katzschner, L., Schmidt, M., & Storch, H. (2015). *Sustainable Ho Chi Minh City: Climate policies for emerging mega cities. Sustainable Ho Chi Minh City: Climate Policies for Emerging Mega Cities*. <https://doi.org/10.1007/978-3-319-04615-0>
- Kim, H. H. (1992). Urban heat island. *International Journal of Remote Sensing*, *13*(12), 2319–2336. <https://doi.org/10.1080/01431169208904271>
- Kim, Y.-H., & Baik, J.-J. (2002). Maximum Urban Heat Island Intensity in Seoul. *Journal of Applied Meteorology*, *41*(6), 651–659. [https://doi.org/10.1175/1520-0450\(2002\)041<0651:MUHIII>2.0.CO;2](https://doi.org/10.1175/1520-0450(2002)041<0651:MUHIII>2.0.CO;2)
- Kipnis, B. A. (1997). Dynamics and Potentials of Israel's Megalopolitan Processes. *Urban Studies*, *34*(3), 489–501. <https://doi.org/10.1080/0042098976096>
- Konopacki, S., & Akbari, H. (2002). Energy Savings of Heat-Island Reduction Strategies in Chicago and

- Houston (Including Updates for Baton Rouge, Sacramento, and Salt Lake City). *Energy*, (February), 1–53. <https://doi.org/LBNL-49638>
- Kotthaus, S., & Grimmond, C. S. B. (2012). Identification of Micro-scale Anthropogenic CO₂, heat and moisture sources - Processing eddy covariance fluxes for a dense urban environment. *Atmospheric Environment*, 57, 301–316. <https://doi.org/10.1016/j.atmosenv.2012.04.024>
- Kovats, R. S., & Hajat, S. (2008). Heat Stress and Public Health: A Critical Review. *Annual Review of Public Health*, 29(1), 41–55. <https://doi.org/10.1146/annurev.publhealth.29.020907.090843>
- Li, F. (2016). Physical activity and health in the presence of China's economic growth: Meeting the public health challenges of the aging population. *Journal of Sport and Health Science*. <https://doi.org/10.1016/j.jshs.2016.06.004>
- Li, J., Song, C., Cao, L., Zhu, F., Meng, X., & Wu, J. (2011). Impacts of landscape structure on surface urban heat islands: A case study of Shanghai, China. *Remote Sensing of Environment*, 115(12), 3249–3263. <https://doi.org/10.1016/j.rse.2011.07.008>
- Li, J., Wang, X., Wang, X., Ma, W., & Zhang, H. (2009). Remote sensing evaluation of urban heat island and its spatial pattern of the Shanghai metropolitan area, China. *Ecological Complexity*, 6(4), 413–420. <https://doi.org/10.1016/j.ecocom.2009.02.002>
- Li, X., Zhou, W., & Ouyang, Z. (2013). Forty years of urban expansion in Beijing: What is the relative importance of physical, socioeconomic, and neighborhood factors? *Applied Geography*, 38(1), 1–10. <https://doi.org/10.1016/j.apgeog.2012.11.004>
- Li, X., Zhou, Y., Asrar, G. R., Imhoff, M., & Li, X. (2017). The surface urban heat island response to urban expansion: A panel analysis for the conterminous United States. *Science of the Total Environment*, 605–606, 426–435. <https://doi.org/10.1016/j.scitotenv.2017.06.229>
- Li, Y., Zhu, L., Zhao, X., Li, S., & Yan, Y. (2013). Urbanization impact on temperature change in china with emphasis on land cover change and human activity. *Journal of Climate*, 26(22), 8765–8780. <https://doi.org/10.1175/JCLI-D-12-00698.1>
- Li, Z.-L., Tang, B.-H., Wu, H., Ren, H., Yan, G., Wan, Z., ... Sobrino, J. a. (2013). Satellite-derived land surface temperature: Current status and perspectives. *Remote Sensing of Environment*, 131, 14–37. <https://doi.org/10.1016/j.rse.2012.12.008>
- Li, Z.-L., Wu, H., Wang, N., Qiu, S., Sobrino, J. A., Wan, Z., ... Yan, G. (2013). Land surface emissivity retrieval from satellite data. *International Journal of Remote Sensing*, 34(9–10), 3084–3127. <https://doi.org/10.1080/01431161.2012.716540>
- Lillesand, T., Kiefer, R., & Chipman, J. (2015). *Remote sensing and image interpretation Seventh Ed.* John Wiley and Sons, Inc., New York.
- Linh, N. H. K., & Van Chuong, H. (2015). Assessing the impact of urbanization on urban climate by remote sensing perspective: A case study in Danang city, Vietnam. In *International Archives of the Photogrammetry, Remote Sensing and Spatial Information Sciences - ISPRS Archives* (Vol. 40, pp. 207–212). <https://doi.org/10.5194/isprsarchives-XL-7-W3-207-2015>
- Liu, Y., He, S., Wu, F., & Webster, C. (2010). Urban villages under China's rapid urbanization: Unregulated assets and transitional neighbourhoods. *Habitat International*, 34(2), 135–144. <https://doi.org/10.1016/j.habitatint.2009.08.003>
- Lo, C. P., & Quattrochi, D. A. (2003). Land-use and land-cover change, urban heat island phenomenon, and health implications: A remote sensing approach. *Photogrammetric Engineering and Remote Sensing*, 69(9), 1053–1063.

<https://doi.org/https://doi.org/10.14358/PERS.69.9.1053>

- Luo, J., & Wei, Y. H. D. (2009). Modeling spatial variations of urban growth patterns in Chinese cities: The case of Nanjing. *Landscape and Urban Planning*, *91*(2), 51–64. <https://doi.org/10.1016/j.landurbplan.2008.11.010>
- Malekipirbazari, M., & Aksakalli, V. (2015). Risk assessment in social lending via random forests. *Expert Systems with Applications*, *42*(10), 4621–4631. <https://doi.org/10.1016/j.eswa.2015.02.001>
- Mao, X., Zhou, J., & Corsetti, G. (2014). How well have Chinas recent five-year plans been implemented for energy conservation and air pollution control? *Environmental Science and Technology*, *48*(17), 10036–10044. <https://doi.org/10.1021/es501729d>
- Martin, P., Baudouin, Y., & Gachon, P. (2015). An alternative method to characterize the surface urban heat island. *Int J Biometeorol*, *59*(7), 849–861. <https://doi.org/10.1007/s00484-014-0902-9>
- Maxwell, S. K., Schmidt, G. L., & Storey, J. C. (2007). A multi-scale segmentation approach to filling gaps in Landsat ETM+ SLC-off images. *International Journal of Remote Sensing*, *28*(23), 5339–5356. <https://doi.org/10.1080/01431160601034902>
- McPherson, E. G., van Doorn, N., & de Goede, J. (2016). Structure, function and value of street trees in California, USA. *Urban Forestry and Urban Greening*, *17*, 104–115. <https://doi.org/10.1016/j.ufug.2016.03.013>
- Memon, A. R., Leung, D., & Chunho, L. (2008). A review on the generation, determination and mitigation of Urban Heat Island. *Journal of Environmental Sciences*, *20*(1), 120–128. [https://doi.org/10.1016/S1001-0742\(08\)60019-4](https://doi.org/10.1016/S1001-0742(08)60019-4)
- Meng, C. (2017). Mitigating the surface urban heat island: Mechanism study and sensitivity analysis. *Asia-Pacific Journal of Atmospheric Sciences*, *53*(3), 327–338.
- Mingers, J. (1989). An Empirical Comparison of Pruning Methods for Decision Tree Induction. *Machine Learning*, *4*(2), 227–243. <https://doi.org/10.1023/A:1022604100933>
- Mölders, N. (2012). Impact of Land-Cover and Land-Cover Changes. In *Land-Use and Land-Cover Changes: Impact on Climate and Air Quality* (pp. 39–115). https://doi.org/10.1007/978-94-007-1527-1_3
- Nace, T. (2017). China Shuts Down Tens Of Thousands Of Factories In Widespread Pollution Crackdown. *Forbes*. Retrieved from <https://www.forbes.com/sites/kpmg/2018/04/23/the-changing-nature-of-work-why-lifelong-learning-matters-more-than-ever/#1b14ebec1e95>
- National Bureau of Statistics of China. (2004). China statistical yearbook. *Beijing: Chinese Statistical Bureau*, 62791819. <https://doi.org/http://www.stats.gov.cn/tjsj/ndsj/2007/indexee.htm>
- Nikam, B. R., Ibragimov, F., Chouksey, A., Garg, V., & Aggarwal, S. P. (2016). Retrieval of land surface temperature from Landsat 8 TIRS for the command area of Mula irrigation project. *Environmental Earth Sciences*, *75*(16). <https://doi.org/10.1007/s12665-016-5952-3>
- Nowak, D. J., Civerolo, K. L., Trivikrama Rao, S., Gopal Sistla, Luley, C. J., & E. Crane, D. (2000). A modeling study of the impact of urban trees on ozone. *Atmospheric Environment*, *34*(10), 1601–1613. [https://doi.org/10.1016/S1352-2310\(99\)00394-5](https://doi.org/10.1016/S1352-2310(99)00394-5)
- Nyambod, E. M. (2010). Environmental Consequences of Rapid Urbanisation: Bamenda City, Cameroon. *Journal of Environmental Protection*, *1*(1), 15–23. <https://doi.org/10.4236/jep.2010.11003>

- Oke, T. R. (1982). The energetic basis of the urban heat island. *Quarterly Journal of the Royal Meteorological Society*, 108(455), 1–24. <https://doi.org/10.1002/qj.49710845502>
- Oke, T. R. (1987). *Boundary Layer Climates. Earth-Science Reviews* (Vol. 27). [https://doi.org/10.1016/0012-8252\(90\)90005-G](https://doi.org/10.1016/0012-8252(90)90005-G)
- Owen, T. W., Carlson, T. N., & Gillies, R. R. (1998). An assessment of satellite remotely-sensed land cover parameters in quantitatively describing the climatic effect of urbanization. *International Journal of Remote Sensing*, 19(9), 1663–1681. <https://doi.org/10.1080/014311698215171>
- Pachauri, R. K., Allen, M. R., Barros, V. R., Broome, J., Cramer, W., Christ, R., ... van Ypersele, J. P. (2014). Climate Change 2014: Synthesis Report. Contribution of Working Groups I, II and III to the Fifth Assessment Report of the Intergovernmental Panel on Climate Change. *EPIC3 Geneva, Switzerland, IPCC, 151 P., Pp. 151, ISBN: 978-92-9169-143-2*. Retrieved from <http://epic.awi.de/37530/%5Cnpapers2://publication/uuid/27ADFB35-E92B-458D-AB50-DFA2153F5FCF>
- Pal, M., & Mather, P. M. (2003). An assessment of the effectiveness of decision tree methods for land cover classification. *Remote Sensing of Environment*, 86(4), 554–565. [https://doi.org/10.1016/S0034-4257\(03\)00132-9](https://doi.org/10.1016/S0034-4257(03)00132-9)
- Peng, S.-S., Piao, S., Zeng, Z., Ciais, P., Zhou, L., Li, L. Z. X., ... Zeng, H. (2014). Afforestation in China cools local land surface temperature. *Proceedings of the National Academy of Sciences*, 111(8), 2915–2919. <https://doi.org/10.1073/pnas.1315126111>
- Peng, S., Piao, S., Ciais, P., Friedlingstein, P., Ottle, C., Bréon, F. M., ... Myneni, R. B. (2012). Surface urban heat island across 419 global big cities. *Environmental Science and Technology*, 46(2), 696–703. <https://doi.org/10.1021/es2030438>
- Petäjä, T., Järvi, L., Kerminen, V.-M., Ding, A. J., Sun, J. N., Nie, W., ... Kulmala, M. (2016). Enhanced air pollution via aerosol-boundary layer feedback in China. *Scientific Reports*, 6(1), 18998. <https://doi.org/10.1038/srep18998>
- Peterson, T. C. (2003). Assessment of urban versus rural in situ surface temperatures in the contiguous United States: No difference found. *Journal of Climate*, 16(18), 2941–2959. [https://doi.org/10.1175/1520-0442\(2003\)016<2941:AOUVRI>2.0.CO;2](https://doi.org/10.1175/1520-0442(2003)016<2941:AOUVRI>2.0.CO;2)
- Phelan, P. E., Kaloush, K., Miner, M., Golden, J., Phelan, B., Silva, H., & Taylor, R. A. (2015). Urban Heat Island: Mechanisms, Implications, and Possible Remedies. *Annual Review of Environment and Resources*, 40(1), 285–307. <https://doi.org/10.1146/annurev-environ-102014-021155>
- Pongracz, R., Bartholy, J., & Dezso, Z. (2006). Remotely sensed thermal information applied to urban climate analysis. *Advances in Space Research*, 37(12), 2191–2196. <https://doi.org/10.1016/j.asr.2005.06.069>
- Potić, I. (2015). Simple ETM+ gap fill techniques review. *Environment Science and Policy for Sustainable Development*, 3(1), 31–37.
- Practices, U. (2010). *Planning Sustainable Cities Un-Habitat Practices. Sustainable development in Africa a multifaceted*. Retrieved from http://www.unhabitat.org/downloads/docs/GRHS_2009Brief.pdf
- Qiyang, W., Jianquan, C., Dan, L., Li, H., & Yuhong, Y. (2015). Kunming: A Regional International Mega City in Southwest China. In R. B. Singh (Ed.), *Urban Development Challenges, Risks and Resilience in Asian Mega Cities* (pp. 323–347). Springer Japan.
- Qu, W. J., Arimoto, R., Zhang, X. Y., Zhao, C. H., Wang, Y. Q., Sheng, L. F., & Fu, G. (2010). Spatial

- distribution and interannual variation of surface PM10 concentrations over eighty-six Chinese cities. *Atmospheric Chemistry and Physics*, 10(12), 5641–5662. <https://doi.org/10.5194/acp-10-5641-2010>
- Reid, W. V. (1998). Biodiversity Hotspots. *Trends in Ecology & Evolution*, 13(7), 275–280. <https://doi.org/10.1007/978-3-642-20992-5>
- Rooney, C., McMichael, A. J., Kovats, R. S., & Coleman, M. P. (1998). Excess mortality in England and Wales, and in Greater London, during the 1995 heatwave. *J Epidemiol Community Health*, 52(8), 482–486. <https://doi.org/10.1136/jech.52.8.482>
- Rosenfeld, A. H., Akbari, H., Romm, J. J., & Pomerantz, M. (1998). Cool communities: Strategies for heat island mitigation and smog reduction. *Energy and Buildings*, 28(1), 51–62. [https://doi.org/10.1016/S0378-7788\(97\)00063-7](https://doi.org/10.1016/S0378-7788(97)00063-7)
- Roth, M., Oke, T. R., & Emery, W. J. (1989). Satellite-derived urban heat islands from three coastal cities and the utilization of such data in urban climatology. *International Journal of Remote Sensing*, 10(11), 1699–1720. <https://doi.org/10.1080/01431168908904002>
- Roy, A. (2011). Re-Forming the Megacity: Calcutta and the Rural–Urban Interface. In *Megacities: Urban Form, Governance, and Sustainability* (pp. 93–109). <https://doi.org/10.1007/978-4-431-99267-7>
- Rozenstein, O., Qin, Z., Derimian, Y., & Karnieli, A. (2014). Derivation of land surface temperature for landsat-8 TIRS using a split window algorithm. *Sensors (Switzerland)*, 14(4), 5768–5780. <https://doi.org/10.3390/s140405768>
- Salisbury, J. W., & D’Aria, D. M. (1994). Emissivity of terrestrial materials in the 3-5 μm atmospheric window. *Remote Sensing of Environment*, 47(3), 345–361. [https://doi.org/10.1016/0034-4257\(94\)90102-3](https://doi.org/10.1016/0034-4257(94)90102-3)
- Scally. (2013). How bad is Kunming’s air? *Life Newspaper*.
- Scally. (2016). River diversion to flush pollution out of Yunnan’s Dianchi Lake.
- Scally. (2017). Urban re-greening effort to include 37 new Kunming parks. *News*.
- Scaramuzza, P., Micijevic, E., & Chander, G. (2004). SLC Gap-Filled Products Phase One Methodology. *Landsat Technical Notes*, 1–5.
- Scarano, M., & Sobrino, J. A. (2015). On the relationship between the sky view factor and the land surface temperature derived by Landsat-8 images in Bari, Italy. *International Journal of Remote Sensing*, 36(19–20), 4820–4835. <https://doi.org/10.1080/01431161.2015.1070325>
- See, L., Perger, C., Duerauer, M., Fritz, S., Bechtel, B., Ching, J., ... Masson, V. (2015). Developing a community-based worldwide urban morphology and materials database (WUDAPT) using remote sensing and crowdsourcing for improved urban climate modelling. In *2015 Joint Urban Remote Sensing Event, JURSE 2015*. <https://doi.org/10.1109/JURSE.2015.7120501>
- Seto, K., Guneralp, B., & Hutyrá, L. (2012). Global forecasts of urban expansion to 2030 and direct impacts on biodiversity and carbon pools. *Proceedings of the National Academy of Sciences*, 109(40), 16083–16088. <https://doi.org/10.1073/pnas.1211658109>
- Shirouzu, N., & Jourdan, A. (2017). China sets 2019 deadline for automakers to meet green-car sales targets. *Business News*.
- Singh, S. K., Srivastava, P. K., Gupta, M., Thakur, J. K., & Mukherjee, S. (2014). Appraisal of land use/land cover of mangrove forest ecosystem using support vector machine. *Environmental*

Earth Sciences, 71(5), 2245–2255. <https://doi.org/10.1007/s12665-013-2628-0>

- Smargiassi, A., Goldberg, M. S., Plante, C., Fournier, M., Baudouin, Y., & Kosatsky, T. (2009). Variation of daily warm season mortality as a function of micro-urban heat islands. *Journal of Epidemiology and Community Health*, 63(8), 659–664. <https://doi.org/10.1136/jech.2008.078147>
- Soares, A. L., Rego, F. C., McPherson, E. G., Simpson, J. R., Peper, P. J., & Xiao, Q. (2011). Benefits and costs of street trees in Lisbon, Portugal. *Urban Forestry & Urban Greening*, 10(2), 69–78. <https://doi.org/10.1016/j.ufug.2010.12.001>
- Sobrino, J. A., Caselles, V., & Coll, C. (1993). Theoretical split-window algorithms for determining the actual surface temperature. *Il Nuovo Cimento C*, 16(3), 219–236. <https://doi.org/10.1007/BF02524225>
- Sobrino, J. A., Jiménez-Muñoz, J. C., Sòria, G., Romaguera, M., Guanter, L., Moreno, J., ... Martínez, P. (2008). Land surface emissivity retrieval from different VNIR and TIR sensors. In *IEEE Transactions on Geoscience and Remote Sensing* (Vol. 46, pp. 316–327). <https://doi.org/10.1109/TGRS.2007.904834>
- Sokolova, M., & Lapalme, G. (2009). A systematic analysis of performance measures for classification tasks. *Information Processing and Management*, 45(4), 427–437. <https://doi.org/10.1016/j.ipm.2009.03.002>
- Solecki, W., Rosenzweig, C., Parshall, L., Pope, G., Clark, M., Cox, J., & Wiencke, M. (2005). Mitigation of the heat island effect in urban New Jersey. *Environmental Hazards*, 6(1), 39–49. <https://doi.org/10.1016/j.hazards.2004.12.002>
- Stewart, I. D. (2011). A systematic review and scientific critique of methodology in modern urban heat island literature. *International Journal of Climatology*. <https://doi.org/10.1002/joc.2141>
- Stewart, I. D., & Oke, T. R. (2006). Methodological Concerns Surrounding the Classification of Urban and Rural Climate Stations To Define Urban Heat Island Magnitude. In *Proceedings of the 6th International Conference on Urban Climate* (pp. 431–444).
- Stewart, I. D., & Oke, T. R. (2012). Local climate zones for urban temperature studies. *Bulletin of the American Meteorological Society*, 93(12), 1879–1900. <https://doi.org/10.1175/BAMS-D-11-00019.1>
- Stewart, I. D., Oke, T. R., Bechtel, B., Foley, M. M., Mills, G., Ching, J., ... Ce, D. (2015). Generating WUDAPT's Specific Scale -dependent Urban Modeling and Activity Parameters: Collection of Level 1 and Level 2 Data. *ICUC9, Toulouse, France (20-24 July)*, 5(4), 1–4. <https://doi.org/10.1017/CBO9781107415324.004>
- Storey, J., Scaramuzza, P., Schmidt, G., & Barsi, J. (2005). Landsat 7 Scan Line Corrector-Off Gap-Filled Product Gap-Filled Product Development Process. In *Proceedings of Pecora*, 16, 23–27. Retrieved from http://www.asprs.org/a/publications/proceedings/pecora16/Storey_J.pdf
- Streutker, D. R. (2002). A remote sensing study of the urban heat island of Houston, Texas. *International Journal of Remote Sensing*, 23(13), 2595–2608. <https://doi.org/10.1080/01431160110115023>
- Su, S., Jiang, Z., Zhang, Q., & Zhang, Y. (2011). Transformation of agricultural landscapes under rapid urbanization: A threat to sustainability in Hang-Jia-Hu region, China. *Applied Geography*, 31(2), 439–449. <https://doi.org/10.1016/j.apgeog.2010.10.008>
- Taha, H. (1997). Urban climates and heat islands: albedo, evapotranspiration, and anthropogenic

- heat. *Energy and Buildings*, 25(2), 99–103. [https://doi.org/10.1016/S0378-7788\(96\)00999-1](https://doi.org/10.1016/S0378-7788(96)00999-1)
- Teh, C. Y., Budiman, P. M., Shak, K. P. Y., & Wu, T. Y. (2016). Recent Advancement of Coagulation-Flocculation and Its Application in Wastewater Treatment. *Industrial and Engineering Chemistry Research*. <https://doi.org/10.1021/acs.iecr.5b04703>
- The state council. (2016). China announces action plan to tackle water pollution. Retrieved from http://english.gov.cn/policies/latest_releases/2015/04/16/content_281475090170164.htm
- The world bank. (2014). *Urban China: Toward Efficient, Inclusive, and Sustainable Urbanization*. Retrieved from <https://www.worldbank.org/content/dam/Worldbank/document/EAP/China/WEB-Urban-China.pdf>
- Thi Van, T., & Xuan Bao, H. D. (2010). Study of the impact of urban development on surface temperature using remote sensing in Ho Chi Minh City, Northern Vietnam. *Geographical Research*, 48(1), 86–96. <https://doi.org/10.1111/j.1745-5871.2009.00607.x>
- Tran, H., Uchihama, D., Ochi, S., & Yasuoka, Y. (2006). Assessment with satellite data of the urban heat island effects in Asian mega cities. *International Journal of Applied Earth Observation and Geoinformation*, 8(1), 34–48. <https://doi.org/10.1016/j.jag.2005.05.003>
- Un. (2004). *World Urbanization Prospects: The 2003 Revision. New York* (Vol. 17). Retrieved from http://opac.rero.ch/get_bib_record.cgi?db=ne&rero_id=R004601639
- Un-Habitat. (2003). *The Challenge of Slums - Global Report on Human Settlements. Earthscan Publications on behalf of UN-Habitat*. <https://doi.org/http://dx.doi.org/10.1108/meq.2004.15.3.337.3>
- United Nations, D. of E. and S. A.-P. D. (2014). World Urbanization Prospects: The 2014 Revision (CD-ROM Edition). *World Urbanization Prospects: The 2014 Revision, CD-ROM Edition, CD-ROM Edition*. <https://doi.org/10.4054/DemRes.2005.12.9>
- Verdonck, M., Okujeni, A., Linden, S. Van Der, & Demuzere, M. (2017). Influence of neighbourhood on Local Climate Zone mapping in heterogeneous cities. *Int J Appl Earth Obs Geoinformation*, 62(Figure 1), 1–13. <https://doi.org/10.3390/www.mdpi.com/journal/remotesensing>
- Vlassova, L., Perez-Cabello, F., Nieto, H., Martín, P., Riaño, D., & Riva, J. D. La. (2014). Assessment of methods for land surface temperature retrieval from landsat-5 TM images applicable to multiscale tree-grass ecosystem modeling. *Remote Sensing*, 6(5), 4345–4368. <https://doi.org/10.3390/rs6054345>
- Voogt, J. ., & Oke, T. . (2003). Thermal remote sensing of urban climates. *Remote Sensing of Environment*, 86(3), 370–384. [https://doi.org/10.1016/S0034-4257\(03\)00079-8](https://doi.org/10.1016/S0034-4257(03)00079-8)
- Wan, Z. (1996). A generalized split-window algorithm for retrieving land-surface temperature from space. *IEEE Transactions on Geoscience and Remote Sensing*, 34(4), 892–905. <https://doi.org/10.1109/36.508406>
- Wang, R., Tao, S., Wang, W., Liu, J., Shen, H., Shen, G., ... Ma, J. (2012). Black carbon emissions in China from 1949 to 2050. *Environmental Science and Technology*, 46(14), 7595–7603. <https://doi.org/10.1021/es3003684>
- Wang, X., Guo, W., Qiu, B., Liu, Y., Sun, J., & Ding, A. (2016). Quantifying the contribution of land use change to surface temperature in the lower reaches of Yangtze River. *Atmospheric Chemistry and Physics Discussions*, 1–13. <https://doi.org/10.5194/acp-2016-1013>
- Wang, X., Yao, J., Yu, S., Miao, C., Chen, W., & He, X. (2018). Street trees in a Chinese forest city:

- Structure, benefits and costs. *Sustainability (Switzerland)*, 10(3), 1–16.
<https://doi.org/10.3390/su10030674>
- Wu, J., Wei-Ning Xiang, & Zhao, J. (2014). Urban ecology in China: Historical developments and future directions. *Landscape and Urban Planning*, 125, 222–233.
<https://doi.org/10.1016/j.landurbplan.2014.02.010>
- Wu, N., Qiao, M., Zhang, B., Cheng, W. Da, & Zhu, Y. G. (2010). Abundance and diversity of tetracycline resistance genes in soils adjacent to representative swine feedlots in China. *Environmental Science and Technology*, 44(18), 6933–6939. <https://doi.org/10.1021/es1007802>
- Wulder, M. A., White, J. C., Masek, J. G., Dwyer, J., & Roy, D. P. (2011). Continuity of Landsat observations: Short term considerations. *Remote Sensing of Environment*, 115(2), 747–751.
<https://doi.org/10.1016/j.rse.2010.11.002>
- Xiao, M., Lin, Y., Han, J., & Zhang, G. (2014). A review of green roof research and development in China. *Renewable and Sustainable Energy Reviews*. <https://doi.org/10.1016/j.rser.2014.07.147>
- Xu, Y., Ren, C., Cai, M., Edward, N. Y. Y., & Wu, T. (2017). Classification of Local Climate Zones Using ASTER and Landsat Data for High-Density Cities. *IEEE Journal of Selected Topics in Applied Earth Observations and Remote Sensing*, 10(7), 3397–3405.
<https://doi.org/10.1109/JSTARS.2017.2683484>
- Yang, F., Tan, J., Zhao, Q., Du, Z., He, K., Ma, Y., ... Zhao, Q. (2011). Characteristics of PM_{2.5} speciation in representative megacities and across China. *Atmospheric Chemistry and Physics*, 11(11), 5207–5219. <https://doi.org/10.5194/acp-11-5207-2011>
- Yang, G., Wang, Y., Zeng, Y., Gao, G. F., Liang, X., Zhou, M., ... Murray, C. J. L. (2013). Rapid health transition in China, 1990-2010: Findings from the Global Burden of disease study 2010. *The Lancet*, 381(9882), 1987–2015. [https://doi.org/10.1016/S0140-6736\(13\)61097-1](https://doi.org/10.1016/S0140-6736(13)61097-1)
- Yang, X., & Lo, C. P. (2002). Using a time series of satellite imagery to detect land use and land cover changes in the Atlanta, Georgia metropolitan area. *International Journal of Remote Sensing*, 23(9), 1775–1798. <https://doi.org/10.1080/01431160110075802>
- Yang, Y.-H., Zhou, F., Guo, H.-C., Sheng, H., Liu, H., Dao, X., & He, C.-J. (2010). Analysis of spatial and temporal water pollution patterns in Lake Dianchi using multivariate statistical methods. *Environmental Monitoring and Assessment*, 170(1–4), 407–416.
<https://doi.org/10.1007/s10661-009-1242-9>
- Yeh, A., Xu, X. ., & Liu, K. (2011). China's post-reform urbanization: retrospect, policies and trends. *Urbanization and Population Issues*, (5).
- Yu, X., Guo, X., & Wu, Z. (2014). Land surface temperature retrieval from landsat 8 TIRS-comparison between radiative transfer equation-based method, split window algorithm and single channel method. *Remote Sensing*, 6(10), 9829–9852. <https://doi.org/10.3390/rs6109829>
- Zhang, H., Qi, Z. fang, Ye, X. yue, Cai, Y. bin, Ma, W. chun, & Chen, M. nan. (2013). Analysis of land use/land cover change, population shift, and their effects on spatiotemporal patterns of urban heat islands in metropolitan Shanghai, China. *Applied Geography*, 44, 121–133.
<https://doi.org/10.1016/j.apgeog.2013.07.021>
- Zhang, P., Imhoff, M. L., Wolfe, R. E., & Bounoua, L. (2010). Characterizing urban heat islands of global settlements using MODIS and nighttime lights products. *Canadian Journal of Remote Sensing*, 36(3), 185–196. <https://doi.org/10.5589/m10-039>
- Zhao, J.Z., Cui, S.H., Yan, C.Z. and Guo, Q. H. (2009). Theoretical thinking in sustainable city

construction of China. *Huan Jing Ke Xue= Huanjing Kexue/[bian Ji, Zhongguo Ke Xue Yuan Huan Jing Ke Xue Wei Yuan hui“ Huan Jing Ke Xue” bian Ji Wei Yuan Hui.]*, 30(4), 1244–1248.

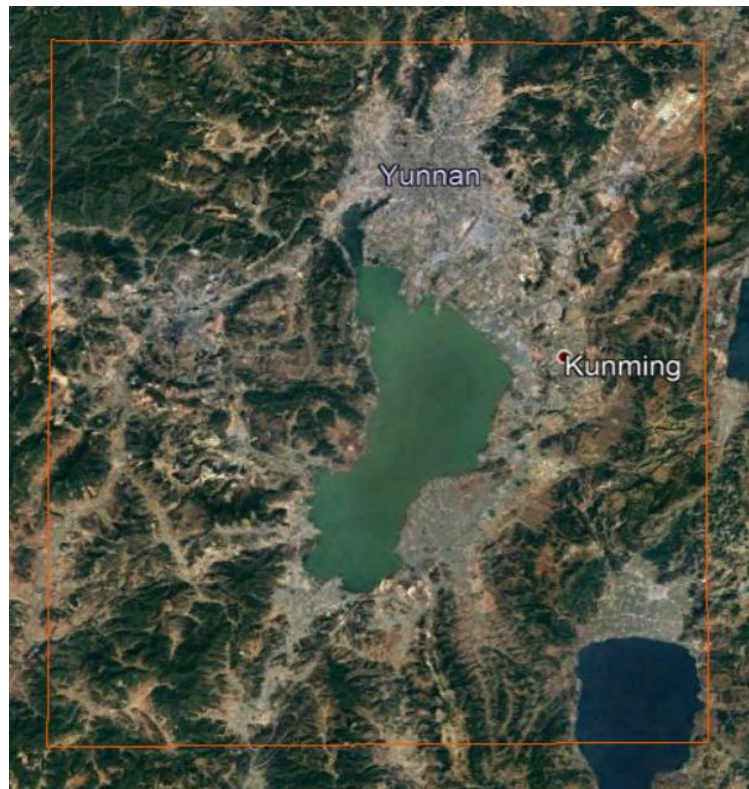
Zhao, J. Z., Liu, H. P., & Dong, R. C. (2008). Sustainable urban development: Policy framework for sustainable consumption and production. *International Journal of Sustainable Development and World Ecology*, 15(4), 318–325. <https://doi.org/10.3843/SusDev.15.4:5>

Zhao, L., Lee, X., Smith, R. B., & Oleson, K. (2014). Strong contributions of local background climate to urban heat islands. *Nature*, 511(7508), 216–219. <https://doi.org/10.1038/nature13462>

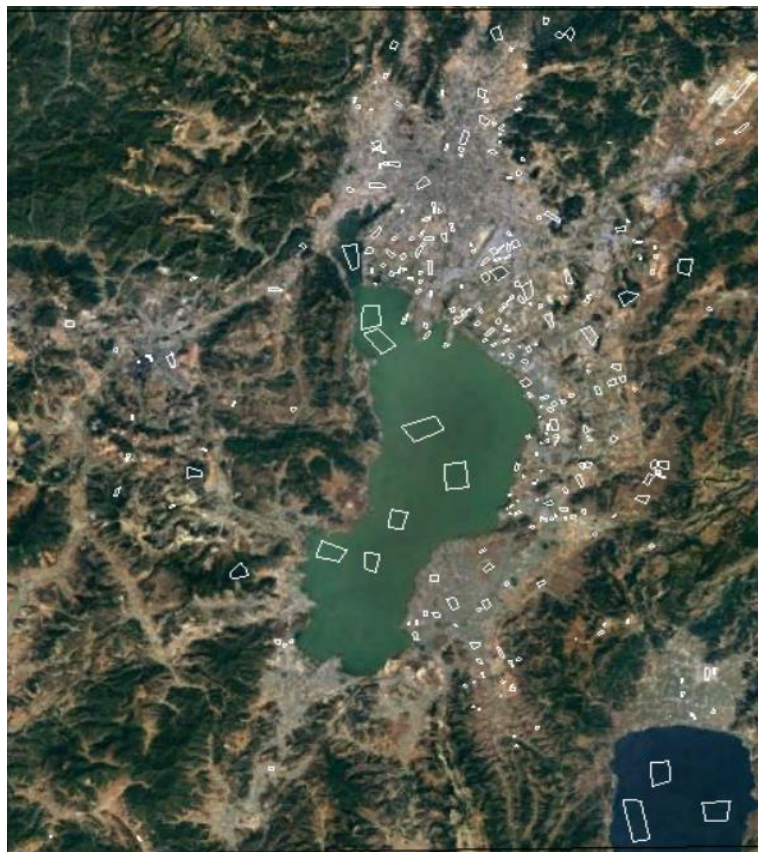
Zhou, W., Huang, G., & Cadenasso, M. L. (2011). Does spatial configuration matter? Understanding the effects of land cover pattern on land surface temperature in urban landscapes. *Landscape and Urban Planning*, 102(1), 54–63. <https://doi.org/10.1016/j.landurbplan.2011.03.009>

Zhou, X., & Wang, Y. C. (2010). Dynamics of Land Surface Temperature in Response to Land-Use/Cover Change. *Geographical Research*, 49(1), 23–36. <https://doi.org/10.1111/j.1745-5871.2010.00686.x>

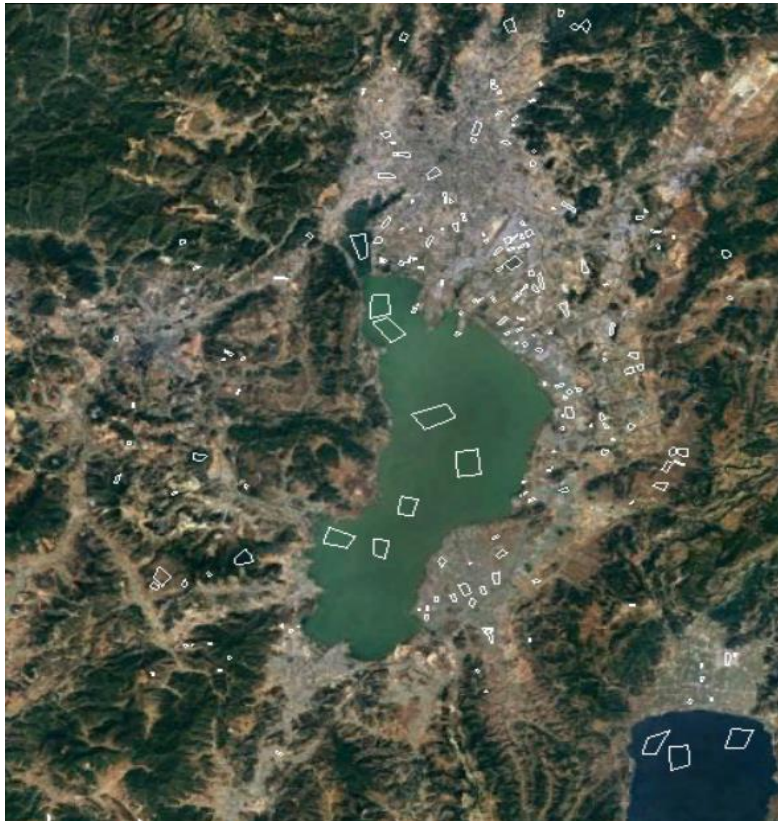
Appendix



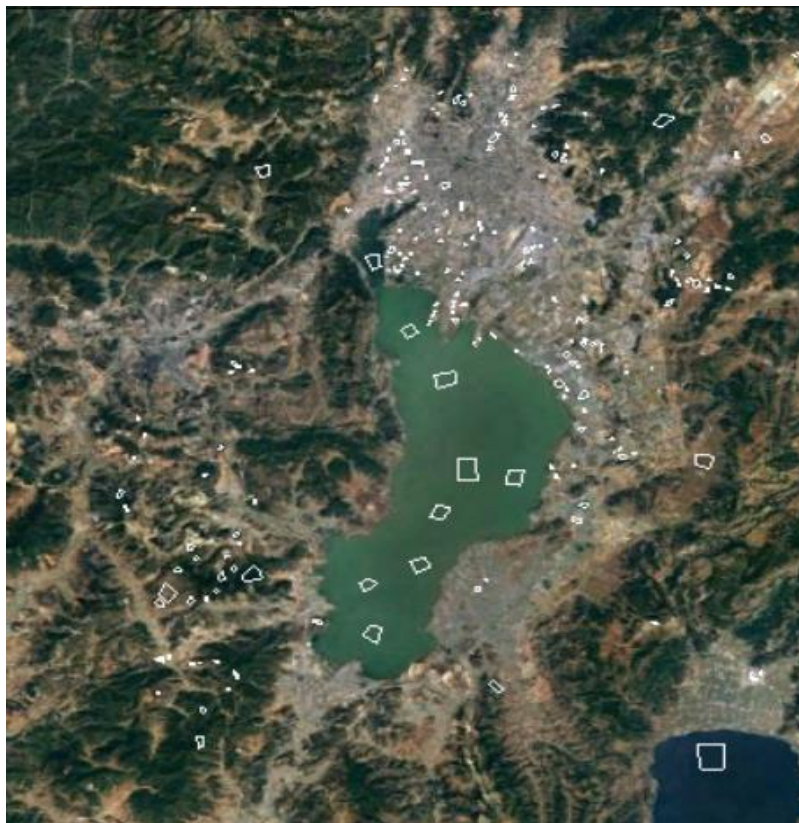
Appendix 1. Region of interest, Kunming (Google Earth © 2017)



Appendix 2. Training areas for the LCZ classification of 2017, Google Earth 2017.



Appendix 3. Training areas for the LCZ classification of 2011, Google Earth 2017.



Appendix 4. Training areas for the LCZ classification of 2005, Google Earth 2017.

Appendix 5. Confusion matrix (%) of LCZ classification for 2017 (workflow A).

	LCZ 1	LCZ 2	LCZ 3	LCZ 4	LCZ 5	LCZ 6	LCZ 8	LCZ 10	LCZ A	LCZ B	LCZ C	LCZ D	LCZ G	LCZ H
LCZ 1	55.32	0.08	0	0.87	0.94	0.18	0.28	0	0	0	0	0	0	0.49
LCZ 2	2.51	82.91	41.59	4.64	18.02	10.05	3.24	42.31	0	0	0	0	0	2.68
LCZ 3	0	0.32	17.4	0.13	0.09	0.88	0.14	0	0	0	0	0.19	0	0.13
LCZ 4	40.29	4.78	17.4	74.56	53.96	24.51	7.93	9.62	0.35	0.14	7.6	0.38	0.01	4.66
LCZ 5	1.04	5.67	10.03	13.73	14.53	28.92	0.9	1.92	0.01	0	2.92	0	0	1.11
LCZ 6	0	0.97	5.9	1.62	5.94	29.98	1.03	0	0	0.28	0.58	1.9	0	0.55
LCZ 8	0.42	4.45	5.9	1.48	0.94	0.18	79.39	11.54	0.03	0	0	1.9	0	2.83
LCZ 10	0	0.32	0	0	0.85	0	1.65	34.62	0	0	0	0	0	0.09
LCZ A	0.21	0	0	0.67	0.09	0.18	0.07	0	80.97	18.73	0.58	0	0	15.55
LCZ B	0	0	0	0.61	0.38	0.53	0.34	0	4.39	22.45	8.77	12.36	0	1.3
LCZ C	0	0.08	0.29	0.07	0.57	0.18	0.14	0	13.95	48.62	16.37	5.7	0	3.72
LCZ D	0	0.08	1.47	0.81	1.04	3	1.17	0	0.23	9.78	62.57	69.58	0	1.08
LCZ G	0.21	0	0	0	0	0	0.34	0	0.08	0	0	0	99.99	62.65
LCZ H	0	0.32	0	0.81	2.64	1.41	3.38	0	0	0	0.58	7.98	0	3.15

Appendix 6. Confusion matrix (%) of LCZ classification for 2005 (workflow B) with kernel size 9x9.

	LCZ 2	LCZ3	LCZ 5	LCZ 6	LCZ 8	LCZ A	LCZ B	LCZ C	LCZ D	LCZ G	LCZ H
LCZ 2	91.26	43.82	19.1	11.03	11.76	0	0	0	0.19	0	0.19
LCZ 3	6.82	49.49	3.43	8.72	0	0	0	0	0	0	0
LCZ 5	0.22	2.23	66.57	13.72	0	0	0	0	0	0	0
LCZ 6	0	4.46	6.48	50.66	0.33	0	0	0	2.89	0	0
LCZ 8	1.59	0	0	0	87.91	0	0	0	0	0	0
LCZ A	0	0	0	0	0	99.32	27.48	0	1.54	0	0
LCZ B	0	0	0	4.14	0	0.38	70.99	7.4	1.93	0	0
LCZ C	0	0	0	0	0	0.13	1.53	85.23	0	0.02	0
LCZ D	0	0	4.42	8.97	0	0.05	0	7.37	87.48	0	5.35
LCZ G	0	0	0	0	0	0.12	0	0	0	99.98	0
LCZ H	0.11	0	0	2.76	0	0	0	0	5.97	0	94.46

Appendix 7. Confusion matrix (%) of LCZ classification for 2011 (workflow B) with kernel size 7x7.

	LCZ 2	LCZ 3	LCZ 4	LCZ 5	LCZ 6	LCZ 8	LCZ 10	LCZ A	LCZ B	LCZ C	LCZ D	LCZ G	LCZ H
LCZ 2	93.21	32	0.56	24.56	20	2.02	0	0	0	1.34	0.62	0	0
LCZ 3	0.85	48.5	0	0.1	4.27	1.28	0	0	0	0	0	0	0
LCZ 4	1.32	12.43	94.5	19.24	3.64	0	0	0	0	0	0	0	0
LCZ 5	2.17	2.19	4.94	49.68	25.25	0	0	0	0	0	0	0	0
LCZ 6	0	4.66	0	2.46	45.59	0	3.75	0	0	0	3.49	0	0
LCZ 8	1.13	0	0	0.1	0	90.7	20	0	0	26.17	4.52	0	0
LCZ 10	1.23	0	0	0	1.25	6	73.75	0	0	0	0	0	0
LCZ A	0	0	0	0	0	0	0	99.54	21.49	0	0	0	0
LCZ B	0	0	0	0	0	0	0	0.06	50.79	24.16	4.52	0.01	0.11
LCZ C	0	0	0	0	0	0	2.5	0.4	27.72	46.99	0	0	0
LCZ D	0	0.22	0	0	0	0	0	0	0	1.34	82.13	0	7.18
LCZ G	0	0	0	0	0	0	0	0	0	0	0	99.99	0
LCZ H	0.09	0	0	3.86	0	0	0	0	0	0	4.72	0	92.71

Appendix 8. Confusion matrix of the LCZ classification for 2017 (workflow B) with kernel size 5x5.

	LCZ 1	LCZ 2	LCZ3	LCZ 4	LCZ 5	LCZ 6	LCZ 8	LCZ 10	LCZ A	LCZ B	LCZ C	LCZ D	LCZ G	LCZ H
LCZ 1	68.48	0.16	0	2.15	0.09	0	0	0	0	0	0	0	0	0
LCZ 2	0	96.68	19.47	0.87	23.02	1.59	1.59	0	0	0	0	0	0	0
LCZ 3	0	0.73	59.29	0.07	0.47	0	0.55	0	0	0	0	0	0	0.11
LCZ 4	31.52	0.24	1.47	88.83	31.85	13.76	0.76	0	0	0	0	0.19	0	0.17
LCZ 5	0	0.49	15.04	5.92	37.97	38.98	0.28	0	0	0	0	0	0	0.62
LCZ 6	0	0.24	4.72	1.89	5.75	42.15	0	0	0	0	0	1.14	0	0.62
LCZ 8	0	1.3	0	0.07	0	0	96.82	1.92	0	0	0	0	0	0
LCZ 10	0	0.16	0	0.2	0.47	0	0	98.08	0	0	0	0	0	0
LCZ A	0	0	0	0	0	0.35	0	0	97.31	33.33	0	0	0	0
LCZ B	0	0	0	0	0	0.35	0	0	2.69	56.34	5.85	11.98	0.01	0
LCZ C	0	0	0	0	0	0.18	0	0	0	10.33	88.3	3.61	0	0
LCZ D	0	0	0	0	0.38	1.76	0	0	0	0	5.85	75.29	0	0
LCZ G	0	0	0	0	0	0	0	0	0	0	0	0	99.99	0
LCZ H	0	0	0	0	0	0.88	0	0	0	0	0	7.79	0	98.47

